Travelling Waves for the Nonlinear Schrödinger Equation with General Nonlinearity in Dimension Two

David Chiron, Claire Scheid

Travelling waves for the Nonlinear Schrödinger Equation with general nonlinearity in dimension two

David CHIRON* & Claire SCHEID†

Abstract

We investigate numerically the two dimensional travelling waves of the Nonlinear Schrödinger Equation for a general nonlinearity and with nonzero condition at infinity. In particular, we are interested in the energy-momentum diagrams. We propose a numerical strategy based on the variational structure of the equation. The key point is to characterize the saddle points of the action as minimizers of another functional, that allows us to use a gradient flow. We combine this approach with a continuation method in speed in order to obtain the full range of velocities.

Through various examples, we show that even though the nonlinearity has the same behaviour as the well-known Gross-Pitaevskii nonlinearity, the qualitative properties of the travelling waves may be extremely different. For instance, we observe cusps, a modified (KP-I) asymptotic in the transonic limit, various multiplicity results and "one dimensional spreading" phenomena.

Keywords: Nonlinear Schrödinger Equation; Travelling wave; Kadomtsev-Petviashvili Equation; Constrained minimization; Gradient flow; Continuation method.

MSC (2010): 35B38; 35C07; 35J20; 35J61; 35Q40; 35Q55; 35J60.

1 The (NLS) equation with nonzero condition at infinity

In this paper, we consider the Nonlinear Schrödinger Equation in two dimensions

$$i\frac{\partial \Psi}{\partial t} + \Delta \Psi + \Psi f(|\Psi|^2) = 0, \tag{NLS}$$

which is a fundamental model in condensed matter physics. The (NLS) equation is used as a model for Bose-Einstein condensation or superfluidity (*cf.* [50], [1]) and a standard case is the Gross-Pitaevskii equation (GP) for which $f(\varrho) = \varrho - 1$. However, for Bose condensates, other models may be used (see [40]), such as the quintic (NLS) ($f(\varrho) = \varrho^2$) in one space dimension and $f(\varrho) = \frac{d}{d\varrho}(\varrho^2/\ln(a\varrho))$ in two space dimension. The so-called cubic-quintic (NLS) is another relevant model (*cf.* [4]), for which

$$f(\varrho) = \alpha_1 - \alpha_3\varrho + \alpha_5\varrho^2,$$

*Laboratoire J.A. Dieudonné, Université de Nice-Sophia Antipolis, Parc Valrose, 06108 Nice Cedex 02, France. e-mail: chiron@unice.fr.

†Laboratoire J.A. Dieudonné, Université de Nice-Sophia Antipolis, Parc Valrose, 06108 Nice Cedex 02, France *and* INRIA Sophia Antipolis-Méditerranée research center, NACHOS project-team 06902 Sophia Antipolis Cedex, France. e-mail: cscheid@unice.fr.

where α_1, α_3 and α_5 are positive constants such that f has two positive roots. The cubic-quintic (NLS) also appears as a model for elongated Bose-Einstein condensates, see [34], [51]. For superfluid helium II, the nonlinearity

$$f(\varrho) = \alpha\varrho - \beta\varrho^{3.8}$$

with α and β positive, is used to produce a quantitatively correct equation of state (*cf.* [24]). In Nonlinear Optics, the nonlinearity f represents the response of the medium to the intensity $|E|^2$ of the electric field, and Kerr media correspond to f linear ($f(\varrho) = \alpha\varrho$). For non Kerr media, several nonlinearities may then be found (see [37]):

$$f(\varrho) = \mu + \alpha\varrho^\nu - \beta\varrho^{2\nu}, \qquad f(\varrho) = -\alpha\varrho\Big(1 + \gamma\tanh\Big(\frac{\varrho^2 - \varrho_0^2}{\sigma^2}\Big)\Big)$$

where all the parameters are positive, or (see [2]),

$$f(\varrho) = -\alpha\ln(\varrho), \qquad f(\varrho) = \mu + \alpha\varrho + \beta\varrho^2 - \gamma\varrho^3,$$

and when we take into account saturation effects, one may encounter (see [37], [35]):

$$f(\varrho) = \alpha\Big(\frac{1}{(1+\frac{\varrho}{\varrho_0})^\nu} - \frac{1}{(1+\frac{1}{\varrho_0})^\nu}\Big), \qquad f(\varrho) = \exp\Big(\frac{1-\varrho}{\varrho_0}\Big) - 1 \tag{1}$$

for some parameters $\nu > 0$, $\varrho_0 > 0$. For these two nonlinearities, f has a finite limit for large ϱ.

As a model for Bose-Einstein condensates, the natural condition at infinity is ([50])

$$|\Psi|^2 \to r_0^2 \qquad \text{as} \quad |x| \to +\infty, \tag{2}$$

where $r_0 > 0$ is such that $f(r_0^2) = 0$. In Nonlinear Optics, this condition is also relevant for dark solitons (see [37]), but one may also impose the more classical condition $\Psi \to 0$ at spatial infinity. In the paper, we shall then assume the nonlinearity f quite general and work with the condition (2). Without loss of generality, we normalize r_0 to 1.

For solutions Ψ of (NLS) which do not vanish, we may use the Madelung transform

$$\Psi = a\exp(i\phi)$$

and rewrite (NLS) as an hydrodynamical system close to the Euler system for compressible fluids with an additional quantum pressure

$$\begin{cases} \partial_t a + 2\nabla\phi\cdot\nabla a + a\Delta\phi = 0 \\ \\ \partial_t\phi + |\nabla\phi|^2 - f(a^2) - \dfrac{\Delta a}{a} = 0, \end{cases} \qquad \text{or} \qquad \begin{cases} \partial_t\rho + 2\nabla\cdot(\rho u) = 0 \\ \\ \partial_t u + 2(u\cdot\nabla)u - \nabla(f(a^2)) - \nabla\Big(\dfrac{\Delta a}{a}\Big) = 0 \end{cases}$$

with $(\rho, u) \overset{\text{def}}{=} (a^2, \nabla\phi)$. When neglecting the quantum pressure and linearizing this Euler type system around the particular trivial solution $\Psi = r_0 = 1$ (or $(a, u) = (1, 0)$), we obtain the free wave equation

$$\begin{cases} \partial_t\bar{a} + \nabla\cdot\bar{u} = 0 \\ \\ \partial_t\bar{u} - 2f'(1)\nabla\bar{a} = 0 \end{cases}$$

with associated speed of sound

$$\mathfrak{c}_s \stackrel{\text{def}}{=} \sqrt{-2f'(1)} > 0$$

provided $f'(1) < 0$ (that is the Euler system is hyperbolic in the region $\rho \simeq 1$), which we will assume throughout the paper. The speed of sound enters in a crucial way in the existence of travelling waves for (NLS).

The Nonlinear Schrödinger equation formally preserves the energy, which is the (formal) Hamiltonian, involving a kinetic term and a potential term

$$E(\Psi) \stackrel{\text{def}}{=} \int_{\mathbb{R}^2} |\nabla\Psi|^2 + V(|\Psi|^2)\ dx = E_{\text{kin}}(\Psi) + E_{\text{pot}}(\Psi),$$

where $V(\varrho) \stackrel{\text{def}}{=} -\int_1^{\varrho} f(R)\ dR$, and the momentum, associated with the invariance of (NLS) under space translation. In [33], the expression for the momentum $\vec{P}$ is

$$\vec{P}(\Psi) \stackrel{\text{def}}{=} \int_{\mathbb{R}^2} \langle i(\Psi - 1), \nabla\Psi\rangle\ dx,$$

where $\langle\cdot,\cdot\rangle$ denotes the real scalar product in $\mathbb{C}$. This expression has a meaning as an improper integral if Ψ converges to 1 at infinity with a suitable decay. For a definition of the momentum when Ψ is just in the energy space, see [44], [23].

1.1 The travelling waves

For (NLS) with nonzero condition at infinity, the travelling waves play a fundamental role in the dynamics. These are particular solutions of the form

$$\Psi(t,x) = u(x_1 - ct, x_2)$$

where c is the speed of propagation, and u is a solution to the elliptic equation

$$\Delta u + uf(|u|^2) = ic\partial_{x_1} u \qquad (\text{TW}_c)$$

with the condition at infinity $|u(x)| \to 1$ as $|x| \to \infty$. We may assume $c \geq 0$, since conjugation of (TW_c) changes the sign of c. The existence and qualitative properties of the travelling waves of the Gross-Pitaevskii equation ($f(\varrho) = 1 - \varrho$), that is

$$i\frac{\partial\Psi}{\partial t} + \Delta\Psi + \Psi(1 - |\Psi|^2) = 0, \qquad (\text{GP})$$

have been studied by C. Jones and P. Roberts in [33] (see also [32] and [11]) in dimensions two and three. The study relies on numerical simulation and formal asymptotic expansion. For this particular nonlinearity, $\mathfrak{c}_s = \sqrt{2} \simeq 1.4142$ and the function V is the parabola $V(\varrho) = \dfrac{1}{2}(\varrho - 1)^2$. They represented the solutions in the (E, P) diagram in figure 1, where $P \stackrel{\text{def}}{=} \vec{P}_1$ is the momentum in the direction x_1 of propagation. The blue curve is the curve $[0, \mathfrak{c}_s] \mapsto (P(c), E(c))$, where $P(c)$ and $E(c)$ are the momentum and energy of the travelling wave of speed c. In space dimension two, as $c \to 0$, the solution possesses two vortices of degree $+1$ and -1 at distance $\simeq 2/c$, and

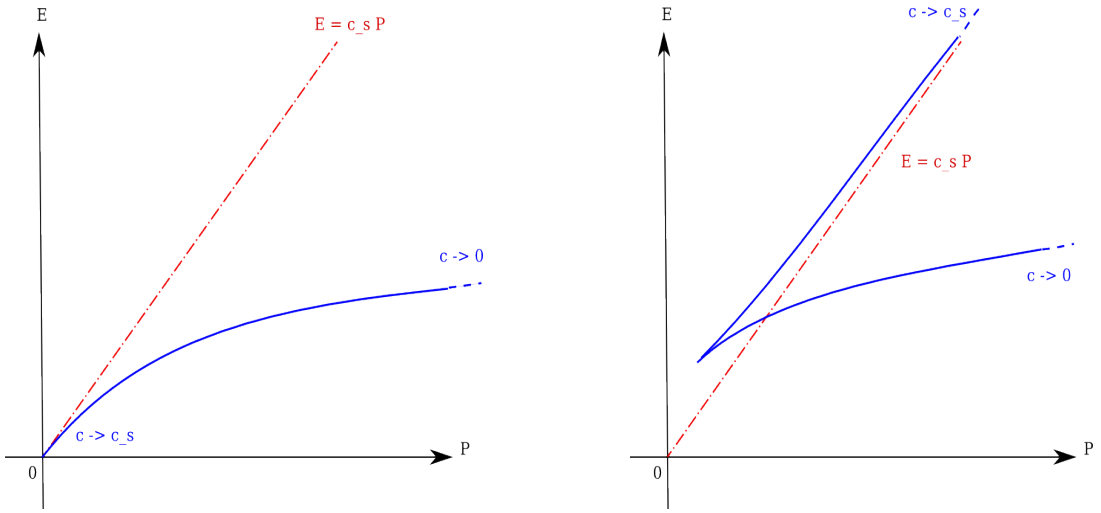

Figure 1: The (E, P) diagram (from [33]) for (GP) in dimensions (a) left: two; (b) right: three (the straight line is $E = \mathfrak{c}_s P$)

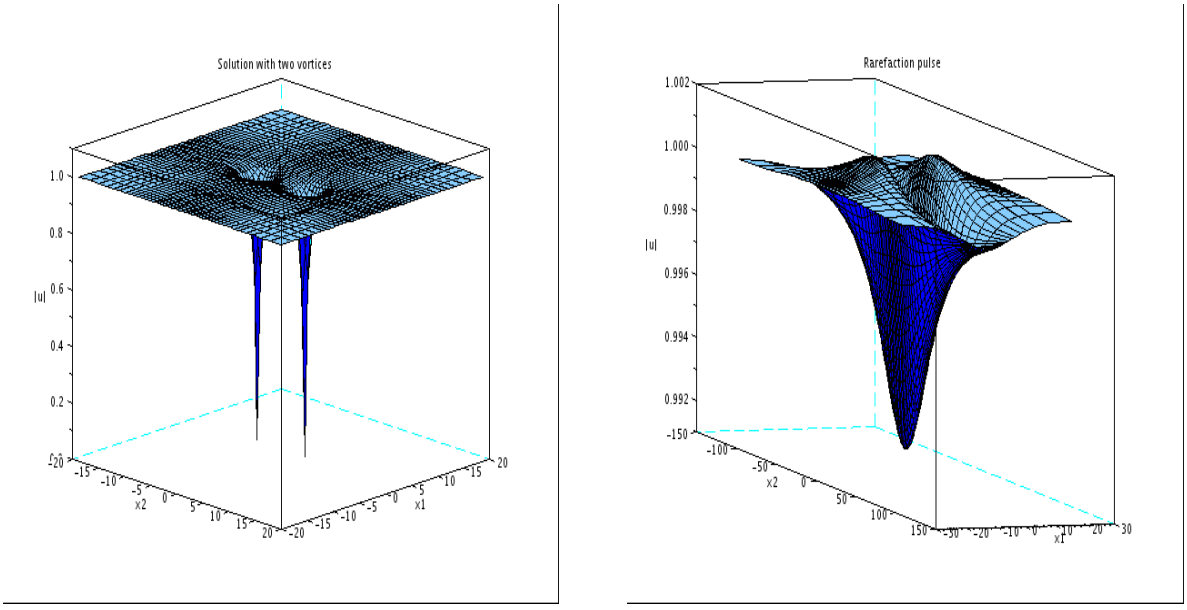

Figure 2: Graphs of (a) left: two vortices ($c \approx 0$) and (b) right: a rarefaction pulse ($c \approx \mathfrak{c}_s$)

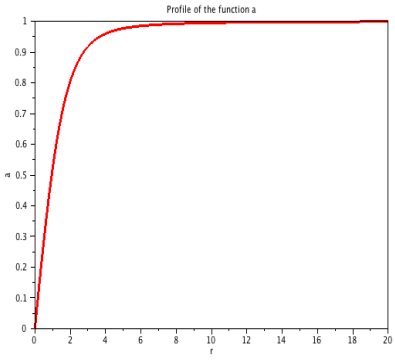

Figure 3: Profile of the function $\mathfrak{a}$ for the (GP) equation ($f(\varrho) = 1 - \varrho$)

for $c \to \mathfrak{c}_s = \sqrt{2}$, the solution is a rarefaction pulse described by the (KP-I) ground state: its modulus is close to one everywhere and it spreads out in the space variable, but much more in the x_2 direction than in the x_1 direction. We have represented in figure 2 the modulus $|u|$ of the travelling waves corresponding to these two extreme cases. The numerical method they used was to start for small speeds with the ansatz of two vortices, and then to increase the speed step by step and solve the equation (TW_c) by Newton algorithm. In dimension three, the solutions are supposed axisymmetric around the x_1-axis. The vortex is then now a vortex ring (a circle). When $c \to \mathfrak{c}_s = \sqrt{2}$, the solution looks qualitatively similar to figure 2 (b) with x_2 replaced by $|(x_2, x_3)|$. For the travelling waves of the Gross-Pitaevskii nonlinearity, C. Jones and P. Roberts ([33]) conjectured (through formal expansions at spatial infinity) an explicit algebraic decay. The paper [30] provides a rigorous proof that finite energy travelling waves satisfy (up to a phase factor) the decay conjectured in [33]. Thanks to this decay, the momentum $\vec{P}$ is well-defined. The proof of [30] certainly extends to more general nonlinearities.

1.2 Vortex solutions

Let us recall that the vortices of degree $d \in \mathbb{Z}$ for (NLS) are special solutions of (TW_c) which are stationary (hence $c = 0$) and of the form

$$U(x) = \mathfrak{a}(r)\mathrm{e}^{id\theta},$$

where we use polar coordinates. The function $\mathfrak{a}$ is real-valued, verifies $\mathfrak{a}(0) = 0$ and $\mathfrak{a}(+\infty) = 1$, is increasing and solves the ODE

$$\mathfrak{a}'' + \frac{\mathfrak{a}'}{r} - \frac{d^2}{r^2}\mathfrak{a} + \mathfrak{a}f(\mathfrak{a}^2) = 0 \tag{3}$$

in $\mathbb{R}_+$. We are interested only in degree ± 1 vortices, and thus we shall restrict ourselves to the case $d = 1$, the case $d = -1$ being deduced by complex conjugation. The profile of the degree one vortex may be found by a shooting method, see figure 3. We have obtained $\mathfrak{a}'(0) \approx 0.583\,189\,495$ for the (GP) equation, which is slightly different from the value $0.582\,781\,187\,8$ given in [9]. The travelling vortex solutions with small speed c as shown in figure 2 (a) consist in two vortices of degrees 1 and -1 at large distance from each other. A good approximation of this solution is given by the expression

$$\mathfrak{a}(|(x_1, x_2 - c^{-1})|)\frac{x_1 + i(x_2 - c^{-1})}{|(x_1, x_2 - c^{-1})|} \times \mathfrak{a}(|(x_1, x_2 + c^{-1})|)\frac{x_1 - i(x_2 + c^{-1})}{|(x_1, x_2 + c^{-1})|}. \tag{4}$$

Here, $\times$ stands for complex multiplication. For mathematical justifications concerning these travelling vortex solutions for the Gross-Pitaevskii equation, see [15] (in space dimension two) and [14], [19] for higher dimensions. These results may be generalized to any nonlinearity f such that $V(\varrho) = -\int_1^\rho f$ is positive for $\varrho \neq 1$. The fact that, as $c \to 0$, the distance between the two vortices is $\sim 2/c$ could be deduced from the arguments in [15].

1.3 The transonic limit

We focus on the transonic limit $c \simeq \mathfrak{c}_s$ but $c < \mathfrak{c}_s$, and thus define, for $0 < \varepsilon < \mathfrak{c}_s$ small,

$$c(\varepsilon) \stackrel{\text{def}}{=} \sqrt{\mathfrak{c}_s^2 - \varepsilon^2} \in (0, \mathfrak{c}_s).$$

The formal convergence to the Kadomtsev-Petviashvili-I (KP-I) solitary wave in dimensions $d = 2$ or $d = 3$ is given in [33] for the Gross-Pitaevskii equation, *i.e.* (NLS) with $f(\varrho) = 1 - \varrho$, where the speed of sound is $\mathfrak{c}_s = \sqrt{2}$. We refer to [37], [38] for the occurence of the two-dimensional (KP-I) in Nonlinear Optics, and to [53] and [35] for the one dimensional case (where (KP-I) reduces to the Korteweg-de Vries (KdV) equation). The argument is as follows (see [20] for the one dimensional case). We insert the ansatz

$$u(x) = (1 + \varepsilon^2 A_\varepsilon(z)) \exp(i\varepsilon\varphi_\varepsilon(z)) \qquad z_1 = \varepsilon x_1, \quad z_2 = \varepsilon^2 x_2 \tag{5}$$

in $(\mathrm{TW}_{c(\varepsilon)})$, cancel the phase factor and separate real and imaginary parts to obtain the hydrodynamical system

$$\begin{cases} -c(\varepsilon)\partial_{z_1} A_\varepsilon + 2\varepsilon^2 \partial_{z_1}\varphi_\varepsilon \partial_{z_1} A_\varepsilon + 2\varepsilon^4 \partial_{z_2}\varphi_\varepsilon \partial_{z_2} A_\varepsilon \\ \qquad\qquad + (1 + \varepsilon^2 A_\varepsilon)\Big(\partial_{z_1}^2 \varphi_\varepsilon + \varepsilon^2 \partial_{z_2}^2 \varphi_\varepsilon\Big) = 0 \\ \\ -c(\varepsilon)\partial_{z_1}\varphi_\varepsilon + \varepsilon^2 (\partial_{z_1}\varphi_\varepsilon)^2 + \varepsilon^4 (\partial_{z_2}\varphi_\varepsilon)^2 - \dfrac{1}{\varepsilon^2} f\Big((1 + \varepsilon^2 A_\varepsilon)^2\Big) \\ \qquad\qquad - \varepsilon^2 \dfrac{\partial_{z_1}^2 A_\varepsilon + \varepsilon^2 \partial_{z_2}^2 A_\varepsilon}{1 + \varepsilon^2 A_\varepsilon} = 0. \end{cases} \tag{6}$$

On the formal level, if A_ε and φ_ε are of order ε^0, we obtain $-\mathfrak{c}_s \partial_{z_1} A_\varepsilon + \partial_{z_1}^2 \varphi_\varepsilon = \mathcal{O}(\varepsilon^2)$ for the first equation of (6). Moreover, since $f(1) = 0$ and $\mathfrak{c}_s^2 = -2f'(1)$, using the Taylor expansion

$$f\Big((1 + \varepsilon^2 A_\varepsilon)^2\Big) = f(1) - \mathfrak{c}_s^2 \varepsilon^2 A_\varepsilon + \mathcal{O}(\varepsilon^4),$$

for the second equation implies $-\mathfrak{c}_s \partial_{z_1}\varphi_\varepsilon + \mathfrak{c}_s^2 A_\varepsilon = \mathcal{O}(\varepsilon^2)$. In both cases, we obtain the single constraint

$$\mathfrak{c}_s A_\varepsilon = \partial_{z_1}\varphi_\varepsilon + \mathcal{O}(\varepsilon^2). \tag{7}$$

We now add $c(\varepsilon)/\mathfrak{c}_s^2$ times the first equation of (6) and $\partial_{z_1}/\mathfrak{c}_s^2$ times the second one. Using the Taylor expansion

$$f\Big((1 + \alpha)^2\Big) = -\mathfrak{c}_s^2 \alpha - \Big(\frac{\mathfrak{c}_s^2}{2} - 2f''(1)\Big)\alpha^2 + f_3(\alpha),$$

with $f_3(\alpha) = \mathcal{O}(\alpha^3)$ as $\alpha \to 0$, this gives

$$\begin{aligned}
&\frac{\mathfrak{c}_s^2 - c^2(\varepsilon)}{\varepsilon^2 \mathfrak{c}_s^2}\,\partial_{z_1} A_\varepsilon - \frac{1}{\mathfrak{c}_s^2}\,\partial_{z_1}\Big(\frac{\partial_{z_1}^2 A_\varepsilon + \varepsilon^2 \partial_{z_2}^2 A_\varepsilon}{1+\varepsilon^2 A_\varepsilon}\Big) + \frac{c(\varepsilon)}{\mathfrak{c}_s^2}(1+\varepsilon^2 A_\varepsilon)\Delta_{z_\perp}\varphi_\varepsilon \\
+\Big\{2\frac{c(\varepsilon)}{\mathfrak{c}_s^2}\partial_{z_1}\varphi_\varepsilon \partial_{z_1} A_\varepsilon + \frac{c(\varepsilon)}{\mathfrak{c}_s^2}\,A_\varepsilon \partial_{z_1}^2\varphi_\varepsilon + \frac{1}{\mathfrak{c}_s^2}\,\partial_{z_1}[(\partial_{z_1}\varphi_\varepsilon)^2] + \Big[\frac{1}{2} - 2\frac{f''(1)}{\mathfrak{c}_s^2}\Big]\partial_{z_1}(A_\varepsilon^2)\Big\} \\
= -2\varepsilon^2 \frac{c(\varepsilon)}{\mathfrak{c}_s^2}\partial_{z_2}\varphi_\varepsilon \partial_{z_2} A_\varepsilon - \frac{\varepsilon^2}{\mathfrak{c}_s^2}\partial_{z_1}[\,(\partial_{z_2}\varphi_\varepsilon)^2] - \frac{1}{\mathfrak{c}_s^2\varepsilon^4}\,\partial_{z_1}[f_3(\varepsilon^2 A_\varepsilon)]. \qquad (8)
\end{aligned}$$

It then follows that if $A_\varepsilon \to A$ and $\varphi_\varepsilon \to \varphi$ as $\varepsilon \to 0$ in a suitable sense, we can infer from (7) that

$$\mathfrak{c}_s A = \partial_{z_1}\varphi, \qquad (9)$$

and since $\mathfrak{c}_s^2 - c^2(\varepsilon) = \varepsilon^2$, (8) gives the solitary waves equation for the (KP-I) equation

$$\frac{1}{\mathfrak{c}_s^2}\,\partial_{z_1} A - \frac{1}{\mathfrak{c}_s^2}\,\partial_{z_1}^3 A + \Gamma A \partial_{z_1} A + \partial_{z_2}^2 \partial_{z_1}^{-1} A = 0. \qquad \text{(SW)}$$

Here, the coefficient Γ depends on f through the formula

$$\Gamma \stackrel{\text{def}}{=} 6 - \frac{4}{\mathfrak{c}_s^2} f''(1).$$

This is this type of solution that we have in figure 2 (b). Note that the modulus is $\mathcal{O}(\varepsilon^2)$ close to 1, and that the variations in x_1 and in x_2 are at the scale ε^{-1} and ε^{-2} respectively, which can be checked on the figure.

For rigorous mathematical results justifying the transonic limit and the convergence to a (KP-I) ground state, see [12] (in two space dimensions for the Gross-Pitaevskii nonlinearity), [22] (in two and three space dimensions for a general nonlinearity) and [20] (in one space dimension, where the (KP-I) equation is replaced by the (KdV) equation). This supposes $\Gamma \neq 0$, and this is the case for instance for the Gross-Pitaevskii nonlinearity ($\Gamma = 6$).

As in [20], the case where Γ vanishes is also of interest, and gives rise to a modified (KP-I) equation (mKP-I) with *cubic* nonlinearity. For the nonlinearities we have mentioned, the case $\Gamma = 0$ occurs for instance for the saturated nonlinearities (1) under the condition $\nu + 1 = 3(\varrho_0 + 1)$ and $\varrho_0 = 1/3$ respectively. More generally, this may happen for nonlinearities which are polynomials of degree three. Note that when $\Gamma = 0$, (SW) becomes linear and thus has no nontrivial solitary wave. When $\Gamma = 0$, which occurs only in the particular case $2f''(1) = 3\mathfrak{c}_s^2$, we may then insert the ansatz

$$u(x) = (1 + \varepsilon A_\varepsilon(z))\exp(i\varphi_\varepsilon(z)) \qquad z_1 = \varepsilon x_1, \quad z_2 = \varepsilon^2 x_2, \qquad (10)$$

for which, compared to (5), we have increased the size of the amplitude A and the phase φ in order to see nonlinear terms. Plugging this in ($\mathrm{TW}_{c(\varepsilon)}$), we obtain similarly the system

$$\left\{\begin{array}{l}
-c(\varepsilon)\partial_{z_1} A_\varepsilon + 2\varepsilon \partial_{z_1}\varphi_\varepsilon \partial_{z_1} A_\varepsilon + 2\varepsilon^3 \partial_{z_2}\varphi_\varepsilon \partial_{z_2} A_\varepsilon + (1+\varepsilon A_\varepsilon)\Big(\partial_{z_1}^2\varphi_\varepsilon + \varepsilon^2 \partial_{z_2}^2 \varphi_\varepsilon\Big) = 0 \\[2ex]
-c(\varepsilon)\partial_{z_1}\varphi_\varepsilon + \varepsilon(\partial_{z_1}\varphi_\varepsilon)^2 + \varepsilon^3(\partial_{z_2}\varphi_\varepsilon)^2 - \dfrac{1}{\varepsilon} f\Big((1+\varepsilon A_\varepsilon)^2\Big) - \varepsilon^2 \dfrac{\partial_{z_1}^2 A_\varepsilon + \varepsilon^2 \partial_{z_2}^2 A_\varepsilon}{1+\varepsilon A_\varepsilon} = 0.
\end{array}\right. \qquad (11)$$

Here again, as $\varepsilon \to 0$ we infer for both equations $\mathfrak{c}_s A_\varepsilon = \partial_{z_1}\varphi_\varepsilon + \mathcal{O}(\varepsilon)$. However, we shall need a higher order expansion. We thus Taylor expand f to next order

$$f\Big((1+\alpha)^2\Big) = -\mathfrak{c}_s^2\alpha - \Big(\frac{\mathfrak{c}_s^2}{2} - 2f''(1)\Big)\alpha^2 + \Big(2f''(1) + \frac{4}{3}f'''(1)\Big)\alpha^3 + \mathcal{O}_{\alpha\to 0}(\alpha^4).$$

To the order $\mathcal{O}(\varepsilon^2)$, the system (11) is (recalling $c^2(\varepsilon) = \mathfrak{c}_s^2 - \varepsilon^2$)

$$\begin{cases} \partial_{z_1}^2\varphi_\varepsilon - c(\varepsilon)\partial_{z_1}A_\varepsilon + 2\varepsilon\partial_{z_1}\varphi_\varepsilon\partial_{z_1}A_\varepsilon + \varepsilon A_\varepsilon\partial_{z_1}^2\varphi_\varepsilon = \mathcal{O}(\varepsilon^2) \\ \\ c^2(\varepsilon)A_\varepsilon - c(\varepsilon)\partial_{z_1}\varphi_\varepsilon + \varepsilon(\partial_{z_1}\varphi_\varepsilon)^2 + \varepsilon\Big(\dfrac{\mathfrak{c}_s^2}{2} - 2f''(1)\Big)A_\varepsilon^2 = \mathcal{O}(\varepsilon^2). \end{cases}$$

Taking into account $\mathfrak{c}_s A_\varepsilon = \partial_{z_1}\varphi_\varepsilon + \mathcal{O}(\varepsilon)$ and since $\Gamma = 0$ implies $2f''(1) = 3\mathfrak{c}_s^2$, we infer for both equations in the above system

$$\partial_{z_1}\varphi_\varepsilon - \mathfrak{c}_s A_\varepsilon = -\frac{3\varepsilon}{2}\mathfrak{c}_s A_\varepsilon^2 + \mathcal{O}(\varepsilon^2). \tag{12}$$

Adding $c(\varepsilon)/\mathfrak{c}_s^2$ times the first equation of (11) and $\partial_{z_1}/\mathfrak{c}_s^2$ times the second one and dividing by ε^2, we get

$$\begin{aligned} &\frac{1}{\mathfrak{c}_s^2}\,\partial_{z_1}A_\varepsilon - \frac{1}{\mathfrak{c}_s^2}\,\partial_{z_1}\Big(\frac{\partial_{z_1}^2 A_\varepsilon + \varepsilon^2\partial_{z_2}^2 A_\varepsilon}{1+\varepsilon A_\varepsilon}\Big) + \frac{c(\varepsilon)}{\mathfrak{c}_s^2}(1+\varepsilon^2 A_\varepsilon)\partial_{z_2}^2\varphi_\varepsilon - \frac{1}{\mathfrak{c}_s^2}\,\Big(6f''(1) + 4f'''(1)\Big)A_\varepsilon^2\partial_{z_1}A_\varepsilon \\ &\quad + \frac{1}{\varepsilon}\Big\{2\frac{c(\varepsilon)}{\mathfrak{c}_s^2}\partial_{z_1}\varphi_\varepsilon\partial_{z_1}A_\varepsilon + \frac{c(\varepsilon)}{\mathfrak{c}_s^2}\,A_\varepsilon\partial_{z_1}^2\varphi_\varepsilon + \frac{1}{\mathfrak{c}_s^2}\,\partial_{z_1}[(\partial_{z_1}\varphi_\varepsilon)^2] + \Big[\frac{1}{2} - \frac{2f''(1)}{\mathfrak{c}_s^2}\Big]\partial_{z_1}(A_\varepsilon^2)\Big\} \\ &\quad = -2\varepsilon\frac{c(\varepsilon)}{\mathfrak{c}_s^2}\partial_{z_2}\varphi_\varepsilon\partial_{z_2}A_\varepsilon - \frac{\varepsilon}{\mathfrak{c}_s^2}\partial_{z_1}[\,(\partial_{z_2}\varphi_\varepsilon)^2] - \frac{1}{\mathfrak{c}_s^2\varepsilon^3}\,\partial_{z_1}[((\varepsilon A_\varepsilon)^4)]. \end{aligned} \tag{13}$$

When $\Gamma = 0$, we have $2f''(1) = 3\mathfrak{c}_s^2$ and, using (12) and $c^2(\varepsilon) = \mathfrak{c}_s^2 - \varepsilon^2$, the second line in (13) seems singular in view of the factor ε^{-1} but is actually equal to

$$\begin{aligned} \frac{1}{\varepsilon}\Big\{ &\frac{2}{\mathfrak{c}_s}\,\partial_{z_1}A_\varepsilon\Big(\mathfrak{c}_s A_\varepsilon - \frac{3\varepsilon}{2}\mathfrak{c}_s A_\varepsilon^2\Big) + \frac{1}{\mathfrak{c}_s}\,A_\varepsilon\partial_{z_1}\Big(\mathfrak{c}_s A_\varepsilon - \frac{3\varepsilon}{2}\mathfrak{c}_s A_\varepsilon^2\Big) \\ &+ \frac{1}{\mathfrak{c}_s^2}\,\partial_{z_1}[(\mathfrak{c}_s A_\varepsilon - \frac{3\varepsilon}{2}\mathfrak{c}_s A_\varepsilon^2)^2] - 5A_\varepsilon\partial_{z_1}A_\varepsilon\Big\} + \mathcal{O}(\varepsilon) = -15A_\varepsilon^2\partial_{z_1}A_\varepsilon + \mathcal{O}(\varepsilon), \end{aligned}$$

since the quadratic terms cancel out. As a consequence, passing to the (formal) limit $\varepsilon \to 0$ in (13) yields

$$\frac{1}{\mathfrak{c}_s^2}\,\partial_{z_1}A - \frac{1}{\mathfrak{c}_s^2}\,\partial_{z_1}^3 A + \Gamma' A^2\partial_{z_1}A + \partial_{z_2}^2\partial_{z_1}^{-1}A = 0, \tag{SW'}$$

where we have set

$$\Gamma' \stackrel{\text{def}}{=} -\frac{4f'''(1)}{\mathfrak{c}_s^2} - 24,$$

which is the solitary waves equation for (mKP-I) with cubic nonlinearity. The solitary wave equation (SW') does have nontrivial solutions if and only if $\Gamma' < 0$, which is the focusing case, see [26]. We may observe that equation (SW') is odd in A, hence the solutions arise by pairs $(A, -A)$.

Let us point out that in two space dimension, a function u given by the ansatz (5) with A a nontrivial solution of (SW) and φ given by (9) is such that $E(u) \sim \mathfrak{c}_s P(u) \approx \varepsilon$ and $E(u) - \mathfrak{c}_s P(u) \approx \varepsilon^3$. On the other hand, for a function u given by the ansatz (10) where A is a nontrivial solution of (SW') and φ_ε given by (see (12))

$$\partial_{z_1} \varphi_\varepsilon = \mathfrak{c}_s A - \frac{3\varepsilon}{2} \mathfrak{c}_s A^2$$

and not only (9), we have $E(u) \sim \mathfrak{c}_s P(u) \approx \varepsilon^{-1}$ and $E(u) - \mathfrak{c}_s P(u) \approx \varepsilon$. This means that if $\Gamma \neq 0$, both E and P are small as $c \to \mathfrak{c}_s$ and the straight line $E = \mathfrak{c}_s P$ is the tangent to the curve at the origin in the (E, P) diagram (see figure 1 (a)), but when $\Gamma = 0 > \Gamma'$, we expect travelling wave solutions with high energy and momentum. Morever, the straight line $E = \mathfrak{c}_s P$ is an asymptote in the (E, P) diagram: we have then a situation rather close to the transonic limit of the Gross-Pitaevskii equation in three dimension (see figure 1 (b)). In the one dimensional case, we refer to [20] for the convergence of the travelling waves in the transonic limit to the (mKdV) solitary wave (when $\Gamma = 0 > \Gamma'$), with indeed the existence of two branches of travelling wave solutions for c near $\mathfrak{c}_s$. In [45], the authors follow the approach in [33] to compute numerically the travelling waves to a Landau-Lifshitz model (see section 3.1). It turns out that the transonic limit is also formally governed by the (mKP-I) solitary wave equation, and that the travelling waves look close to "the" (mKP-I) ground state as $c \to \mathfrak{c}_s$.

In [20], we have studied the travelling waves in dimension one for a general nonlinearity, in particular some f's for which Γ vanishes. We have put forward some behaviours that are rather different from what is obtained for the standard Gross-Pitaevskii nonlinearity, despite the fact that the nonlinearity f and the potential V have qualitatively the same shape. The purpose of this paper is to study the travelling waves for (NLS) with the nonlinearities considered in [20].

1.4 Variational properties

The PDE (TW_c) has a variational structure: the solutions are the critical points of the action functional

$$\mathcal{F}_c(u) \stackrel{\text{def}}{=} E(u) - cP(u)$$

on a suitable energy space $\mathcal{X}$ that we shall not define here (see [44], [23]). It is well-known that the solution to an elliptic PDE such as (TW_c) (satisfying some decay properties at infinity) verifies virial (or Pohozaev) identities. These are obtained by taking the (real) scalar product of (TW_c) by $x_1 \partial_{x_1} u$ and $x_2 \partial_{x_2} u$ and performing various integration by parts (see [43]). In dimension 2, these identities are

$$\begin{cases} E(u) - cP(u) = 2 \displaystyle\int_{\mathbb{R}^2} |\partial_{x_2} u|^2 \, dx \\ \\ E(u) = 2 \displaystyle\int_{\mathbb{R}^2} |\partial_{x_1} u|^2 \, dx, \end{cases}$$

and we can combine them to give

$$cP(u) = 2 \int_{\mathbb{R}^2} V(|u|^2) \, dx = \int_{\mathbb{R}^2} |\partial_{x_1} u|^2 - |\partial_{x_2} u|^2 \, dx. \tag{14}$$

We shall check (as in [33] and [45]) that the numerical solutions we obtain verify these two identities up to a reasonable error.

From the computations in [33], it is natural to believe that the travelling wave is a smooth function of the speed c, although no mathematical proof of this fact has been given. Furthermore, the travelling waves are known to verify the standard Hamilton group relation (see *e.g.* [33])

$$c_* = \frac{\partial E}{\partial P}_{|c=c_*},$$

where the derivative is taken along this (local) branch or, more precisely,

$$\frac{dE}{dc}_{|c=c_*} = c_* \frac{dP}{dc}_{|c=c_*}. \tag{15}$$

Given a smooth family of travelling waves $c \mapsto U_c$, this relation is formally shown by taking the (real) scalar product of (TW_c) with $\dfrac{dU_c}{dc}$ and integrating by parts, assuming good decay properties at infinity. On the (E, P) diagrams in figure 1, this means that the speed c is the slope of the curve $P \mapsto E$. In dimension one, the smooth dependence of U_c on c is easy to show and the Hamilton group relation (15) holds true (see [20]), provided we suitably define the momentum. Indeed, in one space dimension, the travelling waves have different phases at $+\infty$ and $-\infty$ and the phase shift enters in the definition of the momentum (see for instance [39]).

The dynamical stability of the travelling waves of (NLS) is related to the sign of $\dfrac{dP}{dc}$, computed on the local branch. Here is a precise statement in one space dimension.

Theorem 1 ([41], [21]) *Let us consider the* (NLS) *equation in dimension one and* $0 < c_* < \mathfrak{c}_s$. *If* u_{c_*} *is a finite energy travelling wave with speed* c_*, *then* u_{c_*} *belongs to a (unique) local branch of travelling waves* $c \mapsto u_c$ *for* c *near* c_*.
(i) If $\dfrac{dP(u_c)}{dc}_{|c=c_*} < 0$, *then* u_{c_*} *is orbitally stable in the energy space. Moreover,* u_{c_*} *is a local minimizer of the energy* E *at fixed momentum* P.
(ii) If $\dfrac{dP(u_c)}{dc}_{|c=c_*} > 0$, *then* u_{c_*} *is linearly and nonlinearly unstable in the energy space. Moreover,* u_{c_*} *does not minimizes (locally) the energy* E *at fixed momentum* P.

In view of the Hamilton group relation (15) (which holds true in dimension one), we have

$$\frac{d^2E}{dP^2}_{|c=c_*} = \frac{dc}{dP}_{|c=c_*},$$

so that the stability criterion $\dfrac{dP}{dc} < 0$ precisely means that the (local) function $P \mapsto E$ is concave, and that we have instability when the (local) function $P \mapsto E$ is convex. This type of stability criterion appears also in [52] in the study of positive bound state solutions to a Nonlinear Schrödinger equation (see also [3] for related results). A general mathematical framework, which is not restricted to the one dimensional case, for the analysis of stability has been given within the Grillakis-Shatah-Strauss theory [31], and relies on suitable spectral assumptions. Part of the argument in [41] (see also [21]) is to verify the spectral assumptions required in [31].

In the three dimensional setting, a similar statement to Theorem 1 holds true in a space[1] slightly smaller than the energy space and provided that we have a $\mathcal{C}^1$ curve of solutions $c \mapsto u_c$ and the following spectral assumption

($\mathcal{A}$) *the spectrum of the hessian of the action $\mathcal{F}_c$ is of the form $\{\lambda\} \cup \{0\} \cup I_+$, where $\lambda < 0$ is simple, 0 has multiplicity three (the space dimension), and I_+ is closed and $\subset (0, +\infty)$*

is verified. This statement follows from a direct application of [31] combined with the study of the Cauchy problem in [15] (Appendix A). We are not aware of any rigorous verification of the spectral assumption ($\mathcal{A}$) in dimension different from one.

Concerning the two dimensional situation, in addition to the verification of the spectral assumption ($\mathcal{A}$), there is another obstacle that prevents us from using so directly the result in [31]. The mathematical difficulty is to find a suitable space[2] containing the travelling waves and where the Cauchy problem is locally well-posed. This is due to the slow decay of the travelling waves $\int_{\mathbb{R}^2} |u-1|^2 \, dx = +\infty$ (see the algebraic decay in [33] and the rigorous justification in [30]).

Nevertheless, we shall adopt the sign of $\dfrac{dP}{dc}$ as a good criterion for stability, even though it does not rely on a rigorous mathematical proof. Consequently, in view of the diagrams in figure 1, for the Gross-Pitaevskii nonlinearity ($f(\varrho) = 1 - \varrho$), we expect all the travelling wave solutions to be stable in dimension two and, in dimension three, to be stable only for speeds $0 < c < c_{\rm cusp}$ corresponding to the cusp, that is for the lower part of the diagram. In dimension three (*cf.* figure 1 (b)), the upper part of the curve is not expected to be such a local minimum, and not expected to be stable (see [11], [8]).

Another natural way to obtain at least some of the solutions is to minimize the energy under the constraint that the momentum is fixed, that is to consider, for $\mathfrak{p} > 0$,

$$\mathbb{E}_{\rm min}(\mathfrak{p}) \stackrel{\rm def}{=} \inf \Big\{ E(u), u \in \mathcal{X}, P(u) = \mathfrak{p} \Big\}.$$

Since both E and P are invariant by the Schrödinger flow, it is natural to think that any minimizer for this problem is orbitally stable. This idea originates in the work of J. Boussinesq [16] and was rigorously justified by T. Benjamin [5] for the stability of the (KdV) solitary wave. For a general approach in this direction, see [18]. This result does not rely on spectral assumptions as in [31] but is suitable for stability only. The link between the two approaches is the minimization property of E at fixed P, locally or globally. Since we expect that when $\dfrac{d^2E}{dP^2}_{|c=c_*} = \dfrac{dc}{dP}_{|c=c_*} < 0$, the travelling wave is a local minimizer of E for fixed P, it is natural to hope that on the one hand, the solution to this constraint minimization (if they exist) are orbitally stable, and that on the other hand, the function $\mathbb{E}_{\rm min}$ is concave. The properties of the function $\mathbb{E}_{\rm min}$ are summarized in the following proposition, where (16) has to be related with the Hamilton group relation (15).

Proposition 1 ([13], [23]) *We assume that the potential function V is nonnegative.*
(i) The function $\mathbb{E}_{\rm min}$ is concave and increasing. In particular, $\mathbb{E}_{\rm min}$ has a derivative for all $\mathfrak{p}$ except possibly for an at most countable set.

[1] which is actually $1 + H^1(\mathbb{R}^3, \mathbb{C})$
[2] like $1 + H^1(\mathbb{R}^2, \mathbb{C})$

(ii) If $\mathfrak{p}_* > 0$ is such that $\mathbb{E}_{\min}$ has a derivative at $\mathfrak{p}_*$ and $\mathbb{E}_{\min}(\mathfrak{p}_*)$ has a minimizer u_*, then u_* solves (TW_{c_*}) *where the speed c_* is the Lagrange multiplier given by*

$$c_* = \frac{d\mathbb{E}_{\min}}{d\mathfrak{p}}(\mathfrak{p}_*). \tag{16}$$

Existence of at least one minimizer to the problem $\mathbb{E}_{\min}(\mathfrak{p})$, and thus of a solution to (TW_c), have been proved for the (GP) nonlinearity (see [13]) for any $\mathfrak{p} > 0$ in space dimension two. In the case of a general nonlinearity such that the potential function is nonnegative (*i.e.* $V \geq 0$), we have shown in [23] that $\mathbb{E}_{\min}(\mathfrak{p})$ is indeed acheived for any $\mathfrak{p} > 0$ if $\Gamma \neq 0$ but if $\Gamma = 0$, there exists $\mathfrak{p}_0 > 0$ such that $\mathbb{E}_{\min}(\mathfrak{p})$ is acheived only for $\mathfrak{p} \geq \mathfrak{p}_0$ (the space dimension is still equal to two). For the two dimensional (GP) equation, we expect to obtain all the travelling waves in the (E, P) diagram (figure 1 (a)) through the constraint minimization $\mathbb{E}_{\min}(\mathfrak{p})$ for $\mathfrak{p} \in (0, +\infty)$. However, in dimension three (figure 1 (b)), this is no longer the case since $\mathbb{E}_{\min}(\mathfrak{p})$ is not acheived for small $\mathfrak{p}$. Therefore, if $\Gamma = 0$, we are in a situation somehow similar to the three dimensional case for (GP), the value $\mathfrak{p}_0$ being the abscissa of the intersection of the blue curve with the straight line $E = \mathfrak{c}_s P$ (see [13], [23]). In [23], we have shown that the solutions we obtain from the constraint minimization $\mathbb{E}_{\min}(\mathfrak{p})$ are indeed orbitally stable. In particular, the constraint minimization $\mathbb{E}_{\min}(\mathfrak{p})$ does not provide the orbitally unstable travelling waves corresponding to the convex part of the (E, P) diagram in figure 1 (b), since then $\dfrac{dP}{dc} > 0$. The travelling waves associated with the concave part of the (E, P) diagram in figure 1 (b) but located above the straight line $E = \mathfrak{c}_s P$ (that is when $\dfrac{dP}{dc} < 0$ but $\mathfrak{p} < \mathfrak{p}_0$) are orbitally stable but are not (*cf.* [13], [23]) *global* minimizers for $\mathbb{E}_{\min}(\mathfrak{p})$: they are instead *local* minimizers.

We are also interested in considering cases where the potentiel V achieves negative values, as it is the case for the cubic-quintic nonlinearity. This situation has been considered in [23], and another minimization problem has been proposed, namely to impose the constraint that the kinetic energy $E_{\mathrm{kin}}(u) = \int_{\mathbb{R}^2} |\nabla u|^2 \, dx$ is fixed and perform the minimization of $E(u) - c_0 P(u)$, or equivalently $G^{c_0}(u) \stackrel{\mathrm{def}}{=} E_{\mathrm{pot}}(u) - c_0 P(u)$. More precisely, for $k \in \mathbb{R}_+$, we consider

$$\mathbb{G}^{c_0}_{\min}(k) \stackrel{\mathrm{def}}{=} \inf \Big\{ G^{c_0}(u) = E_{\mathrm{pot}}(u) - c_0 P(u), \ u \in \mathcal{X}, \ E_{\mathrm{kin}}(u) = k \Big\}.$$

Similarly to Proposition 1, we have the following properties of the function $\mathbb{G}^{c_0}_{\min}$, which do not require the potential to be nonnegative. Statement *(iii)* below shows that the minimization problem $\mathbb{G}^{c_0}_{\min}$ contains the minimization problem $\mathbb{E}_{\min}$.

Proposition 2 ([23]) *(i) The function $\mathbb{G}^{c_0}_{\min}$ is concave, negative and decreasing. In particular, $\mathbb{G}^{c_0}_{\min}$ has a derivative for all k except possibly for an at most countable set.*
(ii) If $k_* > 0$ is such that $\mathbb{G}^{c_0}_{\min}$ has a derivative at k_* and $\mathbb{G}^{c_0}_{\min}(k_*)$ has a minimizer u_*, then the rescaled function $\tilde{u}_* \stackrel{\mathrm{def}}{=} u_*(\frac{c_0}{c_*}\cdot)$ solves (TW_{c_*}) *where the speed $c_* > 0$ is given by*

$$\frac{d\mathbb{G}^{c_0}_{\min}}{dk}(k_*) = -\frac{c_0^2}{c_*^2}. \tag{17}$$

(iii) Let $\mathfrak{p}_* > 0$ be given and assume that the potential function V is nonnegative. If u_* is a minimizer for $\mathbb{E}_{\min}(\mathfrak{p}_*)$ and if $\mathbb{E}_{\min}$ has a derivative at $\mathfrak{p}_*$, then $\hat{u}_* = u_*(\frac{c_*}{c_0}\cdot)$ is a minimizer for $\mathbb{G}^{c_0}_{\min}(E_{\mathrm{kin}}(u_*))$, where $c_* \stackrel{\mathrm{def}}{=} \dfrac{d\mathbb{E}_{\min}}{d\mathfrak{p}}(\mathfrak{p}_*)$.

Remark 1 At first glance, the parameter c_0 seems to introduce an additional indeterminacy in the problem. However, by a simple scaling argument, the minimization properties of G^{c_0} are easily derived from those of G^1. The latter, G^1, is the functional studied in [23]. The freedom in choosing $c_0 \neq 1$ reveals its interest during numerical simulations: we will choose c_0 as close as possible to c_* so that the afore mentioned scaling parameter c_0/c_* is close to one.

1.5 Relaxed functionals

We were motivated by finding a numerical strategy for computing the travelling waves that preserves the variational strucure of the problem (TW_c). We thus looked for methods based on minimization arguments.

In the (E, P) diagrams given in figure 1, some of the solutions are minimizers, or even local minimizers, for the problem $\mathbb{E}_{\min}(\mathfrak{p})$. Therefore, it is natural to believe that these solutions are saddle points of the action functional $\mathcal{F}_c$. However, finding numerically a saddle point of a functional is not so easy. In [45] and [3], respectively, the functionals

$$\mathcal{L}_{PS}(u, \mu) \stackrel{\text{def}}{=} E(u) + \frac{1}{2}\Big(\mu - P(u)\Big)^2,$$

where $\mu \in \mathbb{R}$ is some parameter, and

$$\mathcal{L}_B(u, U_*) \stackrel{\text{def}}{=} E(u) + \frac{M}{2}\Big(P(u) - P(U_*)\Big)^2,$$

where U_* is a travelling wave and $M > 0$ is given, have been introduced. In [45], this was for finding travelling waves to a two dimensional Landau-Lifshitz equation, whereas in [3], this was for the stability analysis of one dimensional travelling wave in the cubic-quintic (NLS), and in both cases "P" is the momentum. This type of functional can be seen as a kind of relaxation of $\mathcal{F}_c$, the parameter μ for the functional $\mathcal{L}_{PS}$ being here to have some control on the momentum P. The interest for these functionals is that in some cases, a saddle point U_* for $\mathcal{F}_c$ is translated to a local minimizer for $\mathcal{L}_B(\cdot, \mu)$, for some particular $\mu = \mu(U_*)$, or for $\mathcal{L}_B(\cdot, U_*)$. This allows to use heat flow techniques in order to capture numerically these local minima. The condition for the saddle point U_* to become a local minimum for $\mathcal{L}_B(\cdot, U_*)$ has been given in [3]: it suffices to assume

$$\frac{dP}{dc} < 0 \qquad \text{and} \qquad M > -\frac{1}{\frac{dP}{dc}}. \tag{18}$$

This means that only orbitally stable travelling waves can be obtained in this way. In dimension one (or more generally under spectral assumptions similar to those in [31]), a rigorous proof to the fact that a travelling wave U_* is a local minimizer of $\mathcal{L}_B(\cdot, U_*)$, provided (18) is satisfied, is given in [21] in a general framework. Actually, the functional $\mathcal{L}_B(\cdot, U_*)$ becomes a Lyapounov functional for proving orbital stability (see [21]). In [45], no such sufficient condition has been given to ensure that the functional $\mathcal{L}_{PS}$ does have a local minimum. Moreover, we see from (18) that the constant M plays a role in the functional $\mathcal{L}_B$ whereas it has been fixed to 1 for $\mathcal{L}_{PS}$, so that we do not expect to capture with $\mathcal{L}_{PS}$ travelling waves with $\dfrac{dP}{dc} > -1$. Since U_* is clearly not known, functionals of the type of $\mathcal{L}_{PS}$ seem more adapted to our problem. Therefore, we have chosen to define, for some parameters $\mu \in \mathbb{R}$, $P_0 \in \mathbb{R}$ and $E_0 \in \mathbb{R}$, the following functional:

$$\mathcal{L}(u, \mu) \stackrel{\text{def}}{=} E(u) + \frac{E_0}{2P_0^2}\left(\mu - P(u)\right)^2.$$

The constant $\dfrac{E_0}{P_0^2}$ plays the same role as M for the functional $\mathcal{L}_B$; we have written it under this form in order to emphasize on its homogeneity.

Let us then consider the minimization problem

$$\mathfrak{L}_{\min}(\mu) \stackrel{\text{def}}{=} \inf\Big\{\mathcal{L}(u,\mu), u \in \mathcal{X}\Big\}.$$

We may also consider the problem of finding not a global minimizer but a local minimizer, with an obvious meaning. The properties of the functional $\mathfrak{L}_{\min}$ are given in the following proposition (see section 4.1 for the proof), where we stress the link between the problems $\mathbb{E}_{\min}(\mathfrak{p})$ and $\mathfrak{L}_{\min}(\mu)$.

Proposition 3 *Let E_0, P_0, μ_* and $\mathfrak{p}_*$ be four positive constants.*
(i) If $u_* \in \mathcal{X}$ is a minimizer for the problem $\mathfrak{L}_{\min}(\mu_*)$, then u_* is a solution of (TW_{c_*}) with $c_* = c_*(u_*,\mu_*) \stackrel{\text{def}}{=} \dfrac{E_0}{P_0}\left(\mu_* - \dfrac{P(u_*)}{P_0}\right)$. Moreover, u_* is a minimizer for the problem $\mathbb{E}_{\min}(P(u_*))$.
(ii) Assume that $\mathbb{E}_{\min}$ has a second order derivative at $\mathfrak{p}_*$. If $u_* \in \mathcal{X}$ is a minimizer for the problem $\mathbb{E}_{\min}(\mathfrak{p}_*)$, then u_* is a solution of (TW_{c_*}) with $c_* = \dfrac{d\mathbb{E}_{\min}}{d\mathfrak{p}}(\mathfrak{p}_*)$. Furthermore, if the constant $\dfrac{E_0}{P_0^2}$ verifies

$$\frac{E_0}{P_0^2} > -\frac{d^2\mathbb{E}_{\min}}{d\mathfrak{p}^2}(\mathfrak{p}_*)$$

then u_* is a local minimizer for the problem $\mathfrak{L}_{\min}(\mu_*)$ with $\mu_* = \mathfrak{p}_* + c_*\dfrac{P_0^2}{E_0}$.

Remark 2 A similar statement holds for local minimizers instead of global minimizers.

The advantage of working with the relaxed functionals is to transform the minimization under constraint into a minimization *without* constraint, which is of great interest numerically. In particular, heat flow techniques (as in [45]) can be applied. However, we do not have a direct control on the quantities of interest: energy, momentum, speed, but only on the parameter μ. Let us remark that minimizing $\mathfrak{L}_{\min}(\mu_*)$ (or even locally minimizing) captures only minima (or local minima) of the energy under the constraint of fixed momentum, which is a strong indication of stability for the Schrödinger flow. In three dimensions (*cf.* figure 1 (b)), the upper part of the curve is not expected to be such a local minimum, and not expected to be stable (see [11], [8]).

Concerning the other constraint minimization, namely $\mathbb{G}_{\min}^{c_0}$, we may also propose a relaxation by considering

$$\mathcal{I}(u,\kappa) \stackrel{\text{def}}{=} E_{\text{pot}}(u) - c_0 P(u) + \frac{1}{2E_0}\Big(E_{\text{kin}}(u) - \kappa\Big)^2$$

and finally consider the minimization problem

$$\mathfrak{I}_{\min}(\kappa) \stackrel{\text{def}}{=} \inf\Big\{\mathcal{I}(u,\kappa), u \in \mathcal{X}\Big\}.$$

Similarly to Proposition 3, the function $\mathfrak{I}_{\min}$ enjoys the following properties (the proof is given in section 4.2).

Proposition 4 *Let E_0, c_0, κ_* and $\mathfrak{K}_*$ be four positive constants.*
(i) If $u_* \in \mathcal{X}$ is a minimizer for the problem $\mathfrak{I}_{\min}(\kappa_*)$, then u_* is a minimizer for the problem $\mathbb{G}^{c_0}_{\min}(E_{\rm kin}(u_*))$. Moreover, $\tilde{u}_* = u_*(\frac{c_0}{c_*}\cdot)$ is a solution of (TW_{c_*}) with $c_* \stackrel{\rm def}{=} c_0\sqrt{\frac{E_0}{\kappa_* - E_{\rm kin}(u_*)}}$.
(ii) Assume that $\mathbb{G}^{c_0}_{\min}$ has a second order derivative at $\mathfrak{K}_*$. If $u_* \in \mathcal{X}$ is a minimizer for the problem $\mathbb{G}^{c_0}_{\min}(\mathfrak{K}_*)$, then the rescaled function $\tilde{u}_* \stackrel{\rm def}{=} u_*(\frac{c_0}{c_*}\cdot)$ solves (TW_{c_*}) with $c_* = \sqrt{-\frac{c_0^2}{\frac{d\mathbb{G}^{c_0}_{\min}}{dk}(\mathfrak{K}_*)}}$.
Furthermore, if the constant E_0 verifies

$$\frac{d^2\mathbb{G}^{c_0}_{\min}}{dk^2}(\mathfrak{K}_*) + \frac{1}{E_0} > 0.$$

then u_* is a local minimizer for the problem $\mathfrak{I}_{\min}(\kappa_*)$ with $\kappa_* = \mathfrak{K}_* - \frac{c_0^2}{c_*^2}E_0$.

Remark 3 Here again, a similar statement holds for local minimizers instead of global minimizers.

Stability and function $\mathbb{G}^{c_0}_{\min}$. In [23], we have shown that every minimizer for $\mathbb{E}_{\min}$ is also a minimizer for $\mathbb{G}^{c_0}_{\min}(k)$ (see Proposition 2 (*iii*)). Moreover, we also know from [23] that every minimizer for $\mathbb{E}_{\min}$ is also an orbitally stable solution to (NLS). Therefore, it is natural to try to give a criterion relative to the function $\mathbb{G}^{c_0}_{\min}$ for the orbital stability of the solution, that is the sign of $\frac{dP}{dc}$. The proof of the following Proposition is provided in section 4.3.

Proposition 5 *We make the assumptions of Proposition 4. Assume moreover that $\mathbb{G}^{c_0}_{\min}$ has a second order derivative at $\mathfrak{K}_*$. If $u_* \in \mathcal{X}$ is a minimizer for the problem $\mathbb{G}^{c_0}_{\min}(\mathfrak{K}_*)$, then*

$$sgn\Big(\frac{dP}{dc}(\tilde{u}_*)\Big) = sgn\left(\mathbb{G}^{c_0}_{\min}(\mathfrak{K}_*)\frac{d^2\mathbb{G}^{c_0}_{\min}}{dk^2}(\mathfrak{K}_*) - 2\left(\frac{d\mathbb{G}^{c_0}_{\min}}{dk}(\mathfrak{K}_*)\right)^2\right). \tag{19}$$

where $\tilde{u}_* = u_*(\frac{c_0}{c_*}\cdot)$.

We recall (*cf.* Proposition 2) that the function $\mathbb{G}^{c_0}_{\min}$ is concave, negative and decreasing, hence $\frac{dP}{dc}(\tilde{u}_*)$ changes sign when

$$\frac{d^2\mathbb{G}^{c_0}_{\min}}{dk^2}(\mathfrak{K}_*) = 2\frac{\left(\frac{d\mathbb{G}^{c_0}_{\min}}{dk}(\mathfrak{K}_*)\right)^2}{\mathbb{G}^{c_0}_{\min}(\mathfrak{K}_*)},$$

which is a negative value. This means that $\mathbb{G}^{c_0}_{\min}$ remains strictly concave when $\frac{dP}{dc}(\tilde{u}_*)$ changes sign, and this is in agreement with the fact that the minimization problem $\mathbb{G}^{c_0}_{\min}$ contains the minimization problem $\mathbb{E}_{\min}$.

2 Numerical methods

We have worked combining two approaches: finding (local) minimizers to functionals associated with the variational structure of the problem and continuation with respect to the speed c.

2.1 Discretization framework

Symmetries. Following [33], [45], we look for solutions that respect two symmetries of the problem: u is thus assumed to satisfy

$$u(x) = u(x_1, x_2) = u(x_1, -x_2) = \bar{u}(-x_1, x_2). \tag{20}$$

This allows us to work on the domain $\mathbb{R}_+ \times \mathbb{R}_+$ instead of $\mathbb{R}^2$. *Domain mapping.* We then map this domain onto the square $(\hat{x}_1, \hat{x}_2) \in [0, \pi/2]^2$ using the stretched variables

$$R_1 x_1 = \tan(\hat{x}_1), \qquad R_2 x_2 = \tan(\hat{x}_2),$$

where R_1 and $R_2 > 0$ are adapted to the lengthscales of the solution we are interested in. This mapping avoids to work on a bounded computational domain and thus to consider artificial type of boundary conditions. But this comes at the price of two arbitrary constants, R_1 and R_2, that have to be fixed along the computation.

The continuous problem is then expressed and solved numerically in this set of streched variables. Indeed, we write (TW_c) in these variables using the formulas for $h(x) = \hat{h}(\hat{x})$, $\hat{x} = \arctan(Rx)$, for $R > 0$, and

$$\frac{\partial h}{\partial x} = R\cos^2(\hat{x})\frac{\partial \hat{h}}{\partial \hat{x}} \qquad \text{and} \qquad \frac{\partial^2 h}{\partial x^2} = R^2\Big(\cos^4(\hat{x})\frac{\partial^2 \hat{h}}{\partial \hat{x}^2} - 2\sin(\hat{x})\cos^3(\hat{x})\frac{\partial \hat{h}}{\partial \hat{x}}\Big).$$

Discretization. We discretize the computational domain, the square $[0, \pi/2]^2$, by a cartesian grid, with $N_{\hat{x}_1}$ points in the direction $\hat{x}_1$ and $N_{\hat{x}_2}$ points in the direction $\hat{x}_2$. We choose to work here with a uniform dicretization with $N := N_{\hat{x}_1} = N_{\hat{x}_2}$. The size of the mesh is denoted by h; here $h = \dfrac{\pi}{2N}$.
We choose to work in the Finite Difference framework, using central approximations of derivatives. These approximations are of order 2.
Numerical computation of energies and momentum. We are interested in the energy-momentum diagrams. These quantities are integral quantities that have to be approximated. They will be computed numerically simply using a trapezoidal rule for the integral.

2.2 Minimization of the relaxed functionals

2.2.1 Heat flow technique

We would like to solve the minimization problems like $\mathfrak{L}_{\min}(\mu)$ for $\mu > 0$ given. Solving this problem leads to solve the equation

$$\Delta u + uf(|u|^2) - i(\mu - P(u))\partial_{x_1} u = 0.$$

Due to the variational structure of this equation and since we look for a (local) minimizer, we choose to use heat flow techniques. In other words, we start with an initial condition and let it evolve along the heat flow

$$\frac{\partial u}{\partial t} = \Delta u + uf(|u|^2) - i(\mu - P(u))\partial_{x_1} u.$$

As already described, this equation is recast in the streched variables setting. Then the spatial part is discretized using second-order Finite Difference scheme. The Ordinary Differential Equation in time resulting from this spatial discretization is solved by a classical explicit Euler scheme, with time step δt. Due to the explicit nature of the scheme, we have to face a CFL type condition that ensures the stability of the scheme. In the sequel, we will choose the time step small enough in order to be numerically stable.

Remark 4 To enhance the reading, we choose to present equations here in the real variables, instead of the streched ones; the exact expressions of discrete equations and discrete operators will thus not be detailed here. We will rather implicitely assume that the change of variable has been performed before discretizing and present the result in the real variables.

The scheme writes

$$u_h^{n+1} = u_h^n + \delta t\Big(\Delta^h u_h^n + u_h^n f(|u_h^n|^2) - i(\mu_* - P_h(u_h^n))\partial_{x_1}^h u_h^n\Big),\ n \in \mathbb{N}^* \tag{21}$$

$$u_0 = u_h^0 \tag{22}$$

with Δ^h and $\partial_{x_1}^h$ respectively the discrete finite difference operators associated to Δ and ∂_{x_1}. Same notation holds for P_h, approximate moment for P. u_h^n stands for the approximation at fictive time $t_n := n\delta t$. The choice of the initialization (22) will be detailed in next paragraph and next subsection. The numerical scheme is stopped when the convergence criterion

$$\eta := \frac{\left\|\Delta u_h^n + u_h^n f(|u_h^n|^2) - i(\mu_* - P_h(u_h^n))\partial_{x_1}^h u_h^n\right\|_{L^\infty(\mathbb{R}^2)}}{\left\|(\mu_* - P_h(u_h^n))\partial_{x_1} u_h^n\right\|_{L^\infty(\mathbb{R}^2)}} \leq tol$$

is verified.

Remark 5 In what follows $tol = 4.10^{-4}$ will in general be sufficient to have an accurate solution. This tolerance can be made smaller to adapt to each situation if necessary.

Numerical strategy. We compute numerically continuous branches of solutions proceeding as follows (see Fig. 4).
For $c \simeq 0$ for instance, say $c = 0.2$, we expect vortices for the travelling waves: we can get an approximate solution u_0 by using Padé approximants for a single vortex (see subsection 2.3.1 below); the momentum is then large and we expect $\mathbb{E}_{\min} \approx 4\pi \ln \mathfrak{p}$ (*cf.* [33], [15]), hence $\dfrac{d^2\mathbb{E}_{\min}}{d\mathfrak{p}^2} \approx -\dfrac{4\pi}{\mathfrak{p}}$, which allows us to choose the constant $\dfrac{E_0}{P_0^2}$ in order to have $\dfrac{E_0}{P_0^2} > -\dfrac{d^2\mathbb{E}_{\min}}{d\mathfrak{p}^2} \approx \dfrac{4\pi}{\mathfrak{p}}$ (see Proposition 3); we then fix the value of μ as $\mu = P(u_0) + c\dfrac{P_0^2}{E_0}$ (see Proposition 3) (with $c = 0.2$); we then use the iterations (21) until numerical convergence. We then iterate in μ ($\mu \leftarrow \mu + \delta\mu$) and start the iterations (21) from the previously computed solution. The same procedure can be employed starting from $c \simeq \mathfrak{c}_s$, provided we have a good approximation of the (KP-I) or (mKP-I) solitary wave. The way we obtain Padé approximants or a numerical approximation of the (KP-I) solitary wave is given in subsections 2.3.1 and 2.3.2.

The accuracy of the scheme is also tested by evaluating the Pohozaev or virial identities, as in [33], [45]. For the solutions we have obtained, the relations (14) are verified up to 2%.

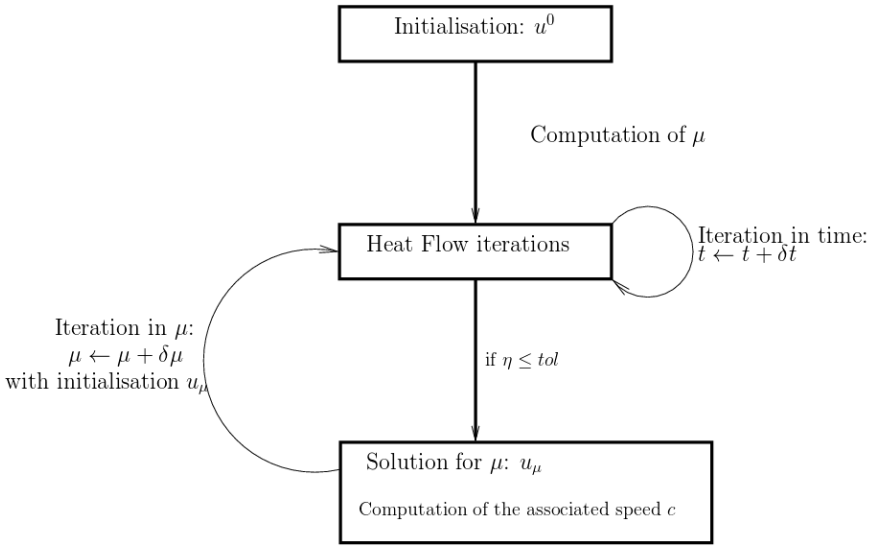

Figure 4: Description of the iterative procedure to compute a minimum of the relaxed functional

2.3 Choices for the initialization

To initiate our algorithm, we may choose to begin either from $c \approx 0$ or from $c \approx \mathfrak{c}_s$ (or both), depending on the nonlinearity and the theoretical knowledge we have for these two respective asymptotic behaviours.

2.3.1 Padé approximants for the vortices

We determine a Padé approximant of the profile $\mathfrak{a}$ of the vortex following the strategy of [9]. We look for an approximate solution $\mathfrak{a}_{\text{Padé}}$ of (3) with $d = 1$ under the form

$$\mathfrak{a}_{\text{Padé}}(r) \stackrel{\text{def}}{=} r\sqrt{\frac{\alpha_1 + \alpha_2 r^2}{1 + \beta_1 r^2 + \beta_2 r^4}},$$

for some coefficients α_1, α_2, α_3, β_1, β_2 to be determined, and where we choose $\beta_2 = \alpha_2$ in order to have $\mathfrak{a}_{\text{Padé}}(+\infty) = 1$. The coefficients α_1, α_2, α_3, β_1 are determined as in [9]: we plug this form of $\mathfrak{a}_{\text{Padé}}$ into (3), perform a Taylor expansion near the origin of the left hand side of (3) up to $\mathcal{O}(r^7)$ (the expansion is odd). By cancelling the coefficients of r, r^3 and r^5, we may eliminate α_2, then β_1, and finally solve numerically the remaining equation on α_1. It turns out that there may exist several solutions, but we find one and only one which provides a function increasing from 0 to 1. The corresponding Padé approximant is given for each nonlinearity we study. In view of (4), we may use this Padé approximant of a single vortex to construct the approximate solution

$$\mathfrak{a}_{\text{Padé}}(|(x_1, x_2 - c^{-1})|)\frac{x_1 + i(x_2 - c^{-1})}{|(x_1, x_2 - c^{-1})|} \times \mathfrak{a}_{\text{Padé}}(|(x_1, x_2 + c^{-1})|)\frac{x_1 - i(x_2 + c^{-1})}{|(x_1, x_2 + c^{-1})|}.$$

We obtain in this way a good numerical error for speeds c typically ≤ 0.2, and this approximate solution is a good initial point for starting heat flows.

2.3.2 Ground state solutions for the (KP-I) and (mKP-I) equations

As already seen, the travelling waves for (NLS) are expected to be close, after rescaling, to a travelling wave of the (KP-I) equation, and more precisely a ground state. For the standard quadratic (KP-I) equation, the ground state is expected to be the well-known lump solitary wave (see [42])

$$\mathcal{W}(z) \stackrel{\text{def}}{=} -24\frac{3-z_1^2+z_2^2}{(3+z_1^2+z_2^2)^2} = -24\partial_{z_1}\Big(\frac{z_1}{3+z_1^2+z_2^2}\Big) = \partial_{z_1}\phi,$$

which solves the adimensionalized version of (SW)

$$\partial_{z_1}\mathcal{W} - \partial_{z_1}^3\mathcal{W} + \mathcal{W}\partial_{z_1}\mathcal{W} + \partial_{z_2}^2\partial_{z_1}^{-1}\mathcal{W} = 0.$$

To our knowledge, no mathematical proof of the fact that $\mathcal{W}$ is indeed a (or the) ground state of (KP-I) has been given. Using the scaling properties of the (KP-I) equation, we then see that

$$A(z) \stackrel{\text{def}}{=} \frac{1}{\mathfrak{c}_s^2\Gamma}\mathcal{W}\Big(z_1, \frac{z_2}{\mathfrak{c}_s}\Big)$$

solves (SW):

$$\frac{1}{\mathfrak{c}_s^2}\,\partial_{z_1}A - \frac{1}{\mathfrak{c}_s^2}\,\partial_{z_1}^3 A + \Gamma A\partial_{z_1}A + \partial_{z_2}^2\partial_{z_1}^{-1}A = 0.$$

The (mKP-I) equation is however presumably not completely integrable, and hence no explicit solution is known. An efficient way to compute numerically "the" ground state of the focusing (mKP-I) is given by the Petviashvili iteration algorithm [47]. On the adimensionalized version of (SW') (where the constants have been set to 1 for simplicity)

$$\partial_{z_1}\mathcal{W}' - \partial_{z_1}^3\mathcal{W}' - (\mathcal{W}')^2\partial_{z_1}\mathcal{W}' + \partial_{z_2}^2\partial_{z_1}^{-1}\mathcal{W}' = 0,$$

this consists in performing the iterations

$$\mathcal{W}'_{n+1} = \sqrt{3}\Big[\frac{\int_{\mathbb{R}^2}(\mathcal{W}'_n)^2 + (\partial_{z_1}\mathcal{W}'_n)^2 + (\partial_{z_2}\partial_{z_1}^{-1}\mathcal{W}'_n)^2\ dz}{\int_{\mathbb{R}^2}(\mathcal{W}'_n)^4\ dz}\Big]^{3/2}\Big(1-\partial_{z_1}^2+\partial_{z_2}^2\partial_{z_1}^{-2}\Big)^{-1}({\mathcal{W}'_n}^3).$$

It turns out that, numerically, taking as starting point the lump of the quadratic (KP-I)

$$\mathcal{W}'_0(z) = \mathcal{W}(z) = -24\frac{3-z_1^2+z_2^2}{(3+z_1^2+z_2^2)^2},$$

we obtain convergence. For a justification of convergence when one starts close to the ground state of the (mKP-I), see [46]. A natural way to implement this algorithm is to work in Fourier space and use the FFT algorithm. However, for our problem, we shall use this numerical solution in a finite differences scheme. Moreover, we have imposed the symmetry (20), which is not completely satisfied when using the FFT algorithm. Finally, we shall need to compute $\partial_{z_1}^{-1}\mathcal{W}'$, which needs an extra computation requiring the exact cancelation of some Fourier coefficients of $\mathcal{W}'_n$. Therefore, we have implemented the Petviashvili iterations directly in terms of $\phi' \stackrel{\text{def}}{=} \partial_{z_1}^{-1}\mathcal{W}'$, that is

$$\phi'_{n+1} = \sqrt{3}\Big[\frac{\int_{\mathbb{R}^2}(\partial_{z_1}\phi'_n)^2 + (\partial_{z_1}^2\phi'_n)^2 + (\partial_{z_2}\phi'_n)^2\ dz}{\int_{\mathbb{R}^2}(\partial_{z_1}\phi'_n)^4\ dz}\Big]^{3/2}\Big(\partial_{z_1}^2 - \partial_{z_1}^4 + \partial_{z_2}^2\Big)^{-1}\partial_{z_1}\Big((\partial_{z_1}\phi'_n)^3\Big),$$

starting here again with the lump

$$\phi_0'(z) = \phi(z) = -\frac{24 z_1}{3 + z_1^2 + z_2^2}.$$

We do not use Fourier transform, but compute the inverse of the negative definite matrix associated to the discretization of the operator $\partial_{z_1}^2 - \partial_{z_1}^4 + \partial_{z_2}^2$. When $\Gamma' < 0$, we may obtain an approximation of the ground state of (SW') through the following scalings

$$A(z) \stackrel{\text{def}}{=} \pm \frac{1}{\sqrt{-\mathfrak{c}_s^2 \Gamma'}} \mathcal{W}'\Big(z_1, \frac{z_2}{\mathfrak{c}_s}\Big).$$

If $\Gamma' > 0$, the (KP-I) equation is defocusing and has no (nontrivial) solitary wave (see [27]). The typical graph of a rarefaction pulse is given in figure 2 (b).

2.4 Continuation with respect to the speed c

The variational method based on relaxed functionnal is very efficient and systematic. However, as discussed before, they suffer from not being able to capture the whole range of speed $c \in [0, \mathfrak{c}_s]$. Indeed, the gradient flow method converges (see Propositions 3 and 4) only in the regions where

- for the functional $\mathcal{L}$, $\dfrac{d^2E}{dP^2} < 0$, or $\dfrac{dP}{dc} < 0$, *i.e.* when the curve $P \mapsto E$ is concave.
- for the functional $\mathcal{I}$, $\dfrac{dE_{\text{kin}}}{dc} < 0$.

Thus, we are compelled to find another way to compute solutions in the remaining range of speeds. Inspired by [28], we choose to work with a continuation method for the speed c; we compute a solution for speed c then use it to compute the solution at speed $c + \delta c$. *Principle.* The equation (TW_c) writes:

$$\Delta u(c) + u(c) f(|u(c)|^2) = ic \partial_{x_1} u(c), \tag{23}$$

where we emphasize the dependency on c of the solution $u = u(c)$. When differentiating with respect to c, this formally gives:

$$\Upsilon_c \left(\frac{\partial u}{\partial c}(c) \right) = i \partial_{x_1} u(c) \tag{24}$$

where

$$\Upsilon_c(v) \stackrel{\text{def}}{=} \Delta v + 2u(c) \langle u(c), v \rangle f'(|u(c)|^2) + f(|u(c)|^2) v - ic \partial_{x_1} v \tag{25}$$

is the linearized operator. We view this as an ODE in c, provided we may invert Υ_c. It should be noticed that the travelling wave we compute are presumably non degenerate, that is the kernel of Υ_c is spanned only by $\partial_{x_1} u(c)$ and $\partial_{x_2} u(c)$. Since the problem (TW_c) is invariant by translation, it follows that $\partial_{x_1} u(c)$ and $\partial_{x_2} u(c)$ belong to the kernel of Υ_c, and assuming non degeneracy of $u(c)$ precisely means that we have no other element in $\ker(\Upsilon_c)$. On the other hand, we impose the symmetries (20) and may observe that if $u(c)$ verifies (20), then $\partial_{x_2} u(c)$ is odd in x_2 and $\partial_{x_1} u(c)$ verifies $\partial_{x_1} u(c)(x_1, x_2) = -\partial_{x_1} \bar{u}(c)(-x_1, x_2)$. Therefore, it is natural to believe that Υ_c becomes invertible when imposing the symmetries (20).

Discretization. Using finite differences setting, one can write the associated discrete operator Υ_h using centered approximations. In the iterative procedure, we initiate the algorithm with an initialization: an approximate solution at speed c_0. From a solution at speed c_k, $u_h(c_k)$, a solution at speed c_{k+1}, $u_h(c_{k+1})$, is computed in the following way:

(a) Computation of $\partial^h_{c_k} u$ with $\partial^h_{c_k} u = \Upsilon_h^{-1}\left(i\partial^h_{x_1} u_h(c_k)\right)$. Computing Υ_h^{-1} in the finite differences framework amounts to solve a linear system. We choose to use a qmr (quasi minimal residual) method to solve it. This step is, of course, the most expensive in computational time.

(b) Then update $u_h(c_{k+1})$ with equation (24) by using a classical ordinary differential equation scheme (*e.g.* Euler scheme, Centered scheme). In the case of Euler scheme, this leads to compute $u_h(c_{k+1})$ with the iteration scheme:

$$u_h(c_{k+1}) = u_h(c_k) + \delta c\, \partial^h_{c_k} u, \text{ with } \delta c > 0 \text{ the chosen step size.} \tag{26}$$

Remark 6 In the variational approach, we decide to stop the simulation for a given criterion $\eta < tol$. In the continuation method, solution at speed c is directly given by the numerical resolution of (24). We can not impose the value of η a priori, but we expect the usual error estimate for approximations of ODE depending on the method. Furthermore at each step, one has to solve a linear system (but only once), that in the transonic limit can be hard to solve (see the discussion in section 2.5).

Remark 7 We could also have chosen to use Newton's method that has the advantage to be very efficient (when it converges) with a control on the residual of the equation. However, Newton's method can require several iterations to converge (which in turn implies to solve the linear system several times) and can also fail to compute a solution especially in the transonic limit. Thus, even if we do not impose η directly with the continuation method, it allows, with a good initial residual (*i.e.* at the begining of the iteration procedure), to compute an accurate solution everywhere and especially in regions where Newton's method may fail to give one.

Discussion on the choice of R_1, R_2. Although the change of variable induced by the choice of R_1 and R_2 has virtually no influence on the continuous setting, the precision of the numerical computations can be however influenced by this choice. Indeed a uniform grid in the mapped domain (here $[0, \frac{\pi}{2}]\times[0, \frac{\pi}{2}]$) is transformed in a non-uniform one in the real domain (here $\mathbb{R}^+\times\mathbb{R}^+$). The mesh is dilated as we approach infinity, leading to bigger cells at infinity. If the solution does not present a significant variation at infinity (recall that $\psi \to 1$ as $\|(x_1, x_2)\| \to \infty$), this has not a big influence on the computation. This is the case for vortex solutions for example, where we can take typically $R_1 = R_2 = 0.2$. However, if this is not the case, one has to take a special care in the choice of R_1 and R_2 in order to keep a good accuracy. For instance, in some of the transonic limits that we consider in the sequel, we know the asymptotic behaviour ((KP-I) or (mKP-I)) and the space variations should be considered in the scaling $(\varepsilon x_1, \varepsilon^2 x_2)$, with $\varepsilon = \sqrt{\mathfrak{c}_s^2 - c^2}$, see section 1.3: the solution tends to spread out (more in the transverse direction x_2 than in the direction of propagation x_1). Choosing R_1 and R_2 respectively close to ε and ε^2 seems to be appropriate in these contexts. In practice, some typical values we had for the transonic limit are $(R_1 = 0.1, R_2 = 0.1)$, $(R_1 = 0.2, R_2 = 0.015)$. These values are rather different from the values for vortex solutions. More generally, R_1^{-1} and R_2^{-1} are typical lengthscales of variations for the travelling wave of interest, hence may vary with c. Thus we will have to adapt R_1 and R_2 along

the computations. Doing so with the variationnal strategy is not a problem, since one iterates the procedure until a convergence criterion is reached. However, if one brutally changes the values of R_1 and R_2 in the continuation procedure, this may result in a degradation of the residual. To solve this problem, we have chosen to extend the continuation strategy: one can similarly construct a continuation algorithm, by considering that R_1 and R_2 are themselves regularly depending on the speed c. The resulting equations are derived in the same manner than the simple continuation (they will not be detailed here) and the numerical resolution follows naturally the same ideas. In [33] and [45], the values of R_1 and R_2 are kept fixed during all the computations.

2.5 Discussion on the transonic limit

The transonic limit turns out to be quite difficult to capture numerically, and we shall give some explanations of this fact. We recall that the small parameter ε is defined through the relation $c(\varepsilon) = \sqrt{\mathfrak{c}_s^2 - \varepsilon^2}$ or $\mathfrak{c}_s^2 = c^2 + \varepsilon^2$.

The first observation is that when $c \to \mathfrak{c}_s$, using the long wave (KP-I) ansatz given by (5), we have, by straightforward computations

$$ic\partial_{x_1} u = \mathsf{e}^{i\varepsilon\phi}\Big(- \varepsilon^2 \mathfrak{c}_s \partial_{z_1}\phi\Big) + \mathcal{O}(\varepsilon^2)$$

and

$$\begin{aligned}\Delta u + uf(|u|^2) - ic\partial_{x_1} u &= \mathsf{e}^{i\varepsilon\phi}\Big(- \varepsilon^2 \mathfrak{c}_s \partial_{z_1}\phi + f((1+\varepsilon^2 A)^2)\Big) + i\varepsilon^3 \mathsf{e}^{i\varepsilon\phi}\Big(\partial_{z_1}^2\phi - \mathfrak{c}_s\partial_{z_1} A\Big) + \mathcal{O}(\varepsilon^4)\\ &= \varepsilon^2 \mathsf{e}^{i\varepsilon\phi}\Big(- \mathfrak{c}_s\partial_{z_1}\phi + \mathfrak{c}_s^2 A\Big) + i\varepsilon^3 \mathsf{e}^{i\varepsilon\phi}\Big(\partial_{z_1}^2\phi - \mathfrak{c}_s\partial_{z_1} A\Big) + \mathcal{O}(\varepsilon^4).\end{aligned}$$

Therefore, as soon as (A, ϕ) verifies the constraint (9), that is $\mathfrak{c}_s A = \partial_{z_1}\phi$, we have a good approximate solution:

$$\frac{\big\|\Delta u + uf(|u|^2) - ic\partial_{x_1} u\big\|_{L^\infty}}{\big\|ic\partial_{x_1} u\big\|_{L^\infty}} \approx \frac{\mathcal{O}(\varepsilon^4)}{\varepsilon^2} = \mathcal{O}(\varepsilon^2).$$

Clearly, this prevents us from computing a precise solution numerically, since the information leading to (SW) is hidden in the higher order terms. The same computations can be carried out with the ansatz (10) and, this time, the preparedness assumption (12) (and not only (7)).

On the other hand, for the continuation in speed c (see section 2.4), one needs to inverse the operator $\Upsilon_{c(\varepsilon)}$. As we shall see, this operator has a rather bad behaviour as $\varepsilon \to 0$. Since we know that the asymptotic behaviour of the solutions to $(\mathrm{TW}_{c(\varepsilon)})$ as $\varepsilon \to 0$ is approximated (through suitable rescalings) by the solitary waves to (KP-I) (or (mKP-I)), we may expect to infer a bound on the linearized operator $\Upsilon_{c(\varepsilon)}$ as $\varepsilon \to 0$ if we have some information on the spectrum of the linearization of (SW).

Proposition 6 *We assume that $\Gamma \neq 0$ and that a family of travelling waves $u_{c(\varepsilon)}$ of* (NLS) *converge to a solitary wave A of* (KP-I) *through the scaling* (5)*, that is $u_{c(\varepsilon)}(x) = (1+\varepsilon^2 A_\varepsilon(z))\mathsf{e}^{i\varepsilon\varphi_\varepsilon(z)}$ with $(z_1, z_2) = (\varepsilon x_1, \varepsilon^2 x_2)$ and $A_\varepsilon \to A$, $\partial_{z_1}\varphi_\varepsilon \to \mathfrak{c}_s A$ as $\varepsilon \to 0$. Then, the linearization of* $(\mathrm{TW}_{c(\varepsilon)})$ *around $u_{c(\varepsilon)}$ admits a negative eigenvalue $\sim \varepsilon^4 \lambda_{\mathrm{KP}}$ as $\varepsilon \to 0$, where λ_{KP} is the negative eigenvalue of the linearization of* (SW) *around A.*

Remark 8 In [11], a similar computation is made to relate the plausible unstable eigenvalue $\sigma_{\mathrm{KP}} \in \mathbb{R}_+^*$ of the linearized (KP-I) equation (for the time dependent problem) in three space dimension

to an unstable eigenvalue of the linearized (NLS) equation. This led the authors to the conjecture that this last unstable eigenvalue should behave like $\varepsilon^3\sigma_{\mathrm{KP}}$ for ε small. Note however that, to our knowledge, no rigorous proof has been given that the ground state of the three dimensional (KP-I) equation is linearly unstable.

We could envisage using Newton's method to compute the travelling waves solutions in the transonic limit. However, due to the rather bad behaviour of the linearized operator $\Upsilon_{c(\varepsilon)}$, Newton's algorithm does not converge in practice in this region if we start from the (KP-I) ansatz. Indeed, either ε is very small so that the linear system is very difficult to solve and the iterates diverge; either ε is not very small and then we are too far from the solution for Newton's algorithm to converge. Another difficulty is that we have two travelling wave solutions which are close: $u = 1$ that is always a trivial solution and the rarefaction pulse given by the (KP-I) ansatz that tends to 1 in L^∞ as $c \to \mathfrak{c}_s$. This is a further argument in favor of the use of both the variational and the continuation method. Indeed, contrary to Newton's method, the variational approach is able to compute solutions even if we start far from the solution and the continuation method is able to deal with the computation of the travelling waves close to the speed of sound. Let us point out that the continuation increases the residual (but it is kept at a reasonable value) as we approach the speed of sound: this no surprise in view of Proposition 6. Furthermore, the use of Newton's method fails to capture the mKP solutions (see example 1, section 3.1). Thus, if we had used Newton's method only, we would have missed some intervals of velocities for several of the examples that follow (sections 3.1 to 3.5).

3 Study of some model cases

For each one of the examples below, we have computed numerically some branches of solutions to (TW_c), with scilab software. For the first three examples, the smooth nonlinearity f has a qualitative behaviour similar to the Gross-Pitaevskii nonlinearity $f(\varrho) = 1 - \varrho$, namely f is decreasing, vanishes for $\varrho = r_0^2 = 1$ and tends to $-\infty$ for $\varrho \gg 1$, which means that the potential function $V(\varrho)$ is convex and tends to $+\infty$ for large ϱ. We then study a nonlinearity with saturation effect and finally the cubic-quintic nonlinearity. For a study of the travelling waves in dimension one for these nonlinearities, we refer to [20], where we may also find the graphs of the functions f and V. In order to see more clearly the behaviour of the solutions as the velocity varies, we have plotted only the modulus $|u|$ and only on the half-plane $\{x_2 \geq 0\}$ (recall the symmetries (20)). Furthermore, for a better visualization, we plotted only one mesh point over three.

3.1 Example 1: a cubic-quintic-septic nonlinearity (i)

We consider the nonlinearity

$$f_1(\varrho) \stackrel{\text{def}}{=} -3(\varrho - 1) + \frac{9}{2}(\varrho - 1)^2 - \frac{5}{2}(\varrho - 1)^3.$$

Then, we compute

$$V_1(\varrho) = \frac{3}{2}(\varrho - 1)^2 - \frac{3}{2}(\varrho - 1)^3 + \frac{5}{8}(\varrho - 1)^4$$

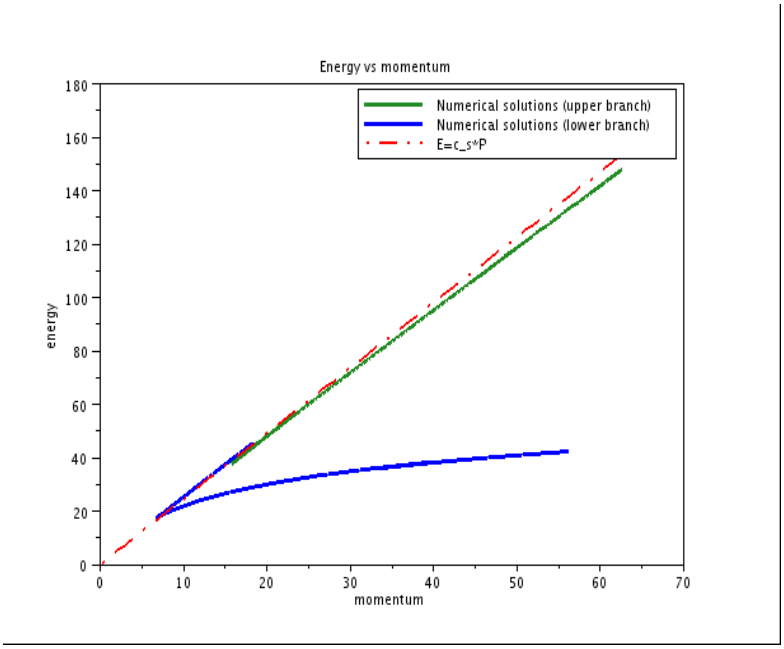

Figure 5: Energy momentum diagram for f_1 with lower and upper branches of solutions

so that $\mathfrak{c}_s^2 = 6$, $\Gamma = 0$ and $\Gamma' = -14 < 0$. The Padé approximant for the amplitude of the degree one vortex solution is found to be

$$\mathfrak{a}_{\text{Padé}}(r) \stackrel{\text{def}}{=} r\sqrt{\frac{2.389314101 + 5.111713038r^2}{1 + 4.639406046r^2 + 5.111713038r^4}}.$$

A peculiarity of this nonlinearity is that $\Gamma = 0 < \Gamma'$. Therefore, from the computations of section 1.3, we expect a transonic limit given by the focusing (mKP-I) equation and not the usual (KP-I) equation. The (E, P) diagram we have obtained is given in figure 5 and consists in *two* distinct branches of solutions we have singled out in figures 6.

The lower branch (figure 6 (a)) has been obtained as follows. We start with the approximation with the two vortices that we expect as $c \approx 0$. We then use the variational method to obtain the concave part of the diagram up the cusp which has parameters $(c = 1.995, P = 6.69, E = 17.45)$, and for this, both minimizations based on $\mathbb{E}_{\min}$ or on $\mathbb{G}_{\min}$ work. The former permits to compute only solutions that are orbitally stable (as explained previously), so that only $\mathbb{G}_{\min}$ is able to compute the solutions (slightly) after the cusp and to reach the values $(c = 2.159, P = 6.89, E = 17.87)$. The variational approach has the advantage of being able to capture a solution in the middle of the curve, like the solution for $(c = 0.556, P = 25.752, E = 33.384)$ that we have obtained from the vortex ansatz with $c = 1$ and imposing $\mu = 25$ despite the fact that we were not so close to the solution we wanted (whereas the Newton algorithm requires to start close to the solution we look for). The variational technique based on $\mathbb{G}_{\min}$ does not cover, however, the whole range of speeds until the speed of sound. Indeed, we only compute numerical solutions that verify $\dfrac{dE_{\text{kin}}}{dc} < 0$. To complete the branch we have used the continuation method as described in section 2.4.

On the qualitative level, we observe in figure 7 that, as the speed increases, the two vortices get closer, then merge for the parameters $(c = 1.998, P = 6.69, E = 17.45)$ (which is almost the

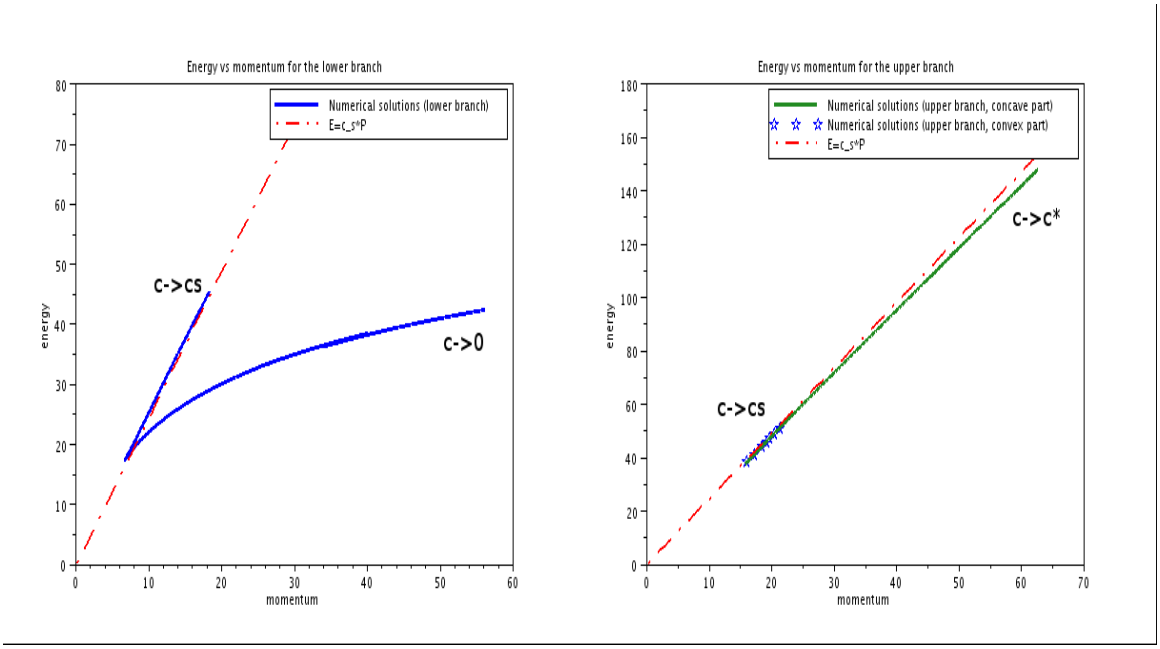

Figure 6: Energy momentum diagram for f_1: (a) left: lower branch; (b) right: upper branch

value of the cusp), and for $c > 1.998$, the solution no longer vanishes. As we approach the speed of sound $\mathfrak{c}_s = \sqrt{6} \approx 2.449$, both energy and momentum increase (upper part of the (E, P) diagram in figure 6 (a), and we expect from the computations in section 1.3 an approximation by the (mKP-I) solitary wave (we have already seen that in this case E and P diverge like $\varepsilon^{-1} \approx (\mathfrak{c}_s - c)^{-1/2}$). In figure 7 (e) and (f), we have plotted the numerical solutions for $c = 2.38$ and $c = 2.422$ (that is $\varepsilon = \sqrt{6 - 2.422^2} \approx 0.3725$). It should be pointed out that scales on both vertical and horizontal axes are different. We may compare figure 7 (f) with figure 8 where we have plotted the modulus of (5) which is the function

$$1 + \varepsilon \mathcal{W}'(\varepsilon x_1, \varepsilon^2 x_2), \tag{27}$$

with the same value of $\varepsilon = 0.3725$ and $A_\varepsilon = \mathcal{W}'$ the solution to (SW'). This last solution may be computed with the help of Petviashvili algorithm (see section 2.3.2). Though not perfect, this approximation is convincing. Note that the convergence rate of A_ε to $\mathcal{W}'$ should be $\mathcal{O}(\varepsilon)$, and that $\varepsilon = 0.3725$ is not so small (in comparison, for the usual (KP-I) limit, we expect a convergence rate $\mathcal{O}(\varepsilon^2)$).

We now turn to the upper branch (figure 6). As in the one dimensional case (see [20], Example 1), these solutions should have a modulus essentially ≥ 1 (contrary to those on the lower branch). One could be tempted to start from speeds c close to $\mathfrak{c}_s$ and use the (mKP-I) solitary wave $-\mathcal{W}'$, but this is difficult for the following reasons. In the transonic limit $c \nearrow \mathfrak{c}_s$, E and P increase up to infinity, thus the curve $P \mapsto E$ has to be convex in view of the Hamilton group relation. As a consequence, we can not capture these travelling waves (if they exist) by the variational methods we have discussed. Therefore, we may choose the continuation method, but then one needs to start with ε very small in order to have an accurate solution, which causes some numerical challenge. Furthermore, we have seen that the transonic limit has some numerical intrinsic difficulties (see

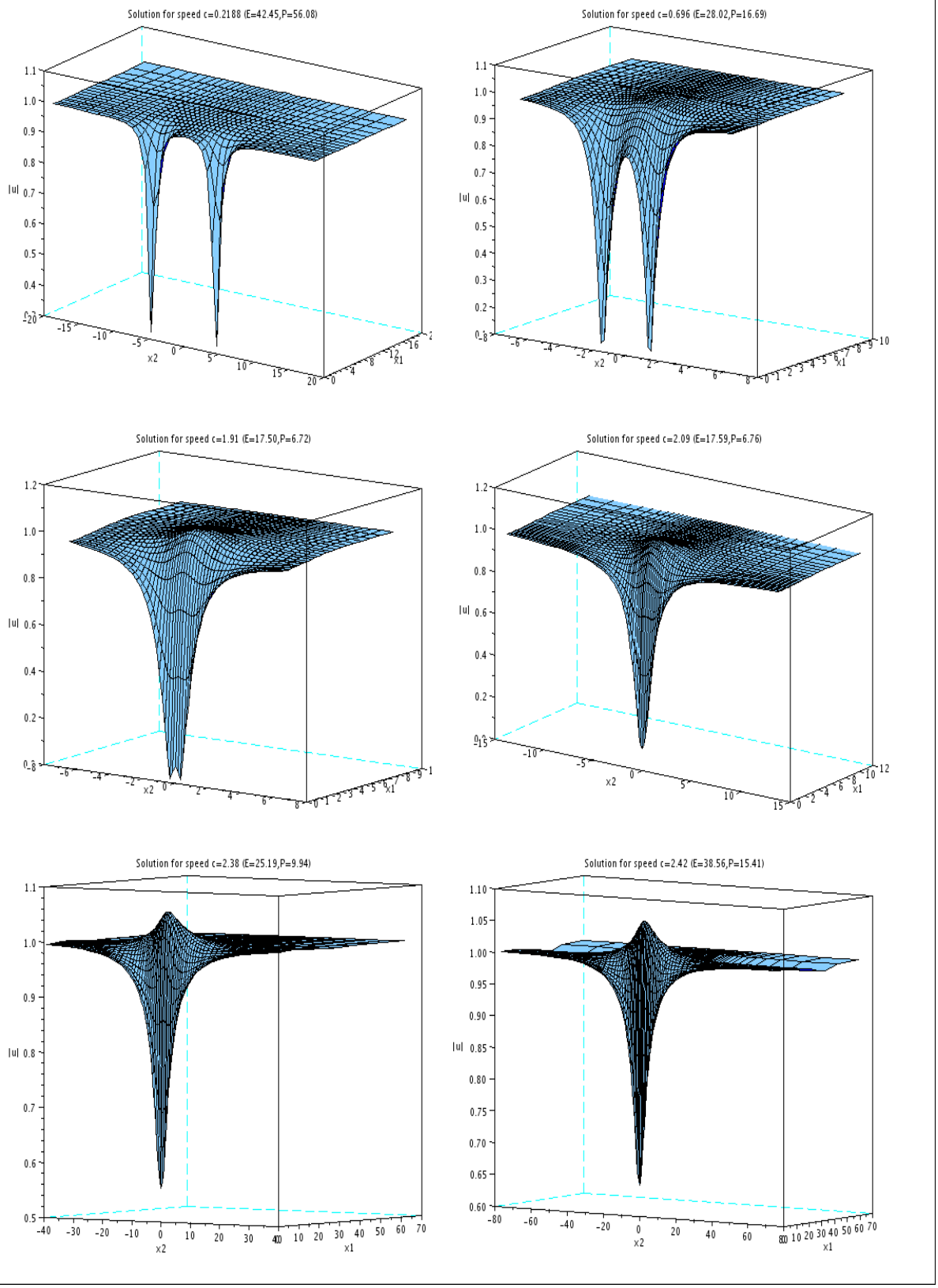

Figure 7: Travelling wave for the nonlinearity f_1 (lower branch) with speed, from left to right and top to bottom: (a) $c = 0.2188$; (b) $c = 0.696$; (c) $c = 1.91$; (d) $c = 2.09$; (e) $c = 2.38$; (f) $c = 2.42$

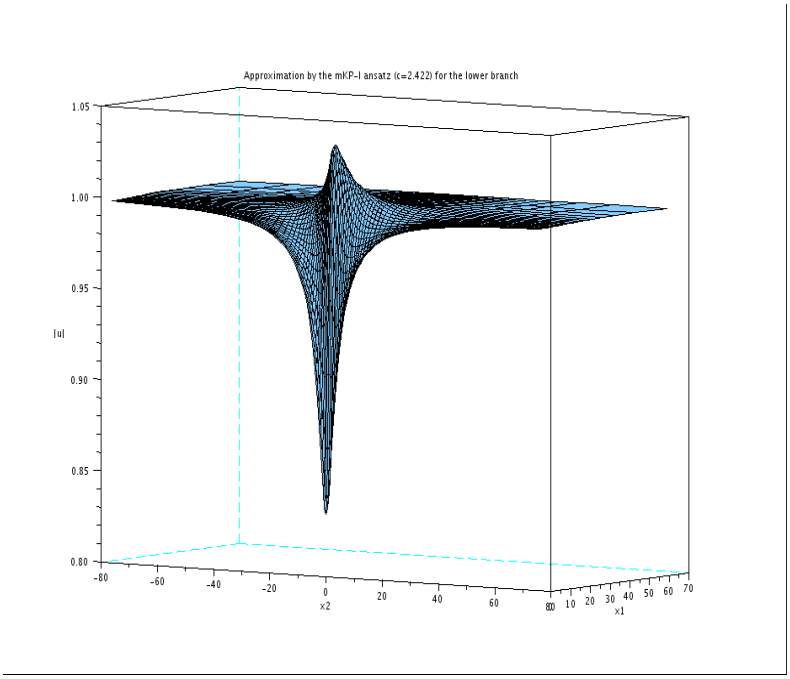

Figure 8: Approximate solution given by the (mKP-I) ansatz (27) for $c = 2.42$ with the help of Petviashvili algorithm.

section 2.5). Finally, since we do not have any theoretical result concerning the (mKP-I) limit for the travelling waves, it should be better to start from solutions rather far from those ones. Instead of starting from $c \approx \mathfrak{c}_s$, it is more convenient to start from the other (diverging) part of the curve. For that purpose, we look for an initial guess given by a Padé function of the form

$$U_{\text{Padé}}(x) = 1 + \frac{a_0 + a_1 x_1^2 + a_2 x_2^2 + i x_1 (b_0 + b_1 x_1^2 + b_2 x_2^2)}{1 + c_1 x_1^2 + c_2 x_2^2 + c_3 x_1^4 + c_4 x_1^2 x_2^2 + c_5 x_2^4}$$

as in [9] and follow the strategy in [9], section 5, by fixing $c = 2.3$. We thus impose $a_2 = c b_1 (1 - c^2/\mathfrak{c}_s^2)$, $b_2 = b_1(1 - c^2/\mathfrak{c}_s^2)$, $c_4 = 2c_3(1 - c^2/\mathfrak{c}_s^2)$ and $c_5 = c_3(1 - c^2/\mathfrak{c}_s^2)$ (these choices are rather arbitrary since we shall not obtain a very accurate initial guess), and optimizing the remaining coefficients as described in [9], section 5. We impose $a_0 > 0$ since we want U to have a modulus ≥ 1 as much as possible and want to avoid the solution on the lower branch, for which $a_0 < 0$ (we also impose the posivity of the coefficients c_j). In this way, we obtain

$$U_{\text{Padé}}(x) = 1 + \frac{0.2152 + 0.1320 x_1^2 + 0.0606 x_2^2 + i x_1 (0.2702 + 0.2225 x_1^2 + 0.0263 x_2^2)}{1 + 0.4222 x_1^2 + 0.001 x_2^2 + 0.0206 x_1^4 + 0.0049 x_1^2 x_2^2 + 0.0003 x_2^4}$$

and start the heat flow with this initial datum. The advantage is that the solutions in the concave part are capturable by the variational methods and that we start sufficiently far from the transonic limit to trust our numerics. Once we have obtained numerical convergence to a (local) minimizer, which gives a point in the middle of the concave part of the diagram in figure 6, we can pursue with variational methods and continuation. This is a big advantage of the heat flow on the functionals we consider since even we start not so close to the local minimum we are looking for, we may reach

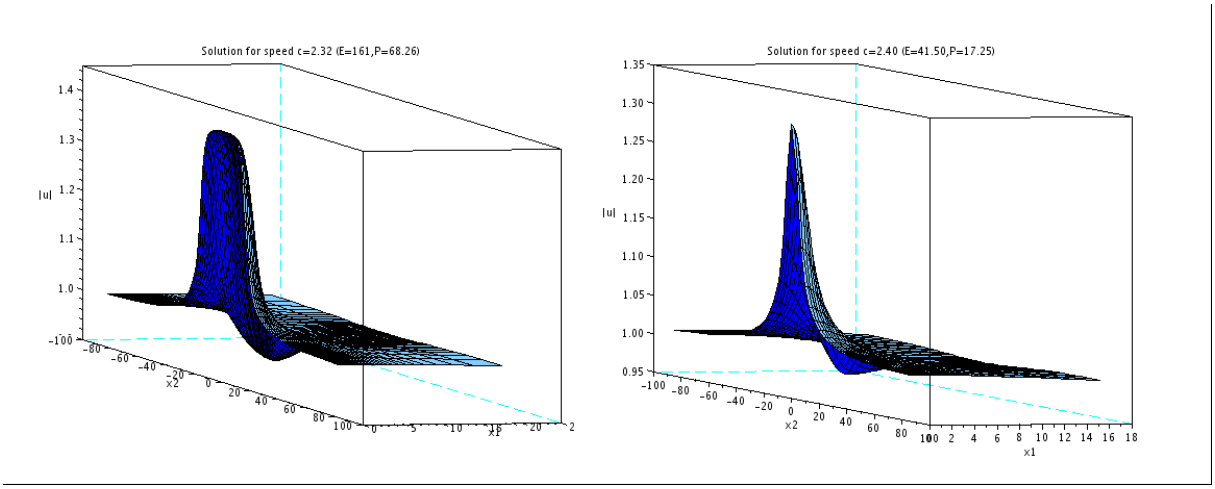

Figure 9: Travelling wave for the nonlinearity f_1 (upper branch) with speed: (a) left $c = 2.32$; (b)

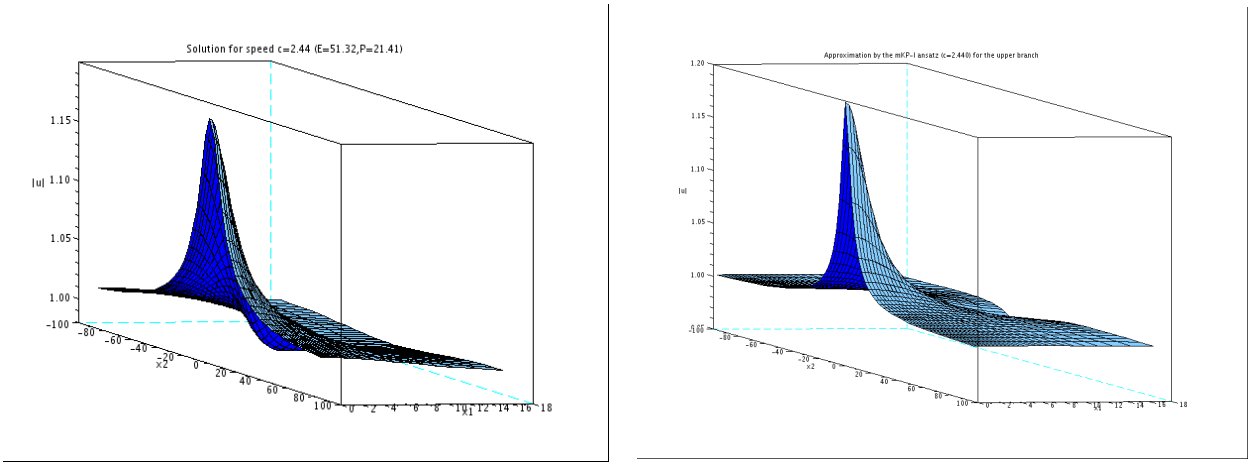

Figure 10: (a) left: travelling wave for the nonlinearity f_1 (upper branch) with speed $c = 2.44$; (b) right: approximate solution given by the (mKP-I) ansatz (27) for $c = 2.44$ with the help of Petviashvili algorithm.

it. At the opposite, the Newton algorithm requires to start not too far from the desired solution, and the continuation procedure needs to start from a sufficiently accurate solution.

Actually, in [20], this is not exactly the nonlinearity f_1 which was considered, but a similar one, say $\tilde{f}_1$. In example 1 in [20], the nonlinearity $\tilde{f}_1$ was such that $\tilde{\mathfrak{c}}_s = \sqrt{2} \approx 1.414\,2$ and as $c \to \tilde{c}_0 \overset{\text{def}}{=} \sqrt{\frac{484}{243}} \approx 1.411\,3$, the modulus of the travelling wave of the upper branch tends (locally uniformly) to ≈ 1.106. It turns out that $\tilde{c}_0$ is extremely close to $\tilde{\mathfrak{c}}_s$, hence we have chosen to modify slightly the nonlinearity in [20] in order to have the same qualitative behaviour but with $\tilde{c}_0$ less close to $\tilde{\mathfrak{c}}_s$. With the nonlinearity f_1, we have now $\mathfrak{c}_s = \sqrt{6} \approx 2.449$ and for the travelling waves in dimension one, as $c \to c_0 \overset{\text{def}}{=} \sqrt{5} \approx 2.236$, the modulus of the solution of the upper branch tends (locally uniformly) to ≈ 1.390.

For our simulation, as c decreases down to $c_* \overset{\text{def}}{=} 2.318$, we have the right part of the green curve in figure 6. In figure 9, we have plotted the solution for $c = 2.32$. It is remarkable that for $x_2 = 0$ and $x_1 \in [-8, +8]$, we observe a plateau where the modulus of the solution is equal to

≈ 1.40 which is precisely the critical amplitude in dimension one. However, the speed $c_* = 2.318$ is different from $c_0 = \sqrt{5} \approx 2.236$. As c increases, the momentum, energy and the maximum of the modulus decrease along the green (concave) part of the (E, P) diagram. We reach the cusp for the parameters $(c = 2.427, P = 15.952, E = 38.320)$, and c is already very close to the speed of sound $\mathfrak{c}_s = \sqrt{6} \approx 2.4494897$. For $c \nearrow \mathfrak{c}_s$, P and E increase and this is the convex part (blue stars) in figure 6. Due to the Hamilton relation (15), one would expect this last part of the curve to be above the staight line $E = \mathfrak{c}_s P$. However, this point is not easy to check due to numerical precision. The solution for $c = 2.44$ in figure 10 is here again quite close to the approximate solution given by the (mKP-I) ansatz (27) for $c = 2.44$ with the other solution $-\mathcal{W}$ of (SW').

In this example, Newton's algorithm converges neither with the (mKP-I) ansatz (10) nor starting from the initial guess $U_{\text{Padé}}$. This method alone does not allow to capture the upper branch of the (E, P) diagram, or to start the lower branch from its upper part.

Comments. Similarly to what we had observed in dimension one in [20], for this nonlinearity f_1, the transonic limit is governed by a focusing (mKP-I) equation and we indeed see two branches of solutions for c close to $\mathfrak{c}_s$. This is, to our knowledge, the first multiplicity result of this type in space dimension two. Let us quote that in [45], the travelling wave solutions to the Landau-Lifshitz equation with an easy plane anisotropy, that is

$$\frac{\partial \mathfrak{m}}{\partial t} = \mathfrak{m} \times (\Delta \mathfrak{m} - \mathfrak{m}_3 \vec{e}_3), \qquad \vec{e}_3 \stackrel{\text{def}}{=} (0, 0, 1). \tag{LL}$$

are simulated. For (LL), the transonic limit is also given by a focusing (mKP-I) equation (see [45]). Therefore, one may also expect two branches of solutions in the transonic limit. However, the model (LL) possesses a discrete symmetry: if $\mathfrak{m}$ solves (LL), then so does $\tilde{\mathfrak{m}}(t, x) = (\mathfrak{m}_1, \mathfrak{m}_2, -\mathfrak{m}_3)(-t, -x)$. Since this symmetry is inherited by the travelling waves, they appear by pairs, with the same energy and momentum. Thus in the (E, P) diagrams for (LL), each curve is actually the superposition of two curves, and this is in particular the case in the transonic limit. Our problem does not possess any discrete symmetry.

The other remarkable fact is the phenomenon of "one dimensional spreading" of the modulus as c approaches $c_* = 2.318$ which, as far as we know, has not been observed before. It is not very easy to propose an ansatz for the travelling wave solution that could give some explanations of this phenomenon. Indeed, in the two dimensional (or higher) case, the travelling wave tends to 1 at infinity (see [30]) at some algebraic rate, but in dimension one, this is no longer the case: the travelling wave has two different phases at $+\infty$ and $-\infty$ and this phase shift has to be included in the definition of the momentum. Therefore, it is not completely clear that we could embed the one dimensional travelling waves in two space dimension. It is probably this phase problem at infinity that implies that the critical speed $c_* = 2.318$ is slightly different from the one dimensional critical speed $c_0 = 2.236$.

3.2 Example 2: a cubic-quintic-septic nonlinearity (ii)

Here, we consider

$$f_2(\varrho) \stackrel{\text{def}}{=} -4(\varrho - 1) - 36(\varrho - 1)^3,$$

for which we compute

$$V_2(\varrho) = 2(\varrho - 1)^2 + 9(\varrho - 1)^4,$$

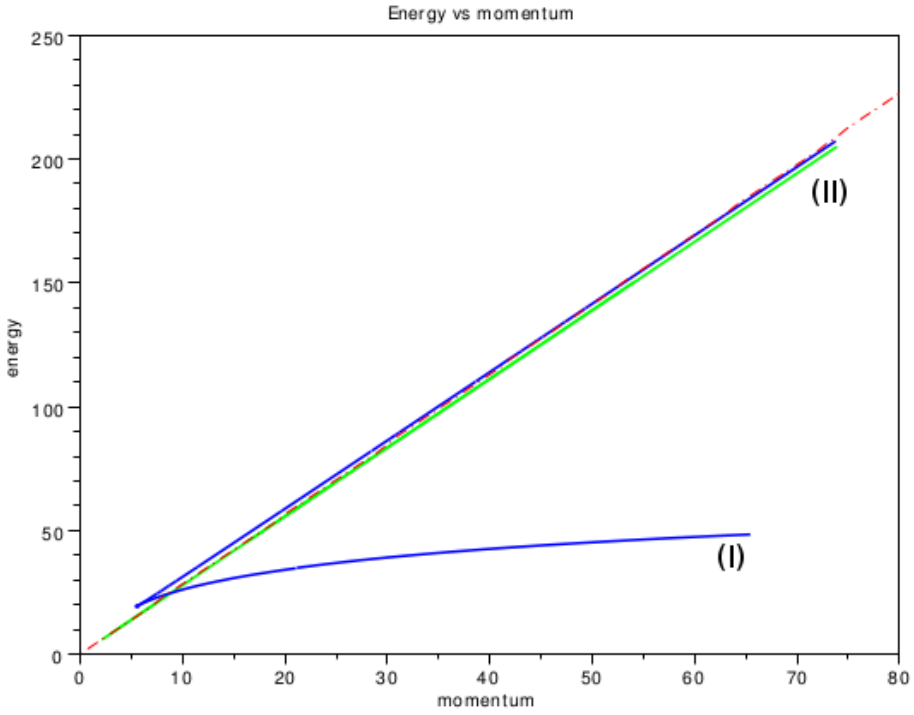

Figure 11: Energy momentum diagram for f_2 with the two branches of solutions (I) and (II)

thus $\mathfrak{c}_s^2 = 8$, $\Gamma = 6$. For this nonlinearity, the Padé approximant for the profile of the degree one vortex is found to be

$$\mathfrak{a}_{\text{Padé}}(r) \stackrel{\text{def}}{=} r\sqrt{\frac{7.459294023 + 33.13690937r^2}{1 + 14.44236536r^2 + 33.13690937r^4}}.$$

The energy momentum diagram has two branches of solutions. The first one corresponding to speed from 0 to $\mathfrak{c}_s \approx 2.8284$ (blue branch (I) on figure 11 and figure 12 (a)). We start our computation by the approximation of the vortices that we expect as $c \approx 0$. We use the variational approach to compute the concave branch of solutions. The cusp occurs at $c = 2.276\,(P = 5.45, E = 19.28)$. The branch is then completed by using the continuation algorithm. Qualitatively, as in the first example, as the speed increases, the vortices come closer and merge (see figure 13). The loss of vorticity occurs for $c = 2.756\,(P = 28.91, E = 83.43)$, which is rather close to the speed of sound. As the speed approaches the speed of sound, energy and momentum become large. As $c \to \mathfrak{c}_s$, the modulus of the solution exhibits a particularly remarkable behaviour: we observe a plateau at a value of ≈ 0.93 in the x_2-direction (see figure 14). It corresponds to the value of the critical amplitude in $1D$ (≈ 0.9269), see [20]. To compute this convex part of the blue branch (I), we could have indifferently used Newton's method for the computation of the upper part of branch (I). Concerning the adaptation of the parameters R_1 and R_2, we start from $R_1 = R_2 = 0.2$ and need to take for the last solution $R_1 = 0.156$, $R_2 = 0.073$. Thus we have to modify their values along the computations.

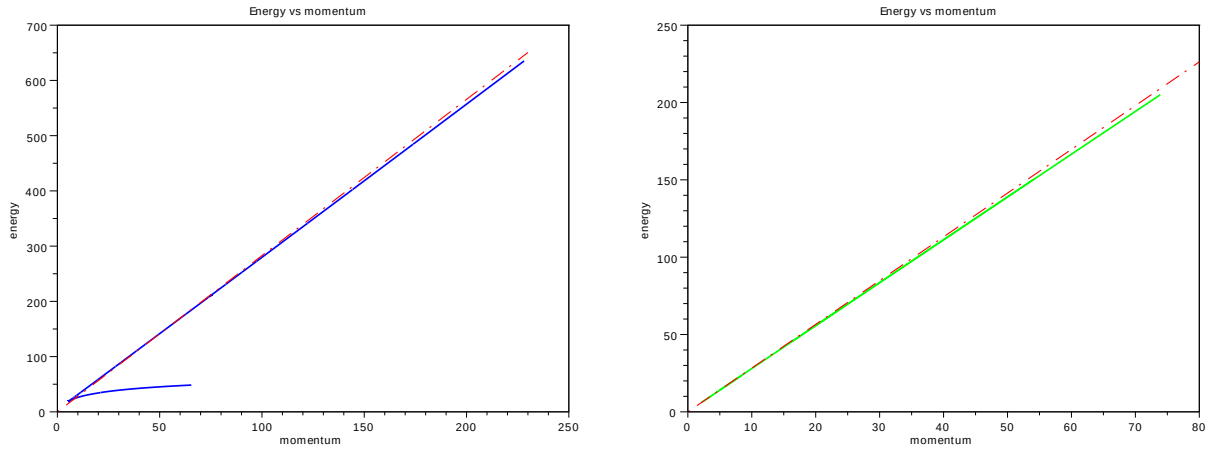

Figure 12: Energy momentum diagram for f_2 with branches of solutions: (a) left (I); (b) right (II)

Turning to the other branch (green branch (II) on figure 11 and figure 12 (b)), we initiate the computation for $c \approx \mathfrak{c}_s \approx 2.8284$ with the (KP-I) ansatz (5) with the $\varepsilon = \sqrt{\mathfrak{c}_s^2 - c^2}$-scaling as described in section 2.3.2. We computed solution from $c \approx \mathfrak{c}_s$ down to the value $c_* \approx 2.77$. This speed appears to be the limit speed we were able to reach numerically. Qualitatively we observe a spreading in the x_2 direction as the speed decreases leading to a sharp plateau at the modulus ≈ 0.90 associated here again to the critical amplitude in $1D$; see the evolution from figure 15 to 16, and the zoom in figure 17. Here again, simply using Newton's method, we would miss the green branch (II).

Comments. Concerning the blue branch (I), as for the nonlinearity f_1, we observe the phenomenon of "one dimensional spreading" as $c \to c_* \approx 2.77$ (see figures 16 and 17), with a plateau in the x_2 variable associated with a one dimensional critical amplitude of ≈ 0.9. The green branch (II) does not possess the same type of "one dimensional spreading" in view of the presence of a small region of relatively small modulus close to the origin. However, the remarkable value of the plateau is still the one dimensional value ≈ 0.9. Another noticeable fact is that we computed *two* numerical solutions for the whole interval of speeds $[c_*, \mathfrak{c}_s]$. The two branches that we have computed both represent solutions with modulus essentially less than one whereas for f_1 one branch corresponds to solution with modulus essentially greater than one. Finally, these two branches cross at $(E \approx 9.2, \mathfrak{p}_* \approx 25.3)$ for the speeds $c \approx 2.80$ and $c \approx 1.19$ corresponding (almost) to figures 16 (a), 13 (b), respectively. The same phenomenon occurs also in $1D$, see [20], example 2. As a consequence, this nonlinearity f_2 has the remarkable property that the function $\mathbb{E}_{\min}$ is *not* differentiable at $\mathfrak{p}_* > 0$ and there exist *two* minimizers for the constrained minimization problem $\mathbb{E}_{\min}(\mathfrak{p}_*)$. We didn't find such configurations in the existing literature.

3.3 Example 3: a cubic-quintic-septic nonlinearity (iii)

We consider here

$$f_3(\varrho) \stackrel{\text{def}}{=} -\frac{1}{2}(\varrho - 1) + \frac{3}{4}(\varrho - 1)^2 - 2(\varrho - 1)^3,$$

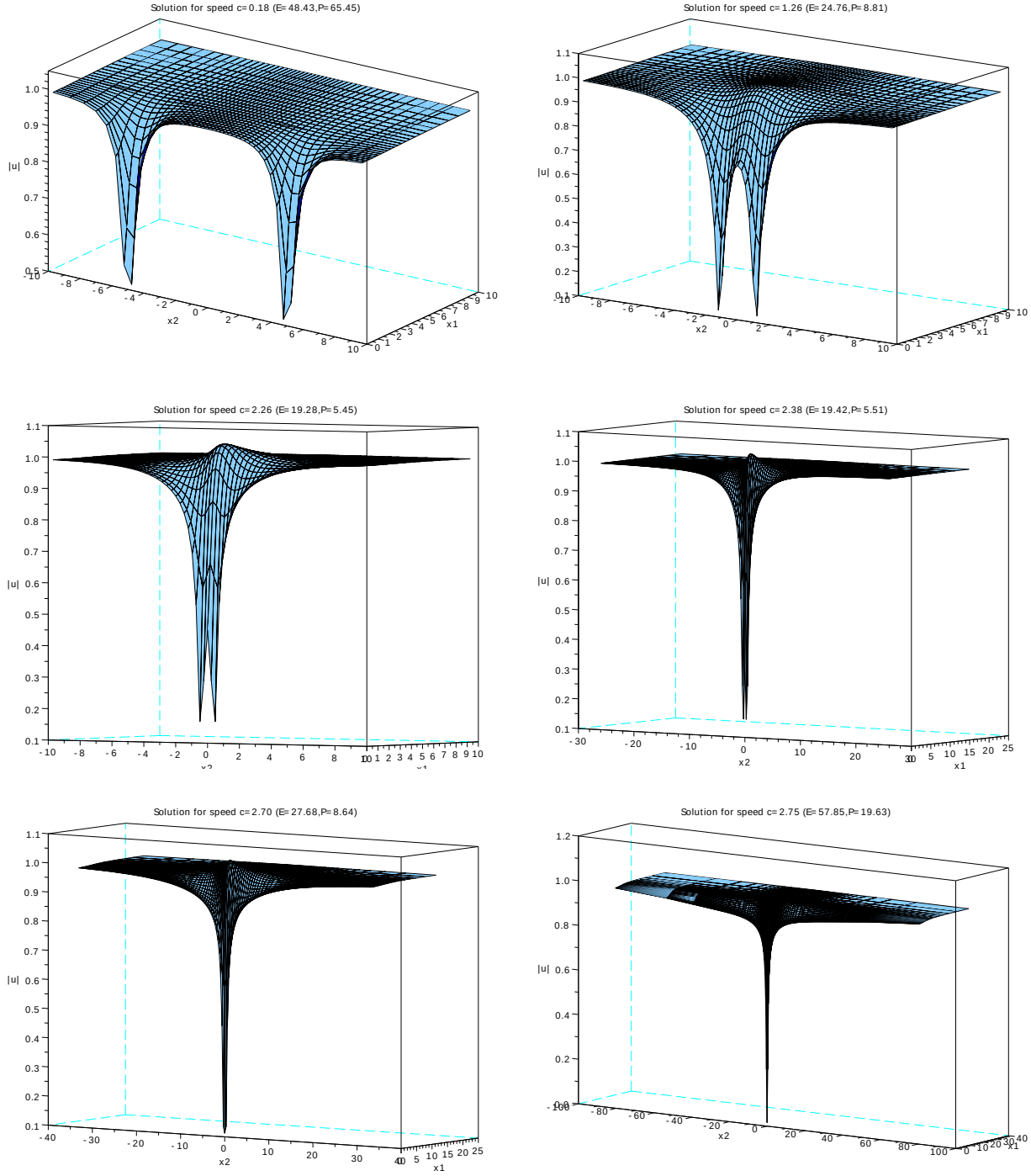

Figure 13: Travelling wave for the nonlinearity f_2 (blue branch (I)) with speed, from left to right and top to bottom: (a) $c = 0.18$; (b) $c = 1.26$; (c) $c = 2.26$; (d) $c = 2.37$; (e) $c = 2.70$; (f) $c = 2.75$

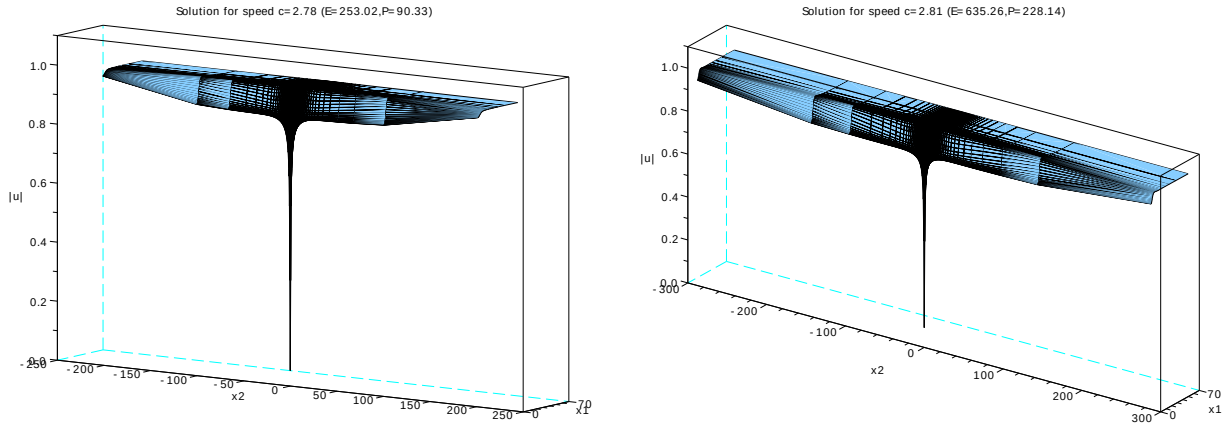

Figure 14: Travelling wave for the nonlinearity f_2 (blue branch (I)) with speed: (a) left $c = 2.78$; (b) right $c = 2.81$

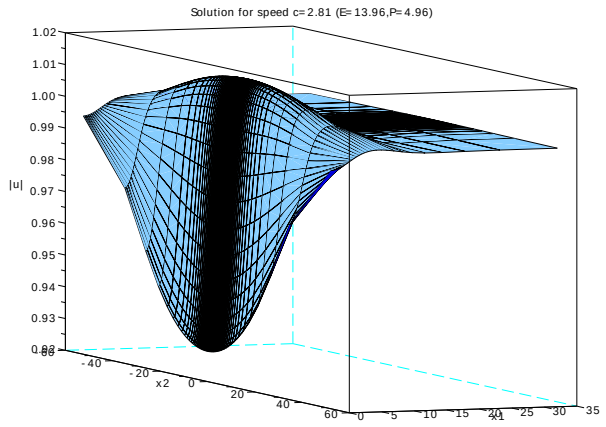

Figure 15: Travelling wave for the nonlinearity f_2 (green branch (II)) with speed $c = 2.81$

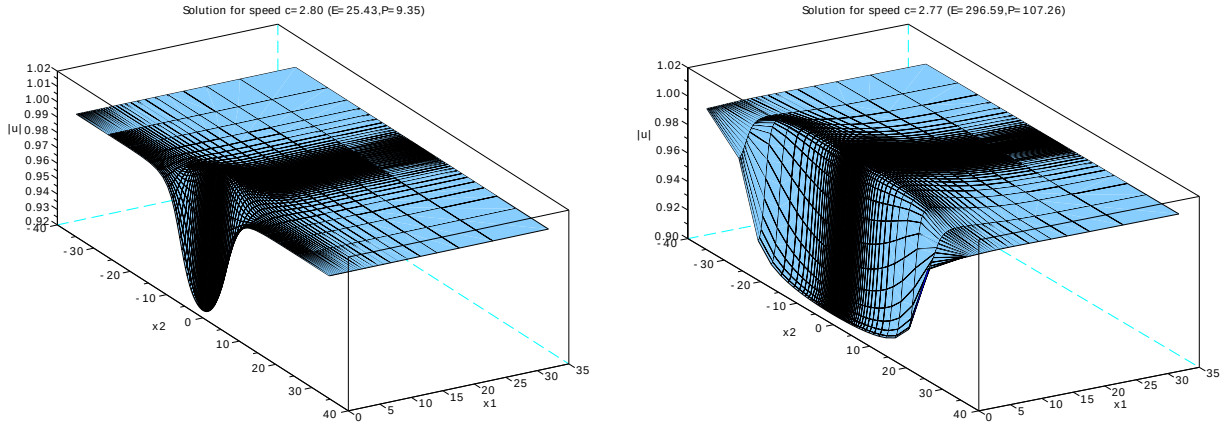

Figure 16: Travelling wave for the nonlinearity f_2 (green branch (II)) with speed: (a) left $c = 2.80$; (b) right $c = 2.77$

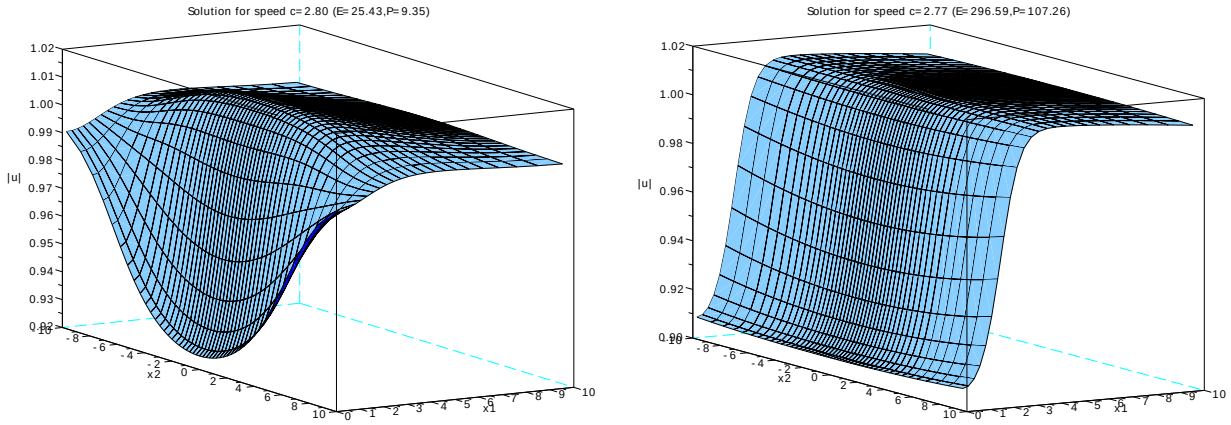

Figure 17: Travelling wave for the nonlinearity f_2 (green branch (II)) with speed: (a) left $c = 2.80$, zoom; (b) right $c = 2.77$, zoom

for which

$$V_3(\varrho) = \frac{1}{4}(\varrho-1)^2 - \frac{1}{4}(\varrho-1)^3 + \frac{1}{2}(\varrho-1)^4,$$

thus $\mathfrak{c}_s^2 = 1$, $\Gamma = 0$, $\Gamma' = 24 > 0$. The peculiarity of f_3 is that we have $\Gamma = 0$, hence we do not have a (KP-I) transonic limit, and the coefficient Γ' is positive which means that the associated (mKP-I) is defocusing (without nontrivial solitary wave), thus we do not have a (mKP-I) transonic limit. Here we find the Padé approximant for the profile $\mathfrak{a}$

$$\mathfrak{a}_{\text{Padé}}(r) \stackrel{\text{def}}{=} r\sqrt{\frac{0.6689784247 + 0.2838394656r^2}{1 + 1.236787922r^2 + 0.2838394656r^4}}.$$

The energy-momentum diagram we have obtained is given in figure 18.

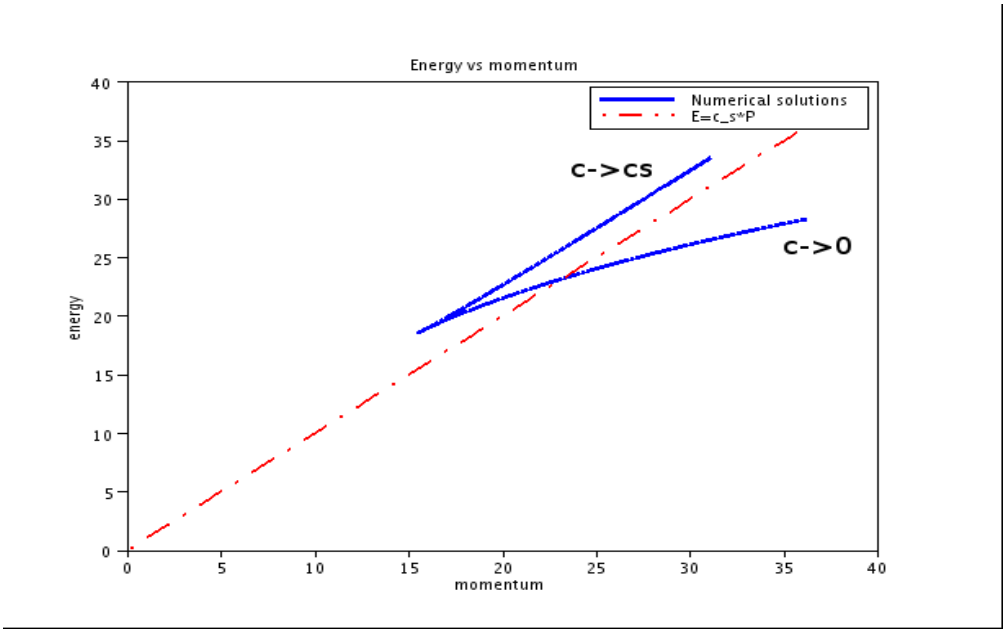

Figure 18: (E, P) diagram for the nonlinearity f_3

We start from c close to zero and let c increase using the minimization based on the functional $\mathcal{I}$. The qualitative behaviour of the solution for $c \leq 0.8$ is rather similar to what we observe on the (GP) equation or for the nonlinearity f_1. For c small, the solution looks like the solution with two vortices as in figure 2 (a) and as c increases, the vortices get closer until we reach the values $(c = 0.795, P = 15.591, E = 18.671)$, which is the solution in figure 19. These solutions correspond to the concave part of the (E, P) diagram in figure 18, but we are actually slightly before the cusp. We have then used the continuation method to obtain the cusp and the upper (convex) part of the (E, P) diagram. The parameters associated with the cusp are $(c = 0.822, P = 15.526, E = 18.613)$. On the convex part, the solution becomes vortexless for the parameters $(c = 0.944, P = 18.163, E = 20.965)$. As $c \nearrow \mathfrak{c}_s$, both energy and momentum increase.

Comments. In one space dimension, we know from [20] that there exists a solution of finite energy and momentum for speed $c = \mathfrak{c}_s$ which has a modulus with minimum value equal to $1/\sqrt{2} \approx 0.707$. Looking at the way the solution evolves close to the speed of sound, it is natural to wonder whether

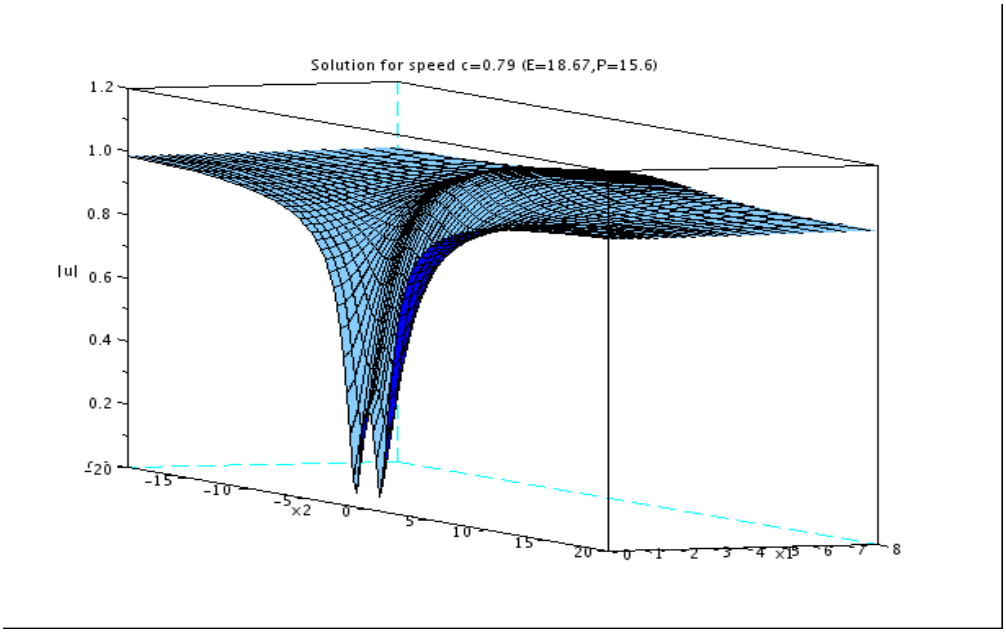

Figure 19: Travelling wave for the nonlinearity f_3 with $c = 0.79$

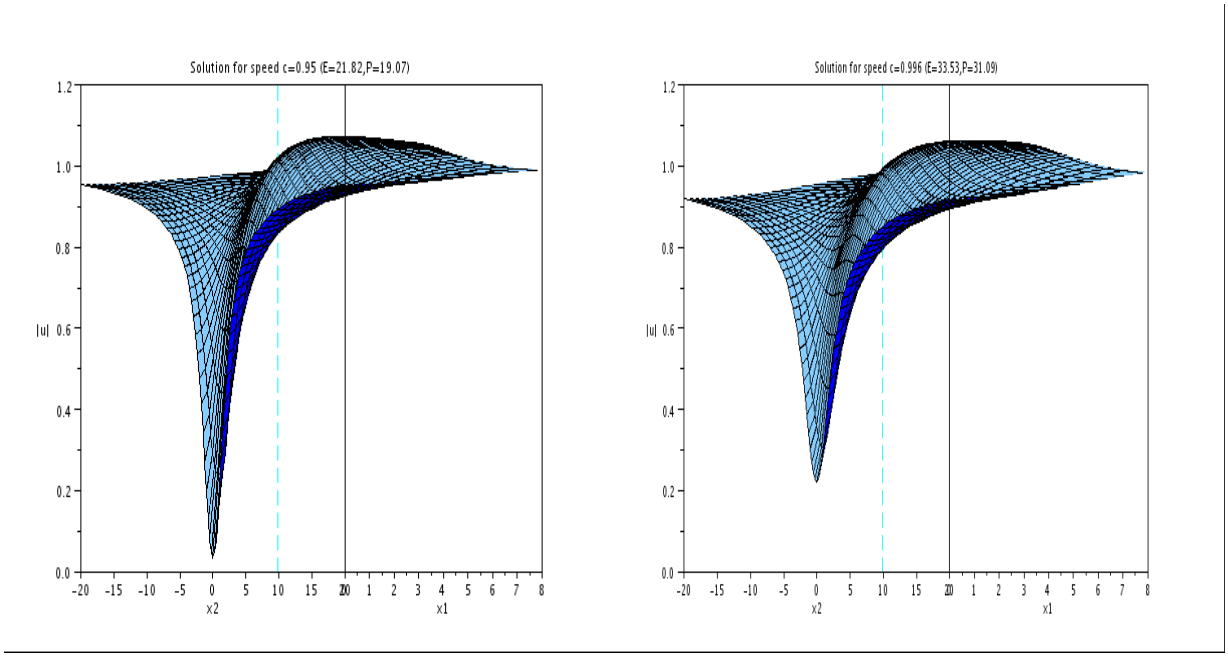

Figure 20: Travelling wave for the nonlinearity f_3 with: (a) left $c = 0.95$; (b) right $c = 0.996$

there exists a nontrivial solution to ($\mathrm{TW}_{\mathfrak{c}_s}$). Indeed, between figures 20 (a) and (c), the speed has increased from $c = 0.95$ to $c = 0.996$ (recall $\mathfrak{c}_s = 1$) the minimum of the modulus has increased, but does not seem to tend to 1 (or even to 0.707). It turns out that if v is a sonic travelling wave of finite energy, then the identity

$$\int_{\mathbb{R}^2} |\nabla v|^2 \, dx = \int_{\mathbb{R}^2} |v|^2 f(|v|^2) + \frac{\mathfrak{c}_s^2}{2}(|v|^2 - 1) \, dx$$

must hold true: see Theorem 3.1 in [43]. For the solution with speed $c = 0.996$, we have computed a kinetic energy ≈ 18.09 and the right-hand side is equal to ≈ 12.18. Since these two values are rather different, we believe that if the travelling wave u_c converges as $c \to \mathfrak{c}_s$ to a nontrivial sonic travelling wave, then the latter must be of infinite energy. In this case, the energy and momentum should diverge to infinity as $c \to \mathfrak{c}_s$. Note that the diagram is similar to the one computed in [33] in $3D$ for the (GP) nonlinearity, see figure 1 (b). In particular there does not exist travelling waves solutions with small energy, see [23] for a mathematical result. We furthermore point out that the transonic limit is not governed by a (KP)-type equation.

We have not performed the numerical simulation for "example 4" in [20]. The point is that this case is very degenerate (we obtain in the transonic limit the sextic (gKdV)), which means that we need to achieve extremely small values of $\varepsilon^2 = \mathfrak{c}_s^2 - c^2$ to see something in the transonic limit. Furthermore, the sextic (gKP-I) does not have nontrivial solitary waves (see [27]). This has led us to think that the (E, P) diagram should probably not be very different from what we have obtained for the nonlinearity f_3. We then pursue with "example 5" in order to keep the notations of [20].

3.4 Example 5: a saturated nonlinearity

In this example, we take, for some $\varrho_0 > 0$,

$$f_5(\varrho) \stackrel{\text{def}}{=} \exp\Big(\frac{1-\varrho}{\varrho_0}\Big) - 1.$$

This type of nonlinearity saturates when ϱ is large and can be found, for instance, in [35]. For this nonlinearity, we have

$$V_5(\varrho) = \varrho_0 \Big\{ \exp\Big(\frac{1-\varrho}{\varrho_0}\Big) - 1 - \frac{1-\varrho}{\varrho_0} \Big\},$$

thus $\mathfrak{c}_s^2 = 2/\varrho_0$, $\Gamma = 6 - \dfrac{2}{\varrho_0}$. Therefore, the coefficient Γ changes sign for $\varrho_0 = 1/3$. We shall focus (as in [20]) on the case $\varrho_0 = 0.4 \in (1/3, 1/2)$, for which $\mathfrak{c}_s = \sqrt{5} \approx 2.236$, $\Gamma = 1$ and the Padé approximant is

$$\mathfrak{a}_{\text{Padé}}(r) \stackrel{\text{def}}{=} r \sqrt{\frac{2.298837694 + 5.902032693 r^2}{1 + 5.363022096 r^2 + 5.902032693 r^4}}.$$

Starting with the approximation of the vortices as $c \approx 0$, we compute the solutions using the variational approach: the qualitative behaviour remains similar to other nonlinearities (see *e.g.* nonlinearity f_2 and figure 13). The solution becomes vortexless at speed $c = 1.83$. To complete the computations, we use the continuation method. The diagram is given in figure 21.

The (E, P) diagram has two cusps. The first one at speed $c_{\text{cusp}\,1} = 1.63$ ($E = 18.64$, $P = 7.84$) (see figure 22, (a) left) it corresponds to a minimum of E and P. The second one occurs after

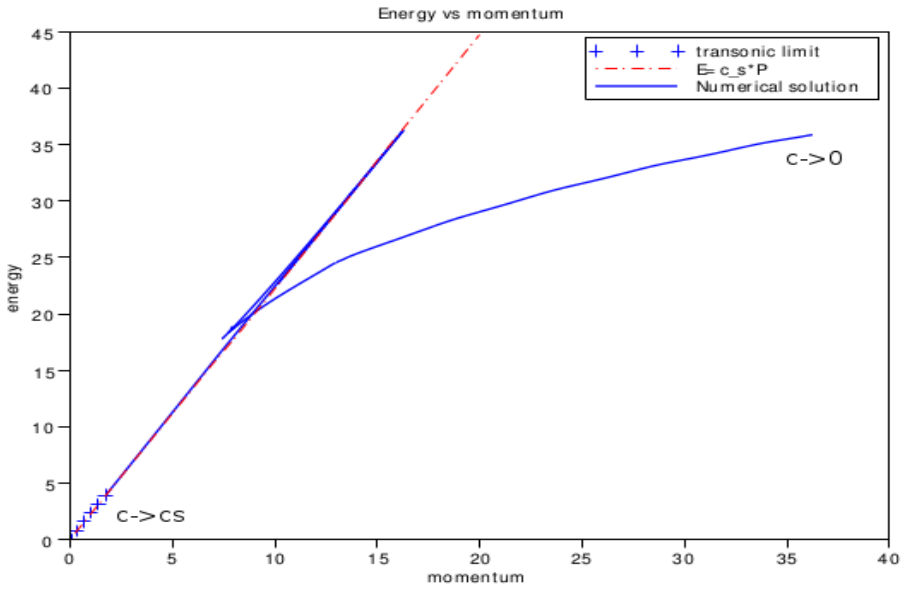

Figure 21: (E,P) diagram for the nonlinearity f_5.

the loss of vorticity at speed $c_{\text{cusp}\,2} = 2.208$ ($E = 36.28$, $P = 16.27$) (see figure 22, (c) left); it corresponds to a maximum of E and P. After this second cusp, energy and momentum decrease down to $(E = 0, P = 0)$, with a (KP-I) transonic limit as $c \to \mathfrak{c}_s \approx 2.236$, see figures 22 (d) and (e). Indeed, for this nonlinearity, the results in [22] may be applied and provide a rigourous convergence result to the (KP-I) limit, and this is why we have inserted the blue crosses in figure 21.

We compared the results obtained with the continuation method to the one obtained with Newton's method. The latter allows for larger speed step sizes but fail to converge in the transonic limit. The continuation method, on the contrary, enables us to pursue the computation if one starts with a solution with a very good residual at the end of the variational computation process. Since we begin to use the continuation method when the variational approach fails, the starting solution for initiating the continuation process can be computed with the desired value of the residual.

*Comments.*The diagram (E, P) exhibits two cusps, reflecting two transitions between stable (concave) branches and unstable (convex) branches. In particular, contrary to the instability cases for the nonlinearities f_1, f_2 and f_3, the instability region is precisely the interval $[c_{\text{cusp}\,1}, c_{\text{cusp}\,2}] \subset]0, \mathfrak{c}_s[$. Furthermore, the two concave regions self-intersect. The two travelling waves at the intersection point belong to the same continuum of solutions corresponding to the interval of velocities $]0, \mathfrak{c}_s[$. In comparison, for the nonlinearity f_2, this happens for two distinct continua. Therefore we find two solutions that have same momentum $\mathfrak{p}_*$ and energy but with two distinct speeds and qualitative behaviours: vortices on the one hand and a rarefaction pulse on the other hand (like in figure 22 (b) and (e)). It is noticeable that for $P \in [9, 16]$, some rarefaction pulses have higher energy than the vortex solutions. In addition, the differentiability properties of $\mathbb{E}_{\min}$ at $\mathfrak{p}_*$ are deeply linked to the question of uniqueness of the minimizer for the constraint minimization problem $\mathbb{E}_{\min}(\mathfrak{p}_*)$. Our nonlinearity, as well as f_2, shows that we have *two* minimizers for $\mathbb{E}_{\min}(\mathfrak{p}_*)$ and $\mathbb{E}_{\min}$ is not differentiable at $\mathfrak{p}_*$.

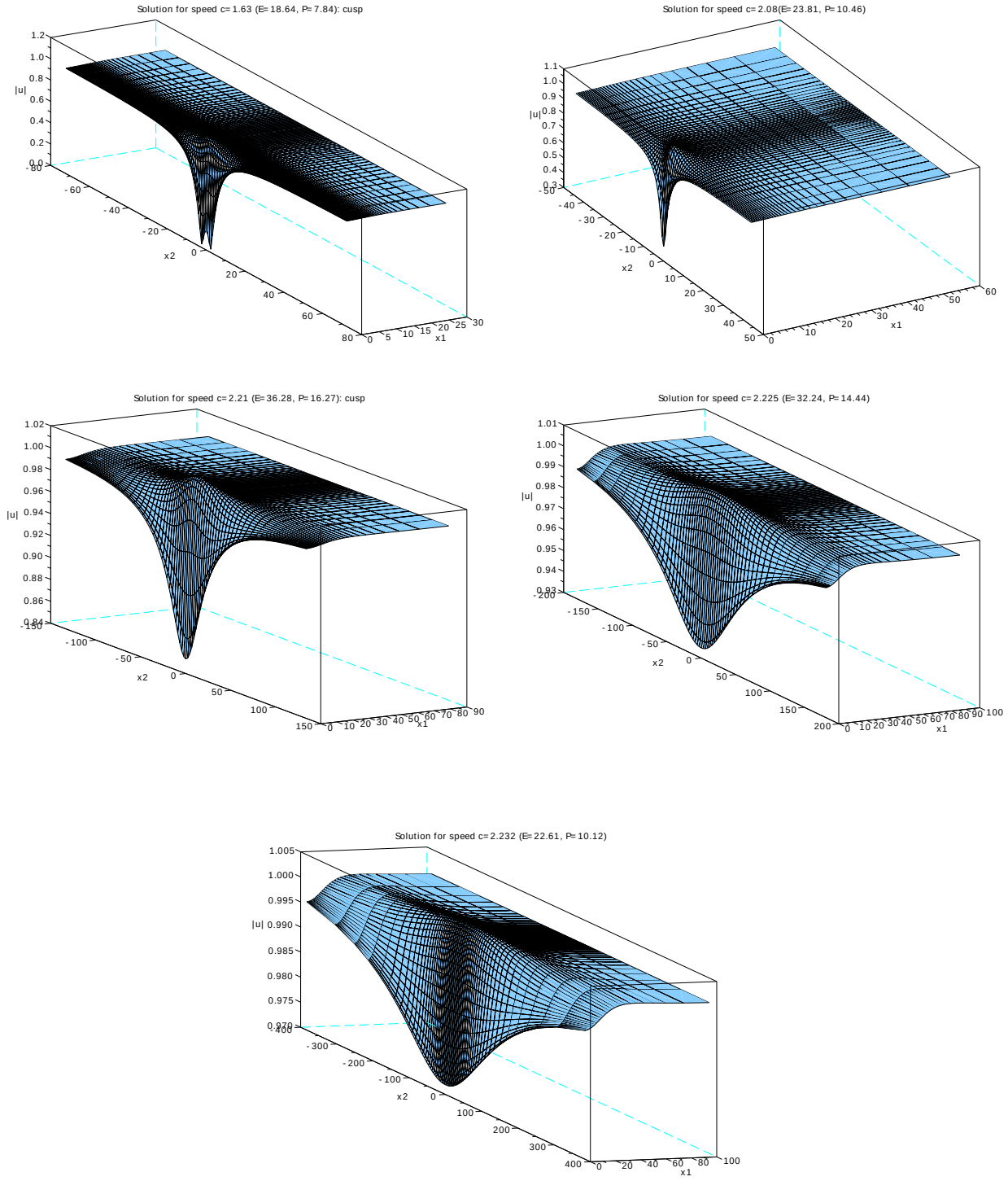

Figure 22: Travelling wave for the nonlinearity f_5 with speed, from left to right and top to bottom: (a) $c = 1.63$, the first cusp; (b) $c = 2.08$; (c) $c = 2.208$, the second cusp; (d) $c = 2.225$; (e) $c = 2.232$

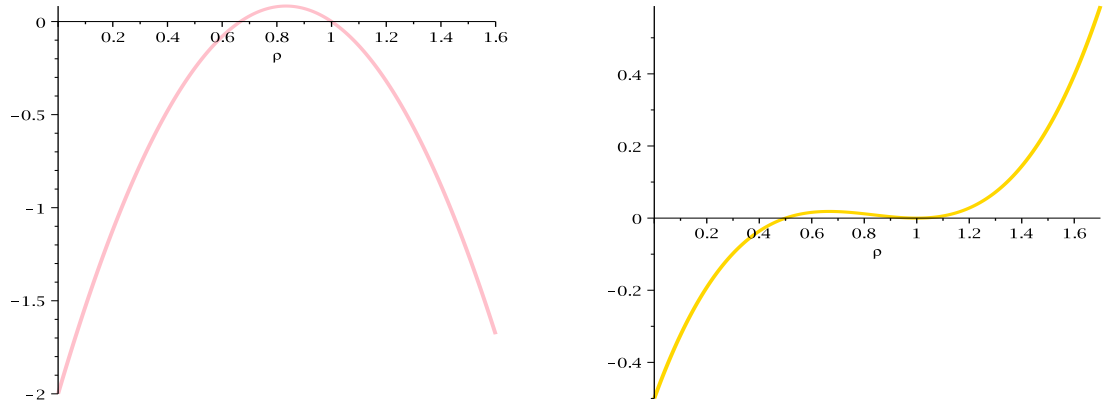

Figure 23: Graphs of (a) left: f_6, (b) right: V_6

In [2], section IV G, a diagram similar to the (E, P) in figure 21 can be found; the corresponding analysis was different and concerned the study of bound states in the $1D$ Nonlinear Schrödinger equation (with zero condition at infinity) with the focusing non monotonic nonlinearity $f(\varrho) = \varrho^{5/2} - \varrho^5 + \frac{1}{2}\varrho^{15/2}$. On the contrary, our framework deals with $2D$ travelling waves with nonzero condition at infinity with a defocusing monotonic nonlinearity. To our knowledge, this is the first occurrence of such a diagram in this last context. This study has led us to try to construct a nonlinearity in $1D$ with the same qualitative properties: see A.1 and figure 28 (b).

The (E, P) diagram in $1D$ with the nonlinearity f_5 does not have any cusp (*cf.* [20]). However, another type of saturated nonlinearity given by

$$f(\varrho) = \alpha \left(\frac{1}{(1 + \frac{\varrho}{\varrho_0})^\nu} - \frac{1}{(1 + \frac{1}{\varrho_0})^\nu} \right)$$

does have one for some particular values of ϱ_0, ν, α. Actually, it corresponds to a local maximum of both P and E. This nonlinearity has already been studied in [36], where they put forward for the first time unstable kinks. Nevertheless their (E, P) diagram should exhibit a cusp as shown in A.2 figure 30 instead of figure 1 in [36].

3.5 Example 6: a cubic-quintic nonlinearity

We consider finally the cubic-quintic nonlinearity

$$f_6(\varrho) \stackrel{\text{def}}{=} -(\varrho - 1) - 3(\varrho - 1)^2,$$

for which

$$V_6(\varrho) = \frac{1}{2}(\varrho - 1)^2 + (\varrho - 1)^3,$$

thus $\mathfrak{c}_s^2 = 2$, $\Gamma = 24$ and the graphs of f_6 and V_6 are given in figure 23. It is important to note that, near the origin, f_6 is increasing and V_6 is negative. This nonlinearity is well-studied in the physical

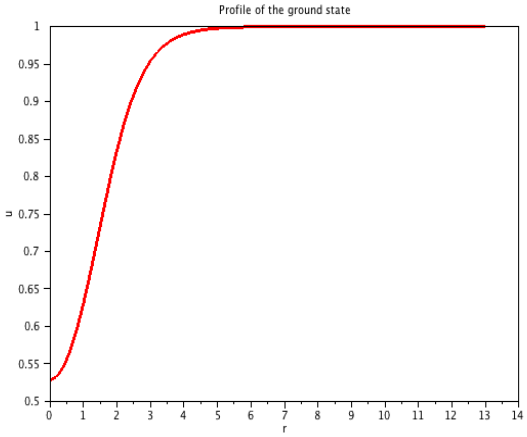

Figure 24: The profile g of the ground state solution for the cubic-quintic nonlinearity f_6

literature: see [4] and other papers by I. Barashenkov and co-authors. However, these studies are in dimension one, and we have not been able to find any study in higher dimensions. In dimension two and three, the paper [10] provides the energy-momentum diagrams in the case of cubic-quintic type nonlinearities but when the potential function V is everywhere nonnegative (hence there exist vortex solutions).

When the potential function V_6 is negative near the origin, there does not exist vortex solutions and we do not expect vortices for small speeds. Actually, for this type of nonlinearity where $\inf V < 0$, there exists a stationary bubble, that is a real-valued solution v to

$$\Delta v + v f_6(v^2) = 0,$$

which is a radially symmetric function $v(x) = g(|x|) = g(r)$, where g is increasing and tends to 1 at infinity. Concerning the existence of such solutions, we may refer to [6] or to the proof of Theorem 3.1 p. 106 in [17] by variational methods. One may also use a shooting argument as in [28] relying on the mathematical justification given in [7]. For our cubic-quintic nonlinearity f_6, we have obtained by the shooting method the profile g given in figure 24, and the minimum value of g is $g(0) \approx 0.528\,621\,847\,110$. This solution is known to be unstable for the corresponding (NLS), see [25]. The (E, P) diagram for f_6 is given in figure 25.

We have started from the transonic limit $c \approx \mathfrak{c}_s$ and used the minimization of the functional $\mathcal{I}$ (that is $\mathbb{G}_{\min}^{c_0}$) starting from ε not too small and the (KP-I) ansatz with the lump solution. The corresponding travelling wave looks like the rarefaction pulse in figure 2 (b). We may notice that we do not reach the value $(P = 0, E = 0)$ in view of the problems associated with the transonic limit (see section 2.5). Here again the results on the transonic limit in [22] may be applied to this nonlinearity (see the blue crosses in figure 25). Then, we increase the kinetic so that E and P increase (concave part of the diagram) until we reach the point with parameters $(c = 0.785, P = 0.721, E = 0.921)$ which corresponds to the cusp. This time, it is associated with a (local) maximum of both E and P whereas those for the nonlinearities f_1, f_2 and f_3 were for a (local) minimum. We pursue the simulation after the cusp: E and P decrease up to ≈ 0.712 and 0 respectively. For $c \approx 0$, we significatively observe numerical convergence towards the bubble as

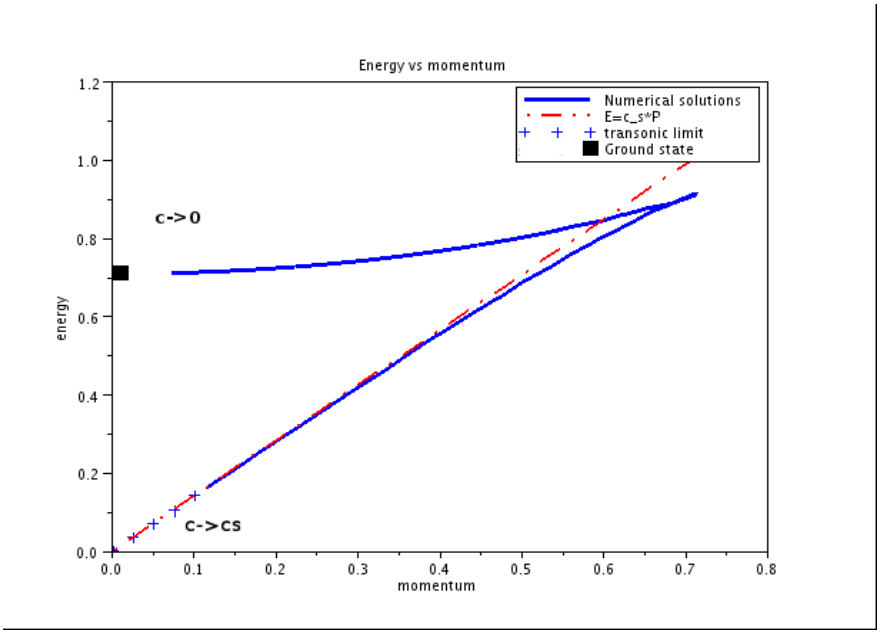

Figure 25: (E, P) diagram for the cubic-quintic nonlinearity f_6

shown in figure 26 (c). In particular, the minimum of the modulus is indeed ≈ 0.529 (see figure 26 (c)), which is the minimum of the ground state solution ($g(0) \approx 0.528$). As c goes to zero, the minimization of $\mathbb{G}_{\min}^{c_0}$ is actually more and more difficult in view of the fact that the derivative $\dfrac{d\mathbb{G}_{\min}^{c_0}}{dk} = -\dfrac{c_0}{c^2}$ (by (17)) tends to $-\infty$ but $\mathbb{G}_{\min}^{c_0}$ has a finite limit. This implies that we spend a lot of time to acheive a (local) minimum. For this reason, we have used the minimization of $\mathbb{G}_{\min}^{c_0}$ up to the solution with parameters $(c = 0.42, P = 0.53, E = 0.81)$ and the rest of the curve is obtained using the continuation method. See the evolution in figure 26.

Comments. The cubic-quintic is a common model, but to the best of our knowledge, the study of the travelling waves for this equation has not been done in dimension two. The specificity of this nonlinearity is that the potential V achieves negative values, which implies the existence of a particular stationary solution: the ground state. The (E, P) diagram is then similar to the one dimensional case, with a cusp corresponding to a maximum for both E and P (see [4]).

4 Proofs

4.1 Proof of Proposition 3

Proof of (i). Since u_* is a minimizer for $\mathfrak{L}_{\min}(\mu_*)$, u_* solves

$$\Delta u_* + u_* f(|u_*|^2) - i\frac{E_0}{P_0^2}\left(\mu_* - P(u_*)\right)\partial_{x_1} u_* = 0$$

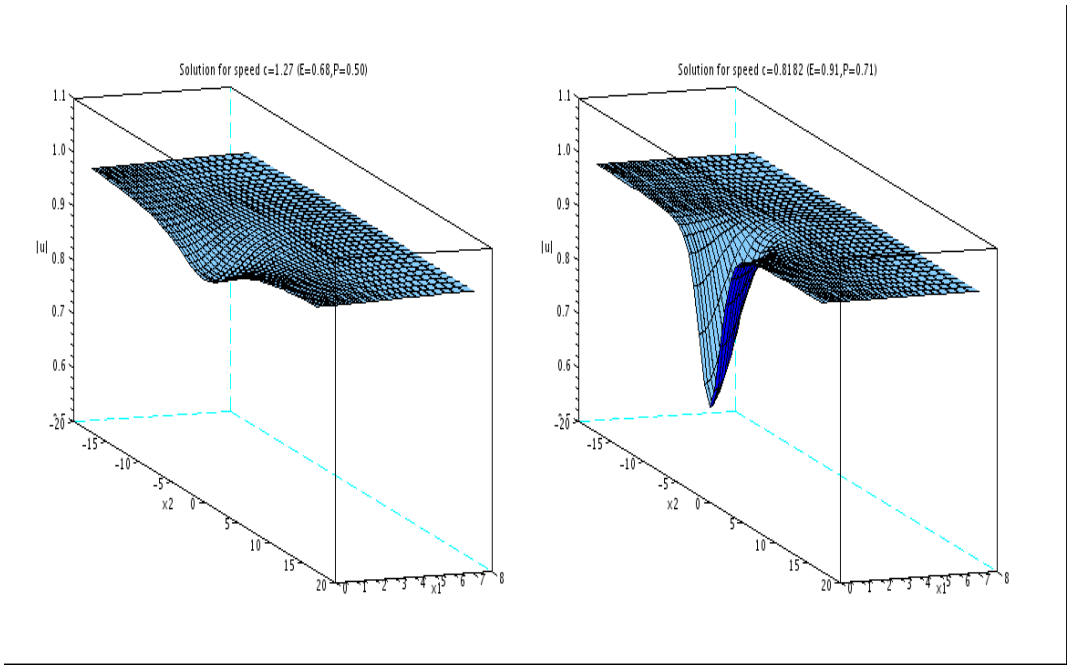

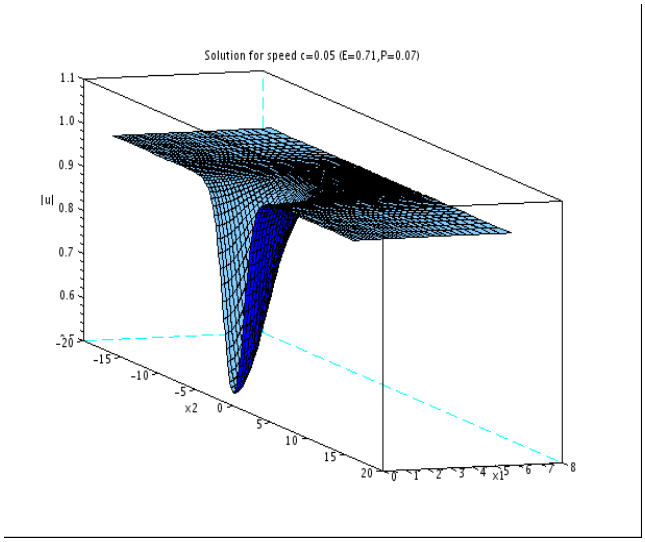

Figure 26: Travelling wave for the cubic-quintic nonlinearity f_6 for speed: (a) top left $c = 1.27$; (b) top right $c = 0.8182$; (c) bottom $c = 0.05$

in $\mathbb{R}^2$, that is (TW_{c_*}) with $c_* = \dfrac{E_0}{P_0^2}(\mu_* - P(u_*))$. Furthermore, for all $w \in \mathcal{X}$ such that $P(w) = P(u_*)$, we have by minimality of u_*

$$E(u_*) + \frac{E_0}{2P_0^2}(\mu_* - P(u_*))^2 = \mathcal{L}(u_*, \mu_*) \leq \mathcal{L}(w, \mu_*) = E(w) + \frac{E_0}{2P_0^2}(\mu_* - P(u_*))^2,$$

hence $E(u_*) \leq E(w)$ as wished.
Proof of (ii). One writes $\forall v \in \mathcal{X}$,

$$\begin{aligned}\mathcal{L}(v, \mu_*) - \mathcal{L}(u_*, \mu_*) &= E(v) - E(u_*) + \frac{E_0}{2P_0^2}(\mu_* - P(v))^2 - \frac{E_0}{2P_0^2}(\mu_* - P(u_*))^2 \\ &= E(v) - E(u_*) + \frac{E_0}{2P_0^2}[2\mu_* - P(u_*) + P(v)][P(u_*) - P(v)].\end{aligned}$$

Since $\mu_* = \dfrac{\mathfrak{p}_*}{P_0} + c_* \dfrac{P_0}{E_0}$ and $P(u_*) = \mathfrak{p}_*$, we deduce

$$\mathcal{L}(v, \mu_*) - \mathcal{L}(u_*, \mu_*) = E(v) - E(u_*) + \frac{E_0}{2P_0^2}(P(u_*) - P(v))^2 - c_*(P(v) - P(u_*)).$$

Since we choose v in the vicinity of u_* and u_* is a minimizer for $\mathbb{E}_{\min}(P(u_*))$,

$$\begin{aligned}\mathcal{L}(v, \mu_*) - \mathcal{L}(u_*, \mu_*) &\geq \mathbb{E}_{\min}(P(v)) - \mathbb{E}_{\min}(P(u_*)) + \frac{E_0}{2P_0^2}(P(u_*) - P(v))^2 - c_*(P(v) - P(u_*)) \\ &\geq \frac{d\mathbb{E}_{\min}}{d\mathfrak{p}}(P(v) - P(u_*)) + \frac{1}{2}\frac{d^2\mathbb{E}_{\min}}{d\mathfrak{p}^2}(P(u_*) - P(v))^2 \\ &\quad + \frac{E_0}{2P_0^2}(P(u_*) - P(v))^2 - c_*(P(v) - P(u_*)) + o((P(u_*) - P(v))^2),\end{aligned}$$

where we have used the second order Taylor expansion of $\mathbb{E}_{\min}$. Furthermore, the speed c_* satisfies the Hamilton group relation (see (16))

$$\frac{d\mathbb{E}_{\min}}{d\mathfrak{p}}(P(u_*)) = c_*,$$

since $\mathbb{E}_{\min}$ has a derivative at $P(u_*)$, thus

$$\mathcal{L}(v, \mu_*) - \mathcal{L}(u_*, \mu_*) \geq \frac{1}{2}\Big(\frac{d^2\mathbb{E}_{\min}}{d\mathfrak{p}^2} + \frac{E_0}{P_0^2} + o(1)\Big)(P(u_*) - P(v))^2$$

and the right hand side is nonnegative under the condition $\dfrac{d^2\mathbb{E}_{\min}}{d\mathfrak{p}^2} + \dfrac{E_0}{P_0^2} > 0$ provided v is sufficiently close to u_*. This concludes the proof. □

4.2 Proof of proposition 4

Proof of (i). Assume that $\kappa_* \in \mathbb{R}^+$ and u_* is a minimizer of the problem $\mathfrak{I}_{\min}(\kappa_*)$. Then for all $v \in \mathcal{X}$, such that $E_{\mathrm{kin}}(v) = E_{\mathrm{kin}}(u_*)$,

$$E_{\mathrm{pot}}(u_*) - c_0 P(u_*) + \frac{1}{E_0}(E_{\mathrm{kin}}(u_*) - \kappa_*)^2 \leq E_{\mathrm{pot}}(v) - c_0 P(v) + \frac{1}{E_0}(E_{\mathrm{kin}}(v) - \kappa_*)^2,$$

which implies

$$E_{\rm pot}(u_*) - c_0 P(u_*) \leq E_{\rm pot}(v) - c_0 P(v),\ \forall v \in \mathcal{X} \text{ such that } E_{\rm kin}(v) = E_{\rm kin}(u_*).$$

Thus $\mathbb{G}^{c_0}_{\rm min}(E_{\rm kin}(u_*)) = G^{c_0}(u_*)$. Furthermore since u_* is a solution of problem $\mathfrak{I}_{\rm min}(\kappa_*)$, u_* solves

$$\frac{1}{E_0}(E_{\rm kin}(u_*) - \kappa_*)\Delta u_* + u_* f(|u_*|^2) - ic_0\partial_{x_1} u_* = 0$$

in $\mathbb{R}^2$. From Proposition 2 (ii), we deduce that

$$\frac{1}{E_0}(E_{\rm kin}(u_*) - \kappa_*) = \left(\frac{c_0}{c_*}\right)^2 > 0,$$

with c_* defined as in (17). Thus if we set $\sigma = \sqrt{\dfrac{E_0}{E_{\rm kin}(u_*) - \kappa_*}} = \dfrac{c_*}{c_0}$, the function $\tilde{u}_* \stackrel{\rm def}{=} u_*(\frac{\cdot}{\sigma})$ is a solution of

$$\Delta \tilde{u}_* + \tilde{u}_* f(|\tilde{u}_*|^2) - ic_*\partial_{x_1}\tilde{u}_* = 0,$$

that is (TW_{c_*}).

Proof of (ii). The first part of the statement is a direct application of Proposition 2. Let then u_* be a minimizer of the problem $\mathbb{G}^{c_0}_{\rm min}(\mathfrak{K}_*)$. One writes $\forall v \in \mathcal{X}$ and $\kappa_* > 0$,

$$\begin{aligned}
\mathcal{I}(v,\kappa_*) - \mathcal{I}(u_*,\kappa_*) &= E_{\rm pot}(v) - c_0 P(v) + \frac{1}{2E_0}(E_{\rm kin}(v) - \kappa_*)^2 \\
&\quad - E_{\rm pot}(u_*) + c_0 P(u_*) - \frac{1}{2E_0}(E_{\rm kin}(u_*) - \kappa_*)^2 \\
&= [(E_{\rm pot} - c_0 P)(v) - (E_{\rm pot} - c_0 P)(u_*)] \\
&\quad + \frac{1}{2E_0}\left[(E_{\rm kin}(v) - \kappa_*)^2 - (E_{\rm kin}(u_*) - \kappa_*)^2\right].
\end{aligned}$$

By choosing $\kappa_* = E_{\rm kin}(u_*) - \frac{c_0^2}{c_*^2}E_0 = \mathfrak{K}_* - \frac{c_0^2}{c_*^2}E_0$, one finds

$$\begin{aligned}
\mathcal{I}(v,\kappa_*) - \mathcal{I}(u_*,\kappa_*) &= [(E_{\rm pot} - c_0 P)(v) - (E_{\rm pot} - c_0 P)(u_*)] \\
&\quad + \frac{1}{2E_0}\left[E_{\rm kin}(v) - E_{\rm kin}(u_*)\right]^2 + \frac{c_0^2}{c_*^2}\left[E_{\rm kin}(v) - E_{\rm kin}(u_*)\right] \\
&\geq \mathbb{G}^{c_0}_{\rm min}(E_{\rm kin}(v)) - \mathbb{G}^{c_0}_{\rm min}(E_{\rm kin}(u_*)) \\
&\quad + \frac{1}{2E_0}\left[E_{\rm kin}(v) - E_{\rm kin}(u_*)\right]^2 + \frac{c_0^2}{c_*^2}\left[E_{\rm kin}(v) - E_{\rm kin}(u_*)\right].
\end{aligned}$$

If we choose v in the vicinity of u_*,

$$\begin{aligned}
\mathcal{I}(v,\kappa_*) - \mathcal{I}(u_*,\kappa_*) \geq{}& \frac{d\mathbb{G}^{c_0}_{\rm min}}{dk}(E_{\rm kin}(u_*))(E_{\rm kin}(v) - E_{\rm kin}(u_*)) \\
&+ \frac{1}{2}\frac{d^2\mathbb{G}^{c_0}_{\rm min}}{dk^2}(E_{\rm kin}(u_*))(E_{\rm kin}(v) - E_{\rm kin}(u_*))^2 + \frac{1}{2E_0}\left[E_{\rm kin}(v) - E_{\rm kin}(u_*)\right]^2 \\
&+ \frac{c_0^2}{c_*^2}\left[E_{\rm kin}(v) - E_{\rm kin}(u_*)\right] + o((E_{\rm kin}(v) - E_{\rm kin}(u_*))^2).
\end{aligned}$$

By (17), we then infer

$$\mathcal{I}(v,\kappa_*)-\mathcal{I}(u_*,\kappa_*)\geq\frac{1}{2}\left[\frac{d^2\mathbb{G}_{\min}^{c_0}}{dk^2}(E_{\rm kin}(u_*))+\frac{1}{E_0}+o(1)\right](E_{\rm kin}(v)-E_{\rm kin}(u_*))^2.$$

This yields the conclusion under the condition: $\dfrac{d^2\mathbb{G}_{\min}^{c_0}}{dk^2}(E_{\rm kin}(u_*))+\dfrac{1}{E_0}>0$, provided v is sufficiently close to u_*. This finishes the proof. □

4.3 Proof of Proposition 5

In the sequel, we shall make a little abuse of notation by using the same notation P for the momentum considered as a function of $\tilde{u}_*$, c or k. Since $P(\tilde{u}_*)=\dfrac{c_*}{c_0}P(u_*)$ and $E_{\rm pot}(\tilde{u}_*)=\left(\dfrac{c_*}{c_0}\right)^2E_{\rm pot}(u_*)$ by scaling, it follows that

$$\mathbb{G}_{\min}^{c_0}(\mathfrak{K}_*)=\left(\frac{c_0}{c_*}\right)^2E_{\rm pot}(\tilde{u}_*)-\frac{c_0^2}{c_*}P(\tilde{u}_*)=-\frac{c_0^2}{2c_*}P(\tilde{u}_*),\tag{28}$$

where we have used the Pohozahev identity $2E_{\rm pot}(\tilde{u}_*)=c_*P(\tilde{u}_*)$. Furthermore, c_* is defined by

$$c_*=\sqrt{-\frac{c_0^2}{\dfrac{d\mathbb{G}_{\min}^{c_0}}{dk}(\mathfrak{K}_*)}}.\tag{29}$$

This implies that $\dfrac{dc}{dk}(\mathfrak{K}_*)<0$ since, by assumption, $\mathbb{G}_{\min}^{c_0}$ has a second order derivative at $\mathfrak{K}_*$ and is concave. This gives $sgn(\frac{dP}{dc})=-sgn(\frac{dP}{dk})$.

Moreover, combining (28) and (29),

$$\frac{dP}{dk}=\frac{d}{dk}\left(-\frac{2}{c_0^2}\mathbb{G}_{\min}^{c_0}\sqrt{-\frac{c_0^2}{\dfrac{d\mathbb{G}_{\min}^{c_0}}{dk}}}\right)=-\frac{1}{c_0}\frac{-2\left(\dfrac{d\mathbb{G}_{\min}^{c_0}}{dk}\right)^2+\mathbb{G}_{\min}^{c_0}\dfrac{d^2\mathbb{G}_{\min}^{c_0}}{dk^2}}{\left(-\dfrac{d\mathbb{G}_{\min}^{c_0}}{dk}\right)^{\frac{3}{2}}},$$

which gives that $-\dfrac{dP}{dk}$ and $\mathbb{G}_{\min}^{c_0}\dfrac{d^2\mathbb{G}_{\min}^{c_0}}{dk^2}-2\left(\dfrac{d\mathbb{G}_{\min}^{c_0}}{dk}\right)^2$ have the same sign, as wished. □

4.4 Proof of Proposition 6

Let us consider a ground state A for (KP-I) (recall $\Gamma\neq0$), that is expected (but not proved) to be the lump solitary wave. Then, A minimizes the energy

$$\int_{\mathbb{R}^2}\frac{1}{\mathfrak{c}_s^2}(\partial_{z_1}\zeta)^2+(\partial_{z_2}\partial_{z_1}^{-1}\zeta)^2+\frac{\Gamma}{3}\zeta^3\,dz$$

among all functions satisfying $\int_{\mathbb{R}^2}\zeta^2\,dz=\int_{\mathbb{R}^2}A^2\,dz$ (see [26] for precise functional spaces). As a consequence, the hessian of the action around A is associated with the self-adjoint operator

$$\Lambda\stackrel{\rm def}{=}\frac{1}{\mathfrak{c}_s}-\frac{1}{\mathfrak{c}_s^2}\,\partial_{z_1}^2+\partial_{z_2}^2\partial_{z_1}^{-2}+\Gamma A$$

has at most one negative eigenvalue (see [48]). Its essential spectrum is $[\mathfrak{c}_s^{-1}, +\infty)$. On the other hand, the scaling properties of (SW) show that for any $\lambda > 0$, the function $A_\lambda(z) = \lambda^2 A(\lambda z_1, \lambda^2 z_2)$ solves

$$\frac{\lambda^2}{\mathfrak{c}_s^2}\,\partial_{z_1} A_\lambda - \frac{1}{\mathfrak{c}_s^2}\,\partial_{z_1}^3 A_\lambda + \Gamma A_\lambda \partial_{z_1} A_\lambda + \partial_{z_2}^2 \partial_{z_1}^{-1} A_\lambda = 0.$$

Differentiating at $\lambda = 1$ provides $\Lambda\Big(\dfrac{\partial A_\lambda}{\partial \lambda}_{|\lambda=1}\Big) = -\dfrac{2}{\mathfrak{c}_s^2} A_1 = -\dfrac{2}{\mathfrak{c}_s^2} A$, hence, by scaling for the third equality,

$$\begin{aligned}\Big\langle \Lambda\Big(\frac{\partial A_\lambda}{\partial \lambda}_{|\lambda=1}\Big), \frac{\partial A_\lambda}{\partial \lambda}_{|\lambda=1}\Big\rangle_{L^2(\mathbb{R}^2)} &= -\frac{2}{\mathfrak{c}_s^2}\Big\langle A_1, \frac{\partial A_\lambda}{\partial \lambda}_{|\lambda=1}\Big\rangle_{L^2(\mathbb{R}^2)} = -\frac{1}{\mathfrak{c}_s^2}\frac{d}{d\lambda}\Big(\|A_\lambda\|^2_{L^2(\mathbb{R}^2)}\Big)_{|\lambda=1} \\ &= -\frac{1}{\mathfrak{c}_s^2}\frac{d}{d\lambda}\Big(\lambda\|A\|^2_{L^2(\mathbb{R}^2)}\Big)_{|\lambda=1} = -\frac{1}{\mathfrak{c}_s^2}\|A\|^2_{L^2(\mathbb{R}^2)} < 0. \end{aligned} \tag{30}$$

Consequently, the operator Λ has exactly one negative eigenvalue, denoted $\lambda_{\rm KP}$, and let $\tilde{A}_* = \mathfrak{c}_s^{-1}\partial_{z_1}^{-1}\tilde{\varphi}_*$ be a corresponding eigenvector, so that

$$\frac{1}{\mathfrak{c}_s}\tilde{A}_* - \frac{1}{\mathfrak{c}_s^2}\,\partial_{z_1}^2 \tilde{A}_* + \partial_{z_2}^2 \partial_{z_1}^{-2}\tilde{A}_* + \Gamma A \tilde{A}_* = \lambda_{\rm KP}\tilde{A}_*.$$

Starting from this eigenpair, we shall construct an approximate eigenvector $\tilde{u}$ for the linearized operator Υ_c (defined in (25)) when $c = c(\varepsilon) \to \mathfrak{c}_s$. Recall that the travelling wave $u_{c(\varepsilon)}(x)$ is searched as $(1 + \varepsilon^2 A_\varepsilon(z))\mathsf{e}^{i\varepsilon\varphi_\varepsilon(z)}$ with $z_1 = \varepsilon x_1$ and $z_2 = \varepsilon^2 x_2$. Therefore, it is natural to look for $\tilde{u}$ under the form

$$\tilde{u}(x) = i\varepsilon(1 + \varepsilon^2 A_\varepsilon(z))\mathsf{e}^{i\varepsilon\varphi_\varepsilon(z)}\tilde{\varphi}(z) + \varepsilon^2 \tilde{A}(z)\mathsf{e}^{i\varepsilon\varphi_\varepsilon(z)}, \tag{31}$$

corresponding to a linearization in (A, φ).
We have already seen that for $u_{c(\varepsilon)}$ given by (5), there holds

$$\begin{aligned}\Big[\Delta u_{c(\varepsilon)} + u_{c(\varepsilon)} f(|u_{c(\varepsilon)}|^2) - ic(\varepsilon)\partial_{x_1} u_{c(\varepsilon)}\Big](x) \\ = \mathsf{e}^{i\varphi_\varepsilon}\left[-\varepsilon^2(1 + \varepsilon^2 A_\varepsilon)\Theta_1(A_\varepsilon, \varphi_\varepsilon) + i\varepsilon^3\Theta_2(A_\varepsilon, \varphi_\varepsilon)\right](z),\end{aligned} \tag{32}$$

where

$$\Theta_2(A_\varepsilon, \varphi_\varepsilon) \stackrel{\rm def}{=} -c(\varepsilon)\partial_{z_1} A_\varepsilon + 2\varepsilon^2 \partial_{z_1}\varphi_\varepsilon \partial_{z_1} A_\varepsilon + 2\varepsilon^4 \partial_{z_2}\varphi_\varepsilon \partial_{z_2} A_\varepsilon + (1 + \varepsilon^2 A_\varepsilon)(\partial_{z_1}^2\varphi_\varepsilon + \varepsilon^2 \partial_{z_2}^2 \varphi_\varepsilon)$$

and

$$\Theta_1(A_\varepsilon, \varphi_\varepsilon) \stackrel{\rm def}{=} -c(\varepsilon)\partial_{z_1}\varphi_\varepsilon + \varepsilon^2(\partial_{z_1}\varphi_\varepsilon)^2 + \varepsilon^4(\partial_{z_2}\varphi_\varepsilon)^2 - \frac{1}{\varepsilon^2} f((1 + \varepsilon^2 A_\varepsilon)^2) - \varepsilon^2 \frac{\partial_{z_1}^2 A_\varepsilon + \varepsilon^2 \partial_{z_2}^2 A_\varepsilon}{1 + \varepsilon^2 A_\varepsilon}.$$

The linearization of (32) (with (5)) gives:

$$\begin{aligned}\Upsilon_{c(\varepsilon)}(\tilde{u}) = \mathsf{e}^{i\varepsilon\varphi_\varepsilon}\Big[-\varepsilon^2(1 + \varepsilon^2 A_\varepsilon) D\Theta_1(A_\varepsilon, \varphi_\varepsilon).(\tilde{A}, \tilde{\varphi}) + i\varepsilon^3 D\Theta_2(A_\varepsilon, \varphi_\varepsilon).(\tilde{A}, \tilde{\varphi}) - \varepsilon^4 \tilde{A}\Theta_1(A_\varepsilon, \varphi_\varepsilon)\Big] \\ + \tilde{\varphi}\mathsf{e}^{i\varepsilon\varphi_\varepsilon}\left[-\varepsilon^2(1 + \varepsilon^2 A_\varepsilon)\Theta_1(A_\varepsilon, \varphi_\varepsilon) + i\varepsilon^3\Theta_2(A_\varepsilon, \varphi_\varepsilon)\right] \\ = \mathsf{e}^{i\varepsilon\varphi_\varepsilon}\Big[-\varepsilon^2(1 + \varepsilon^2 A_\varepsilon) D\Theta_1(A_\varepsilon, \varphi_\varepsilon).(\tilde{A}, \tilde{\varphi}) + i\varepsilon^3 D\Theta_2(A_\varepsilon, \varphi_\varepsilon).(\tilde{A}, \tilde{\varphi})\Big],\end{aligned}$$

since $u_{c(\varepsilon)}$ solves ($\mathrm{TW}_{c(\varepsilon)}$). We now consider, for some λ to be determined later (we shall find $\lambda \sim \varepsilon^4 \lambda_{\mathrm{KP}}$), the expression

$$\Upsilon_{c(\varepsilon)}(\tilde{u}) - \lambda \tilde{u} = \mathsf{e}^{i\varepsilon\varphi_\varepsilon}\Big[-\varepsilon^2(1+\varepsilon^2 A_\varepsilon) D\Theta_1(A_\varepsilon,\varphi_\varepsilon).(\tilde{A},\tilde{\varphi}) + i\varepsilon^3 D\Theta_2(A_\varepsilon,\varphi_\varepsilon).(\tilde{A},\tilde{\varphi}) \\ -\lambda\Big(i\varepsilon(1+\varepsilon^2 A_\varepsilon)\tilde{\varphi} + \varepsilon^2\tilde{A}\Big)\Big].$$

Moreover, in view of (7), it is natural to choose $(\tilde{B},\tilde{\varphi},\tilde{A})$ all of order ε^0, but depending on ε, such that $\mathfrak{c}_s\tilde{A} + \varepsilon^2\mathfrak{c}_s\tilde{B} = \partial_{z_1}\tilde{\varphi} = \mathfrak{c}_s\tilde{A} + \mathcal{O}(\varepsilon^2)$. We now use that $c(\varepsilon) = \sqrt{\mathfrak{c}_s^2 - \varepsilon^2} = \mathfrak{c}_s - \dfrac{\varepsilon^2}{2\mathfrak{c}_s} + \mathcal{O}(\varepsilon^4)$, the definition of $\tilde{\varphi}$ and the convergence of $A_\varepsilon = \dfrac{\partial_{z_1}\varphi}{\mathfrak{c}_s} \to A$, to obtain the expansion

$$\begin{aligned} D\Theta_2(A_\varepsilon,\varphi_\varepsilon).(\tilde{A},\tilde{\varphi}) =& -c(\varepsilon)\partial_{z_1}\tilde{A} + \partial_{z_1}^2\tilde{\varphi} + \varepsilon^2\Big(2\partial_{z_1}\tilde{\varphi}\partial_{z_1}A_\varepsilon + 2\partial_{z_1}\varphi_\varepsilon\partial_{z_1}\tilde{A} + \tilde{A}\partial_{z_1}^2\varphi_\varepsilon + A_\varepsilon\partial_{z_1}^2\tilde{\varphi} + \partial_{z_2}^2\tilde{\varphi}\Big) \\ &+ \mathcal{O}(\varepsilon^4) \\ =& \mathfrak{c}_s\varepsilon^2\Big(\partial_{z_1}\tilde{B} + \frac{1}{2\mathfrak{c}_s^2}\,\partial_{z_1}\tilde{A} + 3\partial_{z_1}(A\tilde{A}) + \partial_{z_2}^2\partial_{z_1}^{-1}\tilde{A}\Big) + o(\varepsilon^2). \end{aligned}$$

Similarly, we obtain

$$D\Theta_1(A_\varepsilon,\varphi_\varepsilon).(\tilde{A},\tilde{\varphi}) = \mathfrak{c}_s\varepsilon^2\Big(\tilde{B} + \frac{1}{2\mathfrak{c}_s^2}\,\tilde{A} + (\Gamma-3)(A\tilde{A}) - \partial_{z_1}^2\tilde{A}\Big) + o(\varepsilon^2),$$

thus

$$\begin{aligned} \Upsilon_{c(\varepsilon)}(\tilde{u}) - \lambda\tilde{u} =& -\mathfrak{c}_s\varepsilon^4\mathsf{e}^{i\varepsilon\varphi_\varepsilon}\Big\{\tilde{B} + \frac{1}{2\mathfrak{c}_s^2}\,\tilde{A} + (\Gamma-3)(A\tilde{A}) - \partial_{z_1}^2\tilde{A} - \frac{\lambda}{\mathfrak{c}_s\varepsilon^2}\tilde{A} + o(1)\Big\} \\ &+ i\mathfrak{c}_s\varepsilon^5\mathsf{e}^{i\varepsilon\varphi_\varepsilon}\Big\{\partial_{z_1}\tilde{B} + \frac{1}{2\mathfrak{c}_s^2}\,\partial_{z_1}\tilde{A} + 3\partial_{z_1}(A\tilde{A}) + \partial_{z_2}^2\partial_{z_1}^{-1}\tilde{A} - \frac{\lambda}{\mathfrak{c}_s\varepsilon^4}(1+\varepsilon^2 A)\tilde{\varphi} + o(1)\Big\}. \end{aligned}$$

In view of this expansion, we fix

$$\lambda \stackrel{\text{def}}{=} \varepsilon^4\lambda_{\mathrm{KP}} \qquad \text{and} \qquad \tilde{B} \stackrel{\text{def}}{=} -\frac{1}{2\mathfrak{c}_s^2}\,\tilde{A} - (\Gamma-3)(A\tilde{A}) + \partial_{z_1}^2\tilde{A} + \frac{\varepsilon^2\lambda_{\mathrm{KP}}}{\mathfrak{c}_s}\tilde{A} + o(1).$$

We then infer

$$\Upsilon_{c(\varepsilon)}(\tilde{u}) - \lambda\tilde{u} = i\mathfrak{c}_s\varepsilon^5\mathsf{e}^{i\varepsilon\varphi_\varepsilon}\Big\{\partial_{z_1}^2\tilde{A} + \Gamma\partial_{z_1}(A\tilde{A}) + \partial_{z_2}^2\partial_{z_1}^{-1}\tilde{A} - \lambda_{\mathrm{KP}}\partial_{z_1}^{-1}\tilde{A}\Big\} + o(\varepsilon^5).$$

and choose $\tilde{A} \stackrel{\text{def}}{=} \tilde{A}_*$ the negative eigenvector as defined previously, so that the term in brackets cancels out. As a consequence,

$$\frac{\big\|\Upsilon_{c(\varepsilon)}(\tilde{u}) - \varepsilon^4\lambda_{\mathrm{KP}}\tilde{u}\big\|_{L^2}}{\big\|\tilde{u}\big\|_{L^2}} = o(\varepsilon^5).$$

We conclude with the help of the following classical result (see, *e.g.*, [49]).

Theorem 4.1 *Let T be a self-adjoint operator on a Hilbert space $\mathcal{H}$. Assume that there exists $(v,\lambda,\delta) \in \mathcal{H}\times\mathbb{R}\times\mathbb{R}_+^*$ such that $v \neq 0$ and $\|Tv - \lambda v\| \leq \delta\|v\|$. Then, $\sigma(T)\cap[\lambda-\delta,\lambda+\delta]$ is not empty.*

Indeed, since the essential spectrum of Υ_c is included in $\mathbb{R}_+$, we deduce the existence of some negative eigenvalue for $\Upsilon_{c(\varepsilon)}$ which is $\sim \varepsilon^4 \lambda_{\rm KP}$ as $\varepsilon \to 0$.

Remark 9 The operator $\Upsilon_{c(\varepsilon)}$ has the same bad behaviour when $\Gamma = 0 > \Gamma'$ provided one can prove that there exists a negative eigenvalue for the linearization of (SW'). This is probably true, but the argument (30) is no longer sufficient in the cubic case.

5 Conclusions

We have investigated numerically the two dimensional travelling waves of the Nonlinear Schrödinger Equation for a general nonlinearity and with nonzero condition at infinity. These travelling waves are saddle points of the action. In order to compute these solutions, we first exhibit, for a certain range of speeds, a functional for which they are local minimizers (Lyapounov functional) so that we can use a gradient flow. We have combined this approach with a continuation method in speed in order to obtain the full range of velocities. Contrary to a Newton's algorithm, our strategy permits to capture the transonic limit of (KP)-type and to compute solutions even without a very accurate initial guess. The consequence is that Newton's method would miss some branches. The variational method was proved to be essential in particular because it can capture solutions lying on a branch which is not connected to the vortex branch ($c \to 0$), which is impossible using only Newton's or the continuation methods.

We have performed simulations for several nonlinearities having the same behaviour as the well-known Gross-Pitaevskii nonlinearity. We obtained a great variety of (E, P) diagrams and qualitative behaviours. We have observed cusps; a modified (KP-I) asymptotic in the transonic limit with two branches of solutions; various multiplicity results: non uniqueness for some interval of speeds, self-intersection of one continuous branch, intersection of two distinct branches, non uniqueness for some constraint minimization problems; some phenomena of "one dimensional spreading" where the modulus has a plateau corresponding to special values associated with the $1D$ problem.

Acknowledgements: D.C. gratefully acknowledges the support of the ANR *ArDyPitEq*. The authors would like to thank L. Di Menza for having suggested to use the continuation method.

A About two diagrams in dimension one

In this appendix, we consider the (NLS) equation in space dimension one as studied in [20]. We wish to give two more (E, P) diagrams showing the variety of possible qualitative behaviours.

A.1 A quasi-degenerate case

We investigate here the quasi-degenerate case

$$f_{\rm qd}(\varrho) \stackrel{\rm def}{=} -2(\varrho-1) + (3-10^{-3})(\varrho-1)^2 - 4(\varrho-1)^3 + 5(\varrho-1)^4 - 6(\varrho-1)^5,$$

which is a perturbation of the degenerate case

$$f_{\rm dege}(\varrho) \stackrel{\rm def}{=} -2(\varrho-1) + 3(\varrho-1)^2 - 4(\varrho-1)^3 + 5(\varrho-1)^4 - 6(\varrho-1)^5$$

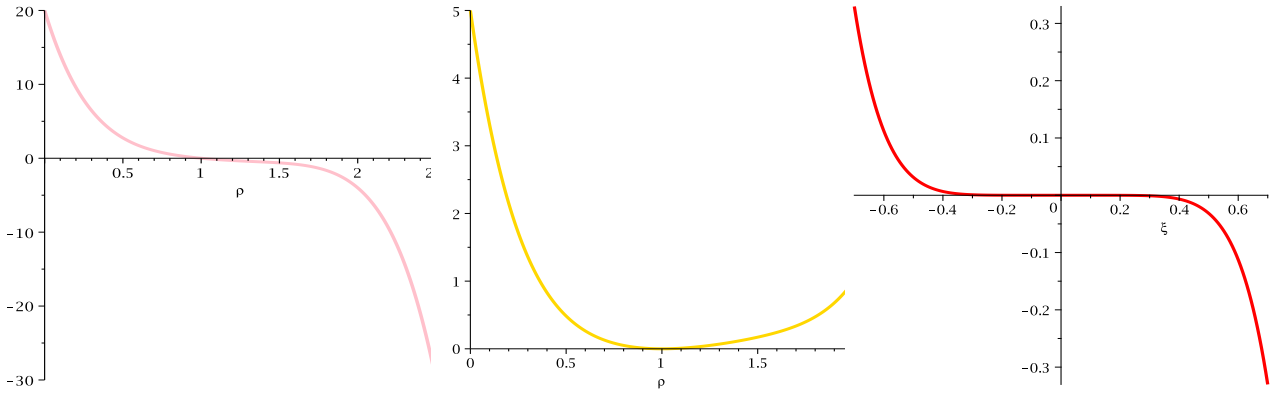

Figure 27: Graphs of (a) left: $f_{\rm qd}$, (b) center: $V_{\rm qd}$ and (c) right: $\mathcal{V}_{\rm qd}$

studied in [20] (example 4 "a degenerate case" there). For the nonlinearity $f_{\rm dege}$, we have $\Gamma = \Gamma' = 0$ (and also other coefficients of the same type) so that the transonic limit is governed by the sextic (gKdV) solitary wave equation

$$\frac{1}{\mathfrak{c}_s^2}\,\partial_z A - \frac{1}{\mathfrak{c}_s^2}\,\partial_z^3 A + \Gamma^{(6)} A^5 \partial_z A = 0,$$

which is supercritical. For the nonlinearity $f_{\rm dege}$, as $c \to \mathfrak{c}_s$, the travelling waves have high energy and momentum (and are unstable, see [20], [21]). For the nonlinearity $f_{\rm qd}$ we are now considering, the coefficient Γ becomes small, but nonzero. Actually, we have

$$V_{\rm qd}(\varrho) = (\varrho-1)^2 - \frac{3-10^{-3}}{3}(\varrho-1)^3 + (\varrho-1)^4 - (\varrho-1)^5 + (\varrho-1)^6$$

and

$$\mathcal{V}_{\rm qd}(\xi) = -\frac{1}{750}\xi^3 - \frac{1}{750}\xi^4 - 4\xi^7,$$

thus $r_0 = 1$, $\mathfrak{c}_s^2 = 4$, $\Gamma = \frac{1}{500}$ and the graphs of $f_{\rm qd}$, $V_{\rm qd}$ and $\mathcal{V}_{\rm qd}$ are given in figure 27.

Since Γ is nonzero, the transonic limit for the nonlinearity $f_{\rm qd}$ is governed by the usual (KdV) solitary wave, and in particular the energy and momentum tend to zero as $c \to \mathfrak{c}_s$. However, in some sense, $f_{\rm qd}$ is close to $f_{\rm dege}$, and we hope that for c close, but not too close, to $\mathfrak{c}_s$, part of the behaviour observed for $f_{\rm dege}$ will be seen for $f_{\rm qd}$. In particular, we hope to have, for the nonlinearity $f_{\rm qd}$, some "large" energy and momentum for c close, but not too close, to $\mathfrak{c}_s$, and then for c very close to $\mathfrak{c}_s$, small energy and momentum.

The numerical computations of the energy and momentum as in [20] provide the diagrams of $c \mapsto E$ and $c \mapsto P$ given in figure 28 (a). Since the variations are rather fast, we have used logarithmic scale: the abscissa is not c but $-\log\left(\dfrac{\mathfrak{c}_s - c}{\mathfrak{c}_s}\right) = -\log(1 - 0.5c)$. Therefore, the corresponding (E, P) diagram is, qualitatively, as in figure 28 (b). Note that we have indeed some

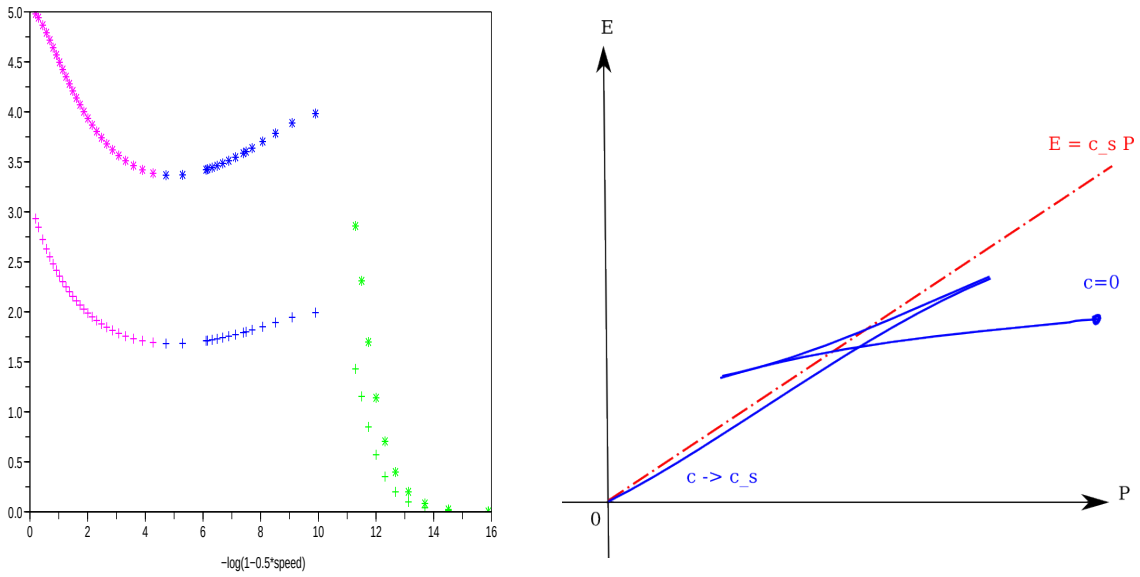

Figure 28: (a) left: Energy (*) and momentum (+) vs. speed in logarithmic scale; (b) right: qualitative (E, P) diagram for nonlinearity $f_{\rm qd}$

"large" energy and momentum for speeds c with $-\log(1-0.5c) \simeq 10$ (for which the dominant behaviour is the one of $f_{\rm dege}$), and finally energy and momentum go to zero since $\Gamma \neq 0$. We have been interested in this nonlinearity since the (E, P) diagram (in dimension one) is qualitatively similar to the one obtained in example 5 for the (exponentially) saturated nonlinearity (in dimension two). As already mentioned, this type of (E, P) diagram can also be found in [2], section IV G, for the study of bound states in the Nonlinear Schrödinger equation (with zero condition at infinity) with the focusing non monotonic nonlinearity $f(\varrho) = \varrho^{5/2} - \varrho^5 + \frac{1}{2}\varrho^{15/2}$. We deal here with travelling waves with a defocusing monotonic nonlinearity.

A.2 Another saturated (NLS) model

We investigate now another classical saturated (NLS) model, which is

$$f_{\rm sat}(\varrho) \stackrel{\rm def}{=} \frac{\varrho_0}{2}\Big(\frac{1}{(1+\varrho/\varrho_0)^2} - \frac{1}{(1+1/\varrho_0)^2}\Big),$$

where $\varrho_0 > 0$ is some parameter. For this nonlinearity, there holds

$$V_{\rm sat}(\varrho) = \frac{(\varrho-1)^2}{2\Big(1+\frac{1}{\varrho_0}\Big)^2\Big(1+\frac{\varrho}{\varrho_0}\Big)} \qquad \text{and} \qquad \mathcal{V}_{\rm sat}(\xi) = -\frac{2\xi^3}{\Big(1+\frac{1}{\varrho_0}\Big)^3\Big(1+\frac{1+\xi}{\varrho_0}\Big)}.$$

This nonlinearity has been studied in [36] and is an example where the "kink", that is the stationary wave ($c = 0$), is unstable if ϱ_0 is small enough. This instability has also been theoretically and numerically studied in [29], where the instability threshold was shown to be $\varrho_0 \simeq 0.134$. However, we would like to point out that the (E, P) diagram given in [36] for $0.08 =$ "I_0" $= \varrho_0 < 0.134$ (figure 1 there) is probably not correct. Indeed, the slope of the curve $P \mapsto E$ must be equal to the speed c in view of the Hamilton group relation (15) (which holds true in dimension one, see [20]).

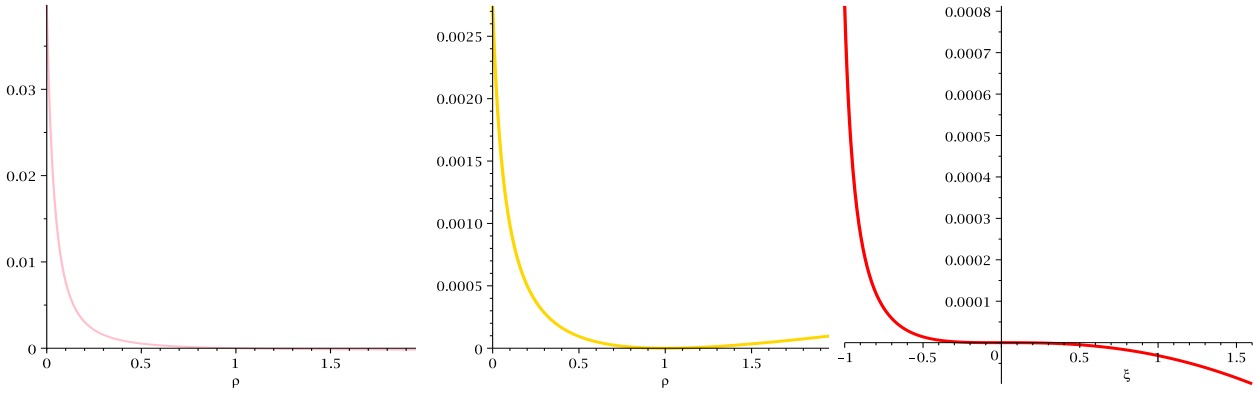

Figure 29: Graphs of (a) f_{sat}, (b) V_{sat} and (c) $\mathcal{V}_{\text{sat}}$

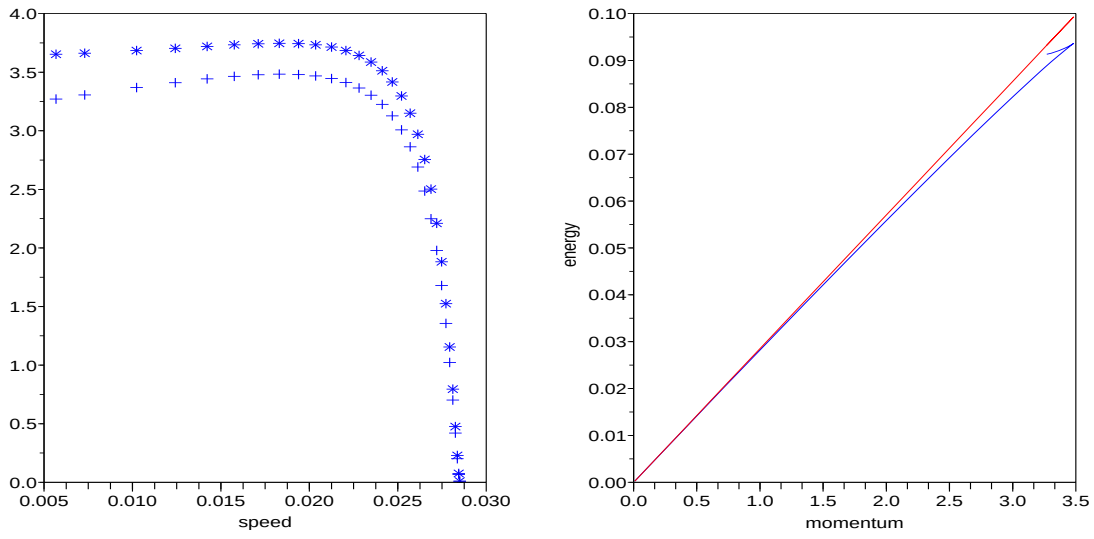

Figure 30: (a) left: 40 × Energy (*) and momentum (+) vs. speed; (b) right: (E, P) diagram for nonlinearity f_{sat}

Hence, there should not exist a point on the curve $c \mapsto (E, P)$ with vertical tangent as given in [36] (figure 1). We have performed the corresponding simulation as in [20].

We shall take $\varrho_0 = 0.08 < 0.134$, thus $r_0 = 1$, $\mathfrak{c}_s^2 = 2(1 + 1/\varrho_0)^{-3} \simeq 0.00081288$, $\Gamma = \frac{6\varrho_0}{\varrho_0+1} = \frac{12}{27} \simeq 0.4444....$ The graphs of $f_{\rm sat}$, $V_{\rm sat}$ and $\mathcal{V}_{\rm sat}$ are given in figure 29. We have computed E and P as the speed c varies, see figure 30 (a), as well as the (E, P) diagram, see figure 30 (b). As we see, the curve possesses a cusp. We see with this example that the (E, P) diagram may exhibit a cusp with a (local) maximum of E and P even though the nonlinearity $f_{\rm sat}$ is increasing. For the cubic-quintic nonlinearity, we also have a cusp with a (local) maximum of E and P, but the nonlinearity is increasing near 0.

References

[1] M. Abid, C. Huepe, S. Metens, C. Nore, C.T. Pham, L.S. Tuckerman, and M.E. Brachet. Gross-Pitaevskii dynamics of Bose-Einstein condensates and superfluid turbulence. *Fluid Dynamics Research*, 33(5-6):509–544, 2003.

[2] N. Akhmediev, A. Ankiewicz, and R. Grimshaw. Hamiltonian-versus-energy diagrams in soliton theory. *Phys. Rev. E*, 59(5):6088–6096, 1999.

[3] I. Barashenkov. Stability Criterion for Dark Solitons. *Phys. Rev. Lett.*, 77:1193–1197, 1996.

[4] I. Barashenkov and E. Panova. Stability and evolution of the quiescent and travelling solitonic bubbles. *Physica D*, 69(1-2):114–134, 1993.

[5] T. Benjamin. The stability of solitary waves. *Proc. Roy. Soc. (London) Ser. A*, 328:153–183, 1972.

[6] H. Berestycki and P.-L. Lions. Nonlinear scalar field equations. I. Existence of a ground state. *Arch. Rational Mech. Anal.*, 82(4):313–345, 1981.

[7] H. Berestycki, P.-L. Lions, and L. Peletier. An ODE approach to the existence of positive solutions for semilinear problems in $\mathbb{R}^N$. *Indiana Univ. Math. J.*, 30(1):141–157, 1981.

[8] N. Berloff. Evolution of rarefaction pulses into vortex rings. *Phys. Rev. B*, 65:174518, 2002.

[9] N. Berloff. Pade approximations of solitary wave solutions of the Gross-Pitaevskii equation. *J. Phys. A: Math. Gen.*, 37(5):1617–1632, 2004.

[10] N. Berloff. Vortex Splitting in Subcritical Nonlinear Schrödinger Equations. *Special issue on vortex rings, Fluid Dynamics Research*, 41:051403, 2009.

[11] N. Berloff and P. Roberts. Motions in a Bose condensate: X. New results on stability of axisymmetric solitary waves of the Gross-Pitaevskii equation. *J. Phys. A: Math. Gen.*, 37:11333–11351, 2004.

[12] F. Béthuel, P. Gravejat, and J-C. Saut. On the KP-I transonic limit of two-dimensional Gross-Pitaevskii travelling waves. *Dynamics of PDE*, 5(3):241–280, 2008.

[13] F. Béthuel, P. Gravejat, and J-C. Saut. Travelling waves for the Gross-Pitaevskii equation. II. *Comm. Math. Phys.*, 285(2):567–651, 2009.

[14] F. Béthuel, G. Orlandi, and D. Smets. Vortex rings for the Gross-Pitaevskii equation. *J. Eur. Math. Soc. (JEMS)*, 6(1):17–94, 2004.

[15] F. Béthuel and J-C. Saut. Travelling waves for the Gross-Pitaevskii equation. I. *Ann. Inst. H. Poincaré Phys. Théor.*, 70(2):147–238, 1999.

[16] J. Boussinesq. Essai sur la théorie des eaux courantes. *Mémoires présentés par divers savants à l'académie des sciences de l'institut de France*, 23, 1877.

[17] H. Brézis and E. H. Lieb. Minimum Action Solutions for Some Vector Field Equations. *Comm. Math. Phys.*, 96:97–113, 1984.

[18] T. Cazenave and P.-L. Lions. Orbital stability of standing waves for some nonlinear Schrödinger equations. *Comm. Math. Phys.*, 85(4):549–561, 1982.

[19] D. Chiron. Travelling waves for the Gross-Pitaevskii equation in dimension larger than two. *Nonlinear Anal., Theory, Methods, Appl.*, 58(1-2):175–204, 2004.

[20] D. Chiron. Travelling waves for the Nonlinear Schrödinger Equation with general nonlinearity in dimension one. *Nonlinearity*, 25:813–850, 2012.

[21] D. Chiron. Stability and instability for subsonic travelling waves of the Nonlinear Schrödinger Equation in dimension one. *Anal PDE*, to appear, 2013.

[22] D. Chiron and M. Mariş. Rarefaction pulses for the Nonlinear Schrödinger Equation in the transonic limit. *Comm. Math. Phys.*, to appear, 2013.

[23] D. Chiron and M. Mariş. Travelling waves for the Nonlinear Schrödinger Equation with nonzero condition at infinity. II. Preprint, 2013.

[24] F. Dalfovo. Structure of vortices in helium at zero temperature. *Phys. Rev. B*, 46(9):5482–5488, 1992.

[25] A. de Bouard. Instability of stationary bubbles. *SIAM J. Math. Anal.*, 26(3):566–582, 1995.

[26] A. de Bouard and J.-C. Saut. *Remarks on the stability of generalized KP solitary waves*, volume 200 of *Contemp. Math.*, pages 75–84. Amer. Math. Soc., Providence, RI, 1996.

[27] A. de Bouard and J.-C. Saut. Solitary waves of generalized Kadomtsev-Petviashvili equations. *Ann. Inst. H. Poincaré Anal. Non Linéaire*, 14(2):211–236, 1997.

[28] L. Di Menza. Numerical computation of solitons for optical systems. *M2AN Math. Model. Numer. Anal.*, 43(1):173–208, 2009.

[29] L. Di Menza and C. Gallo. The black solitons of one-dimensional NLS equations. *Nonlinearity*, 20(2):461–496, 2007.

[30] P. Gravejat. Asymptotics for the travelling waves in the Gross-Pitaevskii equation. *Asymptot. Anal.*, 45(3-4):227–299, 2005.

[31] M. Grillakis, J. Shatah, and W. Strauss. Stability theory of solitary waves in the presence of symmetry I. *J. Funct. Anal.*, 74:160–197, 1987.

[32] C. Jones, S. Putterman, and P. Roberts. Motions in a Bose condensate V. Stability of wave solutions of nonlinear Schrödinger equations in two and three dimensions. *J. Phys A: Math. Gen.*, 19:2991–3011, 1986.

[33] C. Jones and P. Roberts. Motion in a Bose condensate IV. Axisymmetric solitary waves. *J. Phys. A: Math. Gen.*, 15:2599–2619, 1982.

[34] L. Khaykovich and B. Malomed. Deviation from one dimensionality in stationary properties and collisional dynamics of matter-wave solitons. *Phys. Rev. A*, 74:023607, 2006.

[35] Y. Kivshar, D. Anderson, and M. Lisak. Modulational instabilities and dark solitons in a generalized nonlinear Schrödinger-equation. *Phys. Scr.*, 47:679–681, 1993.

[36] Y. Kivshar and W. Krolikowski. Instabilities of dark solitons. *Optics Letters*, 20(14):1527–1529, 1995.

[37] Y. Kivshar and B. Luther-Davies. Dark optical solitons: physics and applications. *Physics Reports*, 298:81–197, 1998.

[38] Y. Kivshar and D. Pelinovsky. Self-focusing and transverse instabilities of solitary waves. *Physics Reports*, 331:117–195, 2000.

[39] Y. Kivshar and X. Yang. Perturbation-induced dynamics of dark solitons. *Phys. Rev. E*, 49:1657–1670, 1994.

[40] E. Kolomeisky, T. Newman, J. Straley, and X. Qi. Low-Dimensional Bose Liquids: Beyond the Gross-Pitaevskii Approximation. *Phys. Rev. Lett.*, 85:1146–1149, 2000.

[41] Z. Lin. Stability and instability of travelling solitonic bubbles. *Adv. Differential Equations*, 7(8):897–918, 2002.

[42] S. Manakov, V. Zakharov, L. Bordag, and V. Matveev. Two-dimensional solitons of the Kadomtsev-Petviashvili equation and their interaction. *Phys. Lett. A*, 63:205–206, 1977.

[43] M. Mariş. Nonexistence of supersonic traveling waves for nonlinear Schrödinger equations with nonzero conditions at infinity. *SIAM J. Math. Anal.*, 40(3):1076–1103, 2008.

[44] M. Mariş. Traveling waves for nonlinear Schrödinger equations with nonzero conditions at infinity. *Ann. of Math.*, 178:107–182, 2013.

[45] N. Papanicolaou and P. Spathis. Semitopological solitons in planar ferromagnets. *Nonlinearity*, 12(2):285–302, 1999.

[46] D. Pelinovsky and Y. Stepanyants. Convergence of Petviashvili's iteration method for numerical approximation of stationary solutions of nonlinear wave equations. *SIAM J. Numer. Anal.*, 42(3):1110–1127, 2004.

[47] V. Petviashvili. Equation of an extraordinary soliton. *Plasma Physics*, 2:469–472, 1976.

[48] M. Reed and B. Simon. *Methods of Modern Mathematical Physics. IV. Analysis of operators.* Academic Press Inc. [Harcourt Brace Jovanovich Publishers], New York, 1978.

[49] M. Reed and B. Simon. *Methods of Modern Mathematical Physics. I. Functional analysis.* Academic Press Inc. [Harcourt Brace Jovanovich Publishers], New York, second edition, 1980.

[50] P. Roberts and N. Berloff. *Nonlinear Schrödinger equation as a model of superfluid helium*, volume 571 of *Lecture Notes in Physics*. Springer-Verlag, Providence, RI, 2001.

[51] S. Sinha, A. Cherny, D. Kovrizhin, and J. Brand. Friction and diffusion of matter-wave bright solitons. *Phys. Rev. Lett.*, 96:030406, 2006.

[52] N. Vakhitov and A. Kolokolov. Stationary solutions of the wave equation in a medium with nonlinearity saturation. *Radiophysics and Quantum Electronics*, 16(7):783–789, 1973.

[53] V. Zakharov and A. Kuznetsov. Multi-scale expansion in the theory of systems integrable by the inverse scattering transform. *Physica D*, 18(1-3):455–463, 1986.